Characterization and Degradation of Fatty Acid Methyl Esters and Biodiesel in Artificial Seawater Under UV Exposure Using Raman Spectroscopy

Julie E. Blanchfield

A thesis

submitted in partial fulfillment of the

requirements for the degree of

Master of Science in Chemical Engineering

University of Washington

2016

Reading Committee:

Qiuming Yu, Chair

Bradley Holt

Jim Pfaendtner

Program Authorized to Offer Degree:

Chemical Engineering

University of Washington

Abstract

Characterization and degradation of fatty acid methyl esters and biodiesel in artificial seawater under UV exposure using Raman Spectroscopy

Julie E. Blanchfield

Chair of the Supervisory Committee:
Research Associate Professor Qiuming Yu
Department of Chemical Engineering

As global concerns over the environmental impact of petroleum fuels increase, alternatives such as biofuels are becoming more prevalent. Most of the world's commodities are shipped over the oceans by large cargo vessels and the carriage of potentially hazardous cargo has safety and environmental risks. The carriage of biofuels is becoming more commonplace and an environmental discharge of such fuels is a potential given international allowances for cargo tank cleaning. The fate of biodiesel in the marine environment is a newer focus of research as the industry expands. This research characterizes the vibrational modes of the building blocks of biodiesel (fatty acid methyl esters (FAMEs)) and a commercial biodiesel sample through Raman spectroscopy. The concentration sensitivity of the Raman spectroscope in concentrations of ultra-pure and artificial seawater was found to be low; concentrations of 20% oil in water were necessary for good spectral resolution. Commercial biodiesel in artificial seawater was exposed under a UV lamp for 23 days to evaluate the degradation mechanisms. Isomerization was evidenced by the decline of the *cis* configurational vibration modes of the =CH bends. Photo-oxidation was apparent as the samples' double bonds broke down over time. It was shown from comparison with a lab-made FAME mix that the antioxidants in commercial biodiesel slowed this process considerably. Hydrolysis occurred breaking down the biodiesel's FAMEs into their

relative free fatty acid and methanol. Methanol evaporated significantly from the sample; its presence was not measured directly through Raman spectroscopy but through a literature review and evaluation of vapor pressures, it was shown that methanol formed. The toxicity of methanol is a concern to marine organisms; however if most of the methanol formed through this degradation evaporates and exists the marine environment through natural physical oceanographic and transport processes, it is unlikely that biodiesel residue into the ocean will cause measurable harm to aquatic organisms.

Table of Contents

List of Figures

List of Tables

Chapter 1. Introduction

1.1 Background

Biodiesel is a renewal energy that is being used more regularly in the global community as the world pushes for sustainable energy products. Countries such as Brazil already produce and use biodiesel regularly and subsidies to users of biodiesel in countries such as the United States work to push the industry forward [1]. Biodiesel, when used in combustion engines, produces fewer emissions than regular petro diesel and the carbon dioxide emissions from burning biodiesel equal the carbon dioxide usage of the biomass used in the feedstock thereby creating a balance [2]. Increased use of biodiesel means more of the fuel is shipped from producers to users all over the globe and increased shipping of any commodity requires transportation safety and environmental scrutiny. Over 90% of the world's commodities are shipped by sea yielding a unique global approach to environmental safety and stewardship [3]. With biofuel being a newer commodity shipped, international and domestic shipping regulations are changing to ensure the safety of personnel and the environment during transport and transfer.

1.2 International and Domestic Shipping of Biodiesel and its Entry into the Aquatic Environment

Regulation of shipping falls internationally to the International Maritime Organization (IMO), which is an agency of the United Nations. Countries that are signatory to the IMO agree to follow the standards and regulations implemented by the IMO and its committees. In the United States (US), shipping by sea is regulated by many agencies of the Executive government including the Department of Transportation's Pipeline and Hazardous Materials Safety Administration (PHMSA) and the Department of Homeland Security's US Coast Guard (USCG). US regulations and law implement requirements for ships that are flagged by foreign countries as

well as vessels. Biofuels, like their petro counterpart, are carried in bulk by large tank ships or tank barges capable of carrying hundreds of thousands of barrels of liquid cargo.

According to the IMO, biofuels "are ethyl alcohol, fatty acid methyl esters (FAMEs), vegetable oils (triglycerides) and alkanes (C10-C26), linear and branched with a flashpoint of either 60°C or less or more than 60°C" as identified by the prevailing code [4]. FAMEs are also termed biodiesel by the industry and used as a petro diesel substitute whereas ethyl alcohol or ethanol is often used as a petro gasoline substitute. The international definition of biofuel and biofuel blends are found in the IMO's International Code for the Construction and Equipment of Ships Carrying Dangerous Chemicals in Bulk (IBC Code) and in supplements to that code. The IBC Code is part of the International Convention for the Prevention of Pollution from Ships (MARPOL), which is a section of the international pollution prevention regulations that regulates hazardous liquid cargoes other than oil; these are defined as "noxious liquid substances" or NLSs. NLSs have specific safety standards for their carriage, vessel design, transfer, and pollution response procedures [5].

MARPOL and the IBC Code clearly outline some specific safety and environmental requirements for biofuels. First, biofuels in their pure form, FAMEs and ethyl alcohol, are classified under the IBC code as a category "Y" NLS. The categories of NLSs are X, Y, and Z. The categories pertain to the assigned hazardous quality of the substance in terms of environmental pollution if or when it is discharged into the sea [5]. Category X is deemed the most detrimental to the environment if discharged into the ocean and has the most stringent requirements relating to discharge of residues and tank cleaning liquids. This hazard level is followed by category Y and thence category Z being the least hazardous to the environment. Specifically, for FAMEs and ethyl alcohols, the definition of a category Y NLS is a "liquid

which if discharged into the sea from tank cleaning or de-ballasting operations are deemed to present a hazard to either marine resources or human health or cause harm to amenities or other legitimate users of the sea and therefore, justify a limitation on the quality and quantity of the discharge" [5]. Blends of biofuels were recently defined by the IMO in 2013 under the IMO's Marine Environmental Protection Committee document MEPC.1/Circ.761/Rev.1 that implements an update to the IBC Code [4]. Blends between 1% and 75% petroleum oil are characterized as NLS category X [4]. Any blend greater than 75% petro-oil is considered oil and is carried under the petro oil pollution prevention regulations in MARPOL. Blends with less than 1% petro are simply identified by their parent biofuel (e.g. FAMEs, ethyl alcohol) [4].

Category Y (and Z) NLSs (pure biofuels) must be pumped to the lowest capacity of the tank pumping equipment possible when the cargo is discharged. Once only "residue" is left in the tank, the vessel can exit the port and flush these cargo tanks with seawater, discharging the water/cargo mix into the ocean under the following specifications: the vessel must be over 12 nautical miles off shore; the vessel must be travelling over 7 knots (nautical miles per hour); the water depth must be greater than 25 m; the discharge must take place over the largest spreadable area possible by safe navigation [5].

Category X NLSs (including most biofuel blends up to 75%), have more stringent requirements. After the tank is emptied completely, the vessel must flush the tank until the resultant residue measures less than 0.1% (1000 ppm) of the original cargo; this waste water from the flushing must be discharged to a shore side facility qualified to handle such waste [5]. Once the flushing has left the tank with less than 0.1% product any further flushing or cleaning that occurs in the tanks may be done in accordance with the requirements for category Y and Z NLSs as discussed in the preceding paragraph. In this manner, biofuels such as biodiesel can

enter the aquatic environment.

US shipping regulations are not yet aligned with these specific International requirements. They do not identify FAMEs or ethyl alcohol as having any specific requirements for carriage by vessel. Current interpretations of the regulations indicate vessels should ship biofuels as oil, requiring vessels to systematically clean all cargo tanks in port as they would regular petro oils. This can be expensive and time consuming for shipping companies. If the US plans to update its regulations pertaining to biofuel, information must be available indicating the outcome of aligning with the already existing International regulations. This research project aims to address this topic through literature research and experimental analysis of the fate of biodiesel in seawater.

1.3 Biodiesel Characteristics

Biodiesel is a blend of fatty acid methyl esters (FAMEs) produced through transesterification of oils or feedstocks such as soybean or rapeseed with methanol [2]. Sources of feedstock are varied, and research continues into new forms of renewable feedstocks. Some sources include: soybean oil, vegetable oil, used cooking oil, animal fats, and even oils produced by algae and other sources [2]. Compared with regular petro diesel, biodiesel has a higher density, lower vapor pressure, and higher heat capacity [6]. Biodiesel generally behaves similar to petro diesel in diesel combustion engines. A small difference in power or torque is noted in some engines with biodiesel decreasing this value; additionally, biodiesel can act as a solvent or cleaner in the engines hoses causing fuel filters to need replacement upon switching to biodiesel [6]. Biodiesel is prone to oxidation when stored long term due to the unsaturation of some of the FAME; this can lead to the product going rancid and commercially available biodiesel often has anti-oxidants added to address this issue [6].

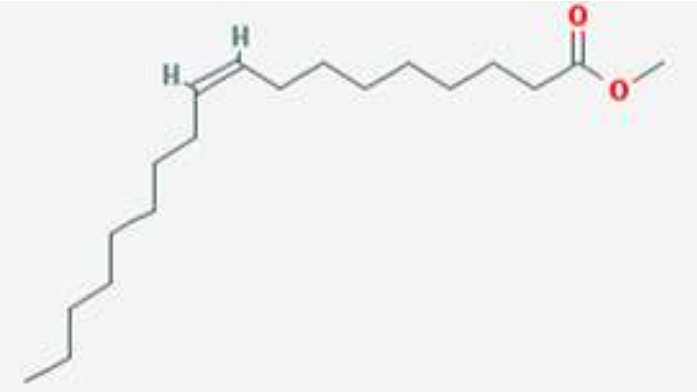

Figure 1.1 Skeletal configuration of oleic acid methyl ester, C18:1 *cis*-9. There are 18 carbons in the backbone, one unsaturation at the 9th carbon from the non-ester end group, and the molecule is bent, indicated by the "*cis*" terminology.

The most common FAMEs in biodiesel are palmitic acid methyl ester, stearic acid methyl ester, oleic acid methyl ester, linoleic acid methyl ester, and linolenic acid methyl ester; commonly oleic acid methyl ester is the most prominent [7]. FAMEs are identified by their carbon backbone chain length, level of saturation or unsaturation (double bonded carbons), the carbonyl group unique to fatty acids, and the ester end group. FAMEs are oftentimes referred to in a nomenclature which indicates the number of carbon atoms in the backbone chain, degree of unsaturation, and geometry of the double bonds [7]. For instance C18:1 *cis*-9 indicates oleic acid methyl ester with a backbone of 18 carbons, one unsaturation at the 9th carbon from the non-ester end group with a *cis* or bent shape. Figure 1.1 is a two-dimensional skeletal image of C18:1 *cis*-9, oleic acid methyl ester. The level of unsaturation in each FAME contributes greatly to the property of the biodiesel. The more unsaturated FAMEs there are, the more susceptible the biodiesel is to oxidation problems; however, unsaturation lowers the cloud point, the temperature at which biodiesel forms solid crystals [2]. Lower cloud points in biodiesels are necessary in cold weather to avoid solidification of the fuel and thus blockage of hoses and filters. Many companies change the saturation level of their biodiesel product seasonally to overcome some of these issues [2].

1.4 Raman Spectroscopy and its Application to Studying Biodiesel

Indian scientist C. V. Raman discovered a light scattering phenomenon named after him, that is, Raman scattering, in 1928. When a light strikes an object it is generally scattered or absorbed by the object. Most light that is scattered is scattered at the same frequency or wavelength of the original light stimulus, which is called Rayleigh scattering and accounts for the colors we see every day. Some of the photons, however, interact with the molecular vibrations of the object's molecules and these vibrations scatter the light at a shifted frequency from the incident light; this is the Raman scattering [8]. Figure 1.2 shows a Jablonski diagram indicating the Raman scattering. Anti-stokes Raman shifts are associated with a shift to a higher vibrational level, and a Stokes Raman shift, the most common, is associated with a shift to a lower vibrational level [9]. The Raman scattering depends on the polarizability change of the molecule and some molecular vibrations exhibit stronger Raman scattering than others.

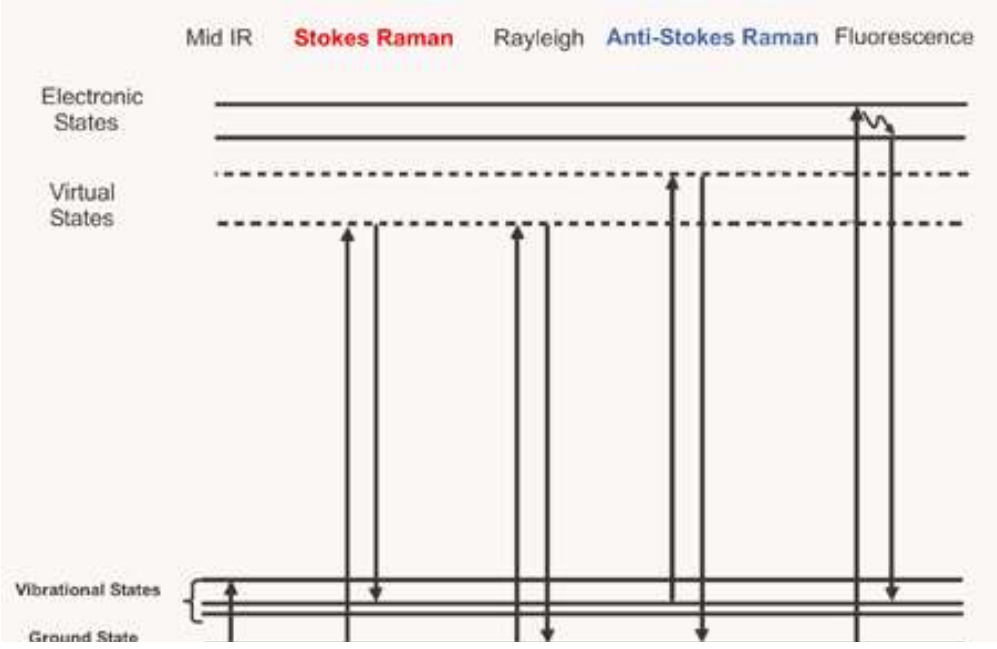

Figure 1.2 Jablonski diagram of vibrational energy states. Stokes Raman scattering is indicated by a shift to a lower energy level and is the most common. Anti-stokes indicates a shift to a higher energy level and is less common. [9]

A Raman spectrometer is the instrument that measures this shift in scattered light. The instrument uses a monochromatic laser with which to excite the sample. Once the sample is excited by the monochromatic laser source, a series of filters, mirrors, and gratings partitions out the Rayleigh scattered light and sends the remaining signal (the Raman signal) to a CCD camera detection device and computer which interprets the signal into a spectroscopy [9].

Raman spectroscopy offers some intriguing advantages. Each substance has its own "fingerprint" due to the unique molecular vibrations associated with each molecule; therefore identification of specific functional groups and molecules are attainable. Raman spectroscopy requires little laboratory preparation as the samples can be placed in the instrument without any additional perturbation. Results are immediate with only some spectral interpretation or data analysis required. Raman spectra can be obtained for samples in a liquid or solid state and even works well for biological samples as the laser power can be controlled for sensitive samples.

Raman spectroscopy does have some disadvantages. The Raman signal can be interrupted by a high background noise due to natural fluorescence of the sample. Additionally, very complex media such as colloidal systems with many components may be too complex for individual molecular vibrational analysis. Not all molecules and vibrational modes give a Raman signal and that is dependent on the polarizability change of the molecule; therefore, knowledge of the sample is useful in interpreting the results that are available. FAMEs are specific molecules and exhibit a strong Raman signal with attributes of specific functional groups. The FAMEs that make up biodiesel are not necessarily identifiable individually, but the functional groups remain present and so offer a good fingerprint region for biodiesel evaluation. Some biodiesel, like petro fuel, have additives such as dyes which may contribute to a fluorescence interruption of the Raman signal; using a longer wavelength excitation laser may resolve this

problem and this issues is explored further in the research.

Chapter 2. Literature Review

Many methods of measurement are used to characterize oil or fuel including infrared spectrometry, gas chromatography, and mass spectrometry. Raman spectroscopy also is used in the evaluation of fuel, but it is not as commonly used as some other methods. More frequently gas or liquid chromatography (GC or LC) is used due to its capability to separate individual compounds from a sample [10]. In this way, each individual fatty acid methyl ester can be separated out from a biodiesel sample and the strength of the signal achieved from each separation is correlated to the concentration in the substance. GC is commonly used with mass spectrometry (MS) to yield identified components in an otherwise unknown substance. This makes GC/MS a very useful tool for forensic study. For instance, the US Coast Guard uses GC/MS in its laboratories to match spilled oil with a suspect vessel [10]. However, GC/MS does require sample preparation that is tedious and it takes a trained professional to process and interpret the chromatograms. Additionally, the equipment to both measure and identify the components of the sample is quite extensive. Therefore, other, less expensive and faster methods are sometimes used such as vibrational spectroscopy.

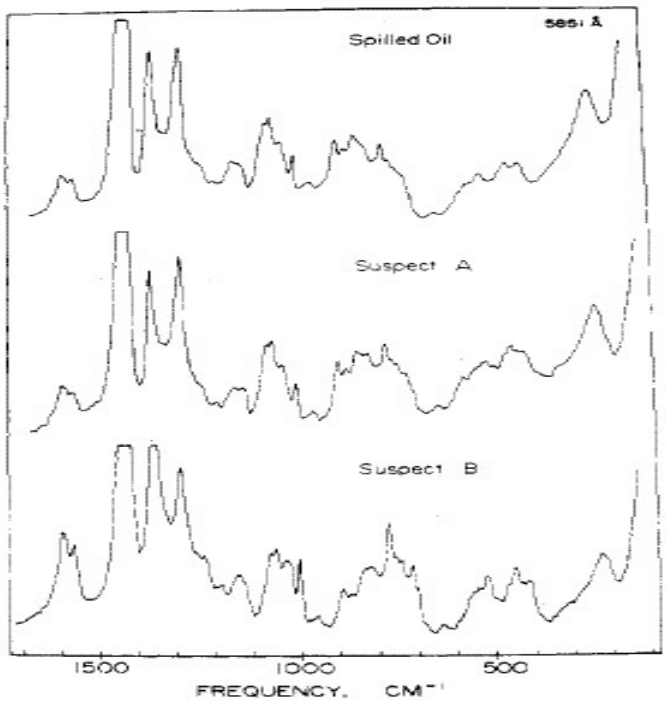

Figure 2.1 Raman spectra from 1976 of spilled petro oil vs. two potential responsible parties. The fingerprint region shown from 100-1700 cm^{-1} indicates that "Suspect A's" sample matched the spill. [11]

As early as 1976, researchers were experimenting with using Raman spectroscopy for the forensic identification of fuels. Ahmadjian and Brown looked into the use of Raman spectroscopy to identify a specific oil spill and compare it to already obtained results from the US Coast Guard [11]. They found the Raman fingerprint region offered a good opportunity to quickly and easily identify the suspected environmental criminal. Figure 2.1 is the Raman spectra from that study showing that the fingerprint region of the fuel (from 100-1700 cm^{-1} wavenumber) can indicate specific enough features to match unknown spilled oil to a suspect responsible party. The authors of this study show the ease and simplicity of Raman spectroscopy, but do suggest that multiple methods of measurement be used in forensic identification in order to build a proper legal case [11].

Even with this early research, the characteristic and identification of oils by Raman spectroscopy continued to constitute a small portion of such studies. In a 2007 article, Cleveland et al. researched the use of a portable Raman spectrometer to identify oil in the marine

environment. Those authors indicated that the use of Raman spectroscopy can be limited by natural fluorescence in the oil, making the Raman signal difficult to interpret [12]. They concurred with Ahmadjian and Brown that further evaluation is required through other measurement techniques [12]. However, the authors recognized that the hand-held Raman spectrometer used in their study was not as powerful as in laboratory instruments. Other techniques such as chemometrics and surface-enhanced Raman spectroscopy may significantly improve this task [12].

2.1 Characterization of Fatty Acid Methyl Esters (FAMEs) and Biodiesel Using Raman Spectroscopy In a 2004 study, Beattie et al. offered a comprehensive study of FAMEs using Raman spectroscopy. These authors, from Queen's University in Northern Ireland, choose to use Raman spectroscopy due to its ease; specifically no sample preparation is required and the

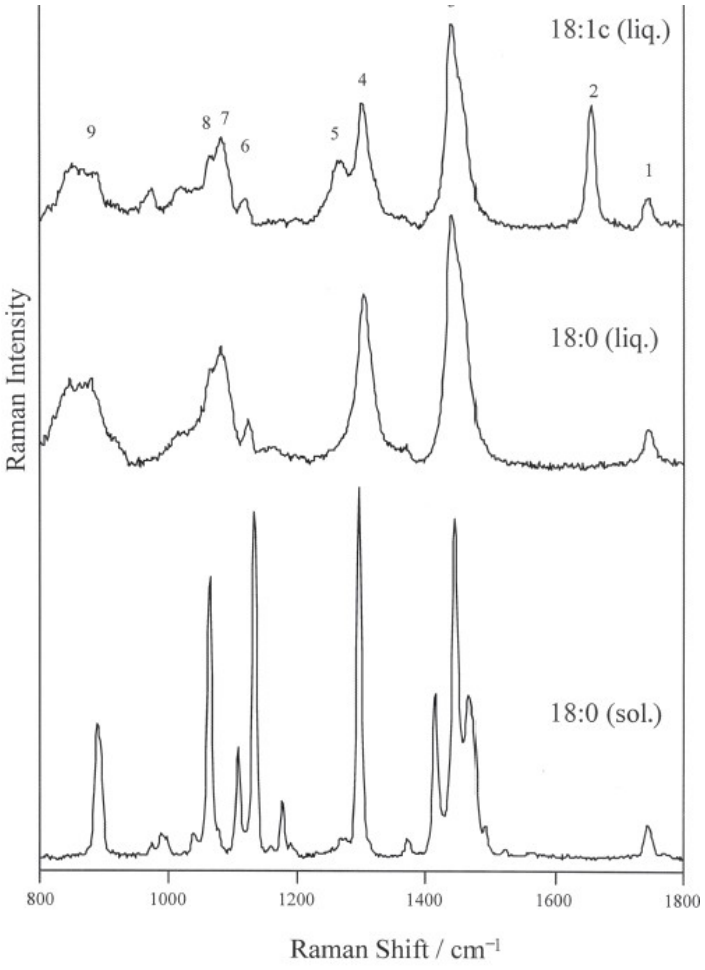

Band	Band position (cm^{-1})	Assignment
1	1730–1750	ν(C=O) Carbonyl stretch (5)
2	1640–1680	ν(C=C) Olefinic stretch (5)
3	1400–1500	$\delta(CH_2)_{sc}$ Methylene scissor deformations (5)
4	1295–1305	$\delta(CH_2)_{tw}$ Methylene twisting deformations (5)
5	1250–1280	$\delta(=CH)_{ip}$ In-plane olefinic hydrogen bend (5)
6	1100–1135	$\nu(C–C)_{ip}$ In-phase aliphatic C–C stretch all-*trans* (36)
7	1080–1110	$\nu(C–C)_{g}$ Liquid: aliphatic C–C stretch in *gauche* (39) and ν(C–C) Solid: aliphatic C–C stretch all-*trans* (38)
8	1060–1065	$\nu(C–C)_{op}$ Out-of-phase aliphatic C–C stretch all-*trans* (37)
9	800–920	$\nu(C_1–C_2)$, $CH_{3,rk}$, ν(C–O) Solid: mixture of stretches and rocks at acyl and methyl terminals. Complex broad plateau in liquid state (28)

Figure 2.2 From Beattie et al., Raman spectra of three FAMEs and the assignment of the identified peaks [13].

samples can be used in any physical state (liquid, gas, solid) [13]. The goal of the research was to determine the capabilities of using Raman spectroscopy for the evaluation of FAMEs and analyze their resultant spectra [13]. This research assigned vibrational modes to many of the common peaks associated with FAMEs, facilitating further study of them with Raman spectroscopy. Figure 2.2 shows the Raman spectra of two FAMEs and some of the peak assignments. The research also looked into the difference of solid vs. liquid states of the sample, also visible in Figure 2.2. The solid state (the bottom spectra) showed sharper peak resolution than the liquid peaks; however, the temperature range of the liquids did not greatly affect its peak resolution [13]. The identification of the vibrational modes and the further discussion regarding comparing the peak ratios of different bands adds comprehensive and strong foundation research into the identification and characterization of FAMEs using Raman spectroscopy.

Although FAMEs makeup the largest components of biodiesel, the study by Beattie et al.

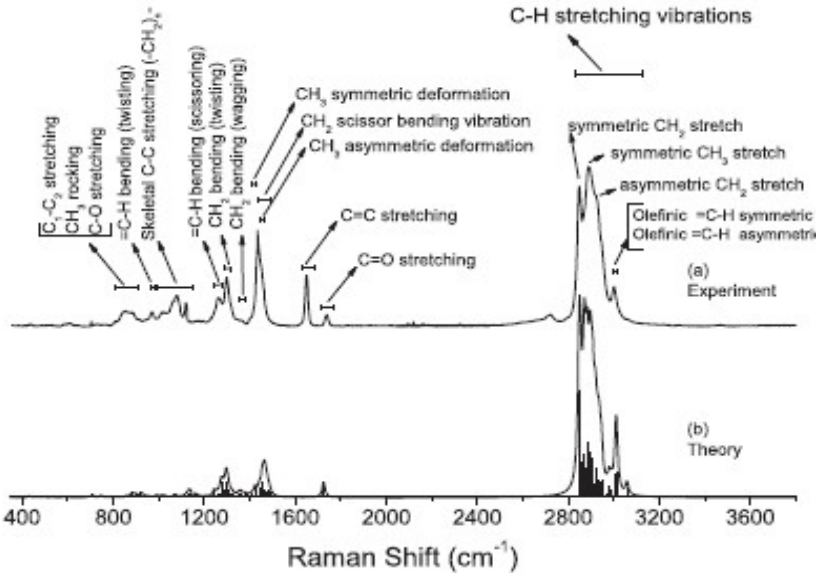

Figure 2.3 Raman spectra (top) and computer simulation (bottom) of Oleic acid methyl ester (C18:1), the most common FAME in biodiesel, discussed by Miranda et al. in their 2014 article. The specific assignment of vibrational modes to peaks offers an excellent resource for biodiesel characterization [15].

was not aimed at researching biodiesels. In 2014 a research group from Brazil, (one of the top five producers of biodiesel in the world) published a journal article that analyzed the Raman spectra specifically of biodiesel [14, 15]. This research, by Miranda et al., yielded the specific line shapes and peak analyses of the Raman spectra of the common FAMEs that make up biodiesel and also offered an equation that can be used to determine the FAME make-up of an unknown biodiesel using Raman spectroscopy [15]. Miranda et al. also compared their experimental results to modeled results using a dynamic simulation calculation, which is indicated in Figure 2.3. Figure 2.3 also very specifically points out the vibrational modes assigned to oleic acid methyl ester (C18:1), the most common FAME in biodiesel [15]. This specific assignment of vibrational modes to peaks offers a very useful resource in further identifying and characterizing FAMEs and biodiesels in general; the resultant discussion in the text of the article is also comprehensive and gives excellent information involving each area of the spectra of FAMEs that make up biodiesel.

Additionally, their work compared the Raman spectra of common FAMEs that make up

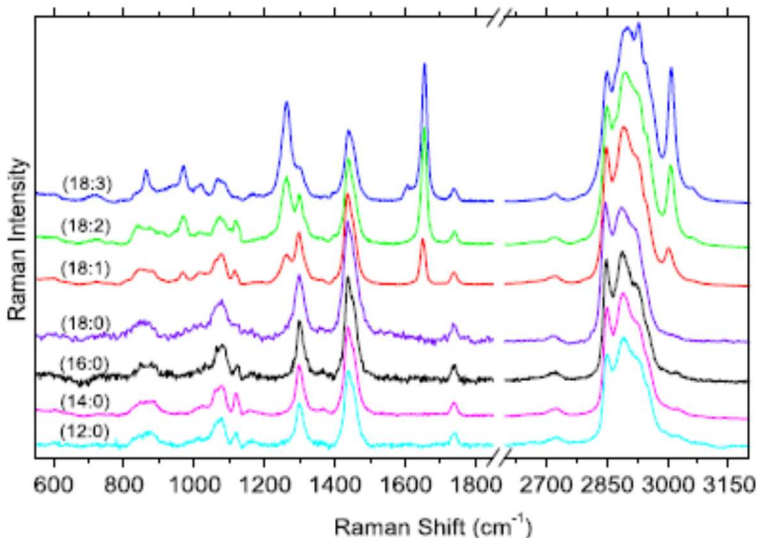

Figure 2.4 Raman spectra for some of the main esters in soybean diesel offering a comprehensive spectral analysis of the range of expected peaks to be found in commercial biodiesel [15].

biodiesel. Figure 2.4 is the Raman spectra for pure esters discussed in Miranda's research including the main esters found in soybean biodiesel [15]. Of interest is the "fingerprint region" which, for FAMEs and biodiesel, is from approximately 700 to 1900 cm^{-1}. Starting from the right to the left within the fingerprint region of Figure 2.4, the carbonyl group (the carbon double bonded to oxygen), common to esters is observed in all of the FAMEs at ~1744 cm^{-1}. Unsaturated FAMEs (having one or more double bonded carbons) have a strong peak at 1657 cm^{-1} and those are only seen in the FAMEs with the double bonded carbons (the top three in Figure 2.4: oleic acid methyl ester C18:1, linoleic acid methyl ester C18:2, and linolenic acid methyl ester C18:3) [15]. The next major peak at approximately 1440 cm^{-1} is the peak associated with CH_3 deformations and a CH_2 bend; this is common to all of the FAMEs and is also more specifically indicated in Figure 2.3 as well. The next set of peaks from approximately 1260-1320 cm^{-1} are associated with another CH_2 bend (~1303 cm^{-1}) and also the unsaturated FAMEs (top three spectra) show a second peak in this area at the lower frequency (~1268 cm^{-1}) which indicates the =CH bend (scissor) [15]. The next set of peaks to the left from approximately 1000-1130 cm^{-1} is contributed to vibrations with the skeletal carbon chain (C-C) [13, 15]. At lower frequencies, a peak to note is located in some of the FAMEs at approximately 973 cm^{-1}. This peak, noted in the top three spectra of Figure 2.4 is associated with the =CH bend (twist) but also it is associated with the conformation of the FAME molecule in either a *cis* (bent) or *trans* (straight) shape. The peak is present in the top three spectra of Figure 2.4, and in the very top spectra in Figure 2.4, because these FAMEs are in the *cis* or bent conformation [13, 15]. For comparison, Figure 2.5 shows three FAMEs common to biodiesel illustrating the *cis* and *trans* shapes.

(a) 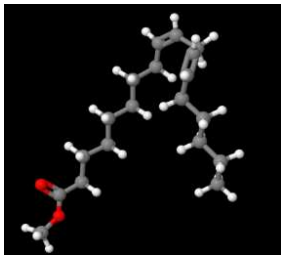 (b) 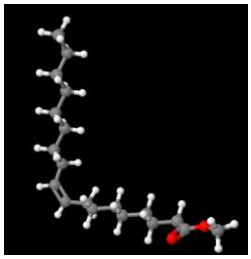 (c) 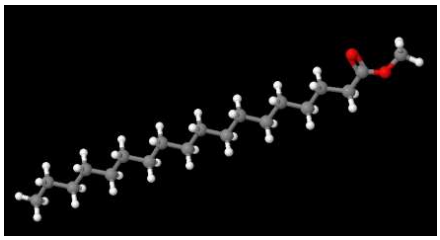

Figure 2.5 Three FAMEs common to biodiesel: (a) linoleic acid methyl ester C18:2 *cis*- 9,12, (b) oleic acid methyl ester C18:1 *cis*-9, and (c) stearic acid methyl ester C18:0, indicating the bent or *cis* ((a) and (b)), and straight or *trans* (c) conformations [43].

The last large broad peaks from 800-900 cm^{-1} are due to the FAME end group vibrations. These are associated with the C-O stretch, the CH_3 rocking, and the C_1-C_2 acyl group stretching [15, 16].

2.2 Degradation of Biodiesel in the Environment

The fate of biodiesel in the environment and its associated degradation mechanisms are fairly well documented by numerous research teams. A large amount of biodegradability research was done by the University of Idaho in the 1990s and that research is summarized in a chapter of the 2010 book "The Biodiesel Handbook" of Knothe et al. Biodegradability was measured through the CO_2 evolution method and gas chromatography. The CO_2 evolution method is the Environmental Protection Agency's recognized method for testing a chemical's biodegradability in the environment and, in general, it measures the amount of CO_2 produced during microbial degradation of the substance in question [17]. The method indicates that a CO_2 production by microbial degradation of >60% indicates a substance is "readily degradable" [17]. The biodegradability studies were conducted in both soil and aquatic environments and the authors found that all of the biodiesels tested were considered "readily biodegradable" in that after 28 days, 84% was degraded from the aqueous system and 88% was degraded from the soil system, well over the 60% required by the EPA standard [17]. The University of Idaho researchers also found that biodiesel in a blend of regular petro diesel increased the extent of the

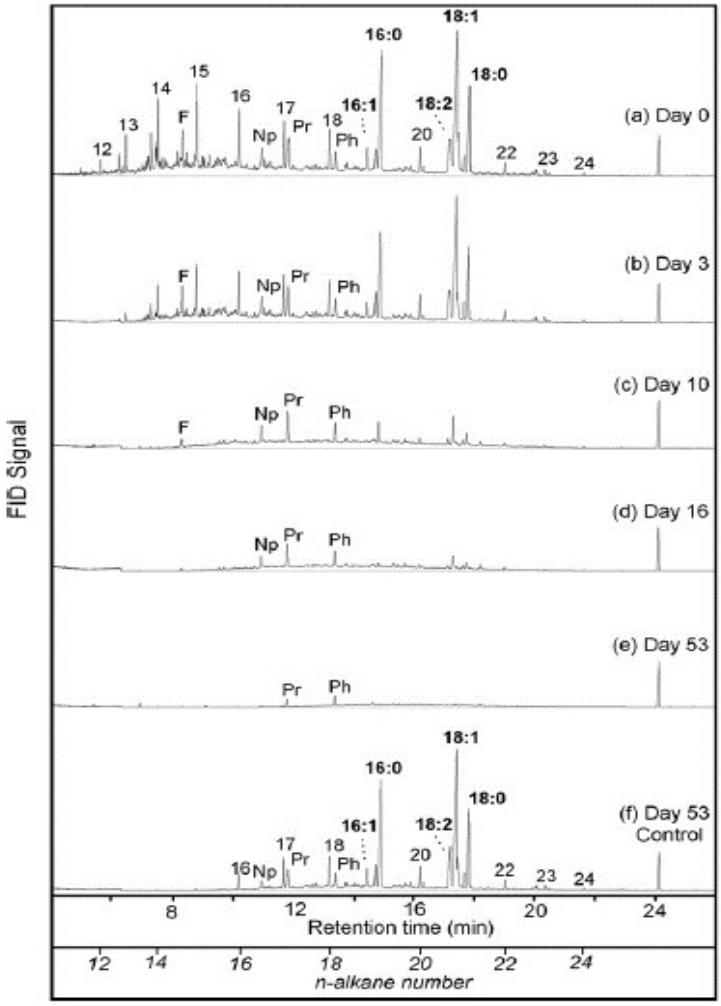

Figure 2.6 Gas chromatogram of B25 over a timeframe from (a) 0 days to (e) 53 days compared with the (f) control. The FAME peaks are annotated using the naming convention discussed in part 1. Plain numbers indicate hydrocarbon chains (alkanes) and some other components of petro diesel such as norpristane (Np) are also noted on the chromatograms [18].

blend's biodegradability, making the petro diesel degrade much faster than it would without any biodiesel [17].

More recently, research into the biodegradation of biodiesels in the marine environment became more available as researchers, environmentalists, and responsible parties became aware of the potential of biodiesel spills into the aquatic environment. An initial study in 2007, contributed by DeMello, et al. out of the Woods Hole Oceanographic Institution, offered a very good analysis of the fate of biodiesel in the marine environment measured using gas

chromatography and a lengthy experiment of over 50 days. The research compared petro diesel with petro/biodiesel blends and 100% biodiesel. They found that the FAMEs in 100% biodiesel degraded to 10% of their original mass within three weeks [18]. Additionally, the presence of FAMEs in a petro/biodiesel blend showed signs of slowing the initial degradation of the n-alkanes in petro diesel. This result was counter to those suggested by the University of Idaho and offers interesting discussion on whether adding biodiesel to a petro diesel spill could potentially act as a mitigation technique [17,18]. In the blended petro/biodiesel samples, the FAMEs degraded faster than the petro diesel components; this is apparent in Figure 2.6 which shows a blend of B25 (25% biodiesel, 75% petro) [18]. By day 10, none of the FAME peaks such as C18:1 remained in the chromatogram indicating they were broken down by microbial degradation. This study was an excellent, specific look at the breakdown of petro diesel vs. biodiesel, but the mechanisms and intermediates of the biodiesel breakdown was not within the scope of this research; likewise, the research relied on aquatic microbial degradation and did not take into account photolytic degradation as the experiment took place in a dark environment [18].

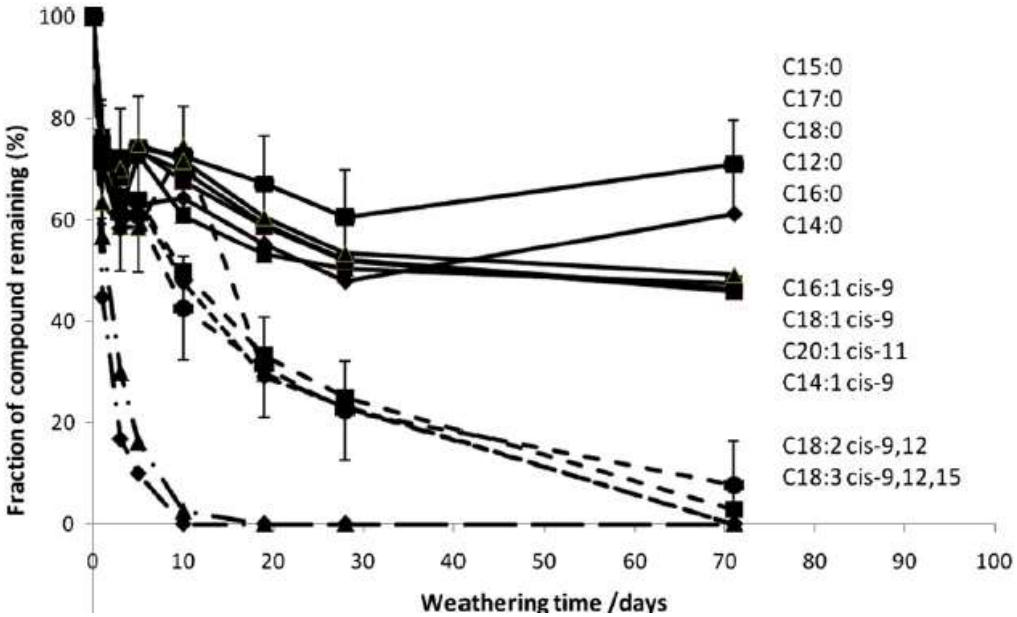

Figure 2.7 Biodiesel weathering results of 71 day exposure to sun and seawater using total ion chromatograms (TICs) of selected components of biodiesel. The solid lines indicate saturated FAMEs; the middle dashed lines are FAMEs with one unsaturation; the lower two dash-dot lines indicate FAMEs with more than one unsaturation. The components are listed in order of stability from most stable (top) to least stable (bottom). [7]

In an effort to more accurately describe the weathering and degradation process of biodiesel in the marine environment, a research group from Australia conducted an experiment of over 70 days in 2011. This group mixed approximately 2.5% biodiesel with seawater in beakers, covered the beakers with a “watch glass” and placed the beakers on the roof of a 12-story building in Sydney and allowed the samples to sit there for 71 days [7]. Samples were

taken periodically through this long weathering experiment and evaluated using gas chromatography. Figure 2.7 summarizes a great deal of results gained from this experiment. It is apparent that the saturated FAMEs were more stable that unsaturated FAMEs; that is, the unsaturated FAMEs degraded quickly with linoleic and linolenic acid methyl esters being undetectable after 10 days of weathering [7]. Additionally Khoury et al. found that FAMEs with the *cis* conformation were more susceptible to degradation due to "oxidation from the unprotected side" [7]. Additionally Khoury et al., separately looked at a neat biodiesel sample in sunlight versus a biodiesel sample in seawater placed in the dark in order to make conclusions about the speed of photolytic versus biological degradation. Figure 2.8 indicates the findings of Khoury et al. in comparing photolytic and biodegradation for 10 days. Their results show that photolytic degradation occurred faster than biodegradation and, similar to the larger weathering experiment, unsaturated components broke down faster under sunlight conditions than saturated components [7]. Overall, in the biodiesel studied, the FAMEs broke down by biodegradation and unsaturated molecules broke down quickly under photolytic conditions [7]. After 71 days remaining FAMEs were saturated FAMEs with between 60-80% of those particular components remaining in the samples [7]. Noting that most biodiesels are made up of >70% unsaturated

FAMEs, this research indicated that most of the biodiesel was degraded over the period studied [7].

Noting the observations of Khoury et al. regarding the faster photolytic degradation of biodiesels, a research groups working from both China and Canada sought specifically to study the photolytic degradation of biodiesel and its blends. This study used total organic carbon (TOC) to measure the breakdown of the commercial biodiesel [19]. In this research, TOC removal rates were a fast and easy method to show the speed of degradation, but it does not indicate intermediates or any information about what portions of the FAMEs were degraded (e.g. unsaturated components, etc.). Yang et al. first found that the degradation rate of biodiesels did not depend greatly on the biodiesel source; biodiesel from soy degraded relative to biodiesel made from canola [19]. Secondly, they found that the concentration of biodiesel ranging from approximately 30 to 150 parts per million (ppm) degraded at a similar rate although the higher concentration initially degraded somewhat slower than the lower concentrations; after 2 hours all concentrations degraded at approximately the same rate [19]. Third, they showed that biodiesel in water with humic acid had a slightly slower degradation rate than ultra-pure water and overall the more complex the water, the slower the degradation. This is illustrated in Figure 2.9 and the

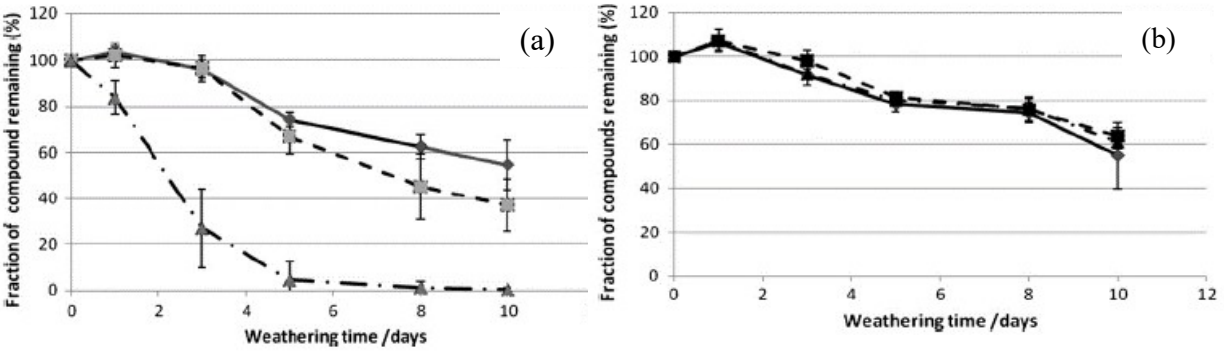

Figure 2.8 Photolytic (a) versus biodegradation (b) of a commercial biodiesel subject to weathering for 10 days. The solid lines are saturated compounds, dashed lines are compounds with one double bond, and the dash-dot lines are compounds with multiple double bonds. [7]

authors contributed this to the other chemicals or substances in the water medium that may absorb some of the UV light [19]. The humic acid was chosen to mimic natural organic matter and the pyrogallic acid was used to mimic synthetic antioxidants [19]. Of interest in this study is the speed at which the biodiesel degraded. This study used a very strong UV light, reportedly at 33.7 mW/cm^2 though the wavelength of the UV light was not indicated. The solar constant, which is the solar irradiance outside the atmosphere at the Earth's mean distance from the sun, is 137 mW/ cm^2 [20]. Of that irradiance, approximately 9% is UV (12.33 mW/cm^2). The UV lamp used in Yang et al.'s research is close to 3 times that value and although it is difficult to compare a monochromatic UV lamp to a UV spectrum of sunlight, it is apparent that the lamp used in this research was very strong. In comparing Figures 2.8 and 2.9 it may seem like the research is contradicting. In Figure 2.8 Khoury et al. found that the C18:1 FAMEs (the dashed line) took almost 10 days to degrade approximately 60% of that component, where in Figure 2.9 Yang et al. show that after 3 hours their samples had degraded to 60%. Though they research similar topics, it remains difficult to compare these results. Khoury et al. used pure biodiesel where Yang et al.'s is diluted in water. Further, Khoury et al., assumedly placed their samples in physical sunlight in the winter of Sydney, Australia whereas Yang et al. used a very strong artificial UV source. Lastly, the degradation was measured differently (total ion chromatograms using GC vs. total organic carbon removal). Both results indicate that photolytic degradation is a significant contributor to the overall degradation of biodiesels in the environment and recommend further study into the mechanism of this degradation.

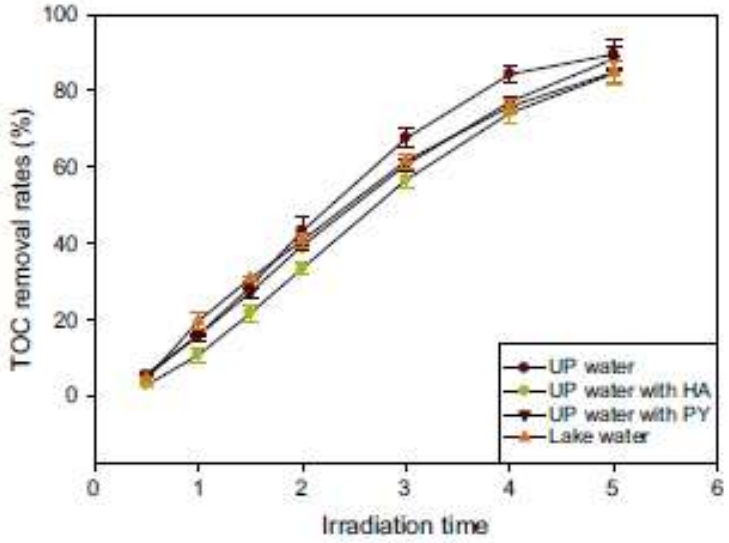

Figure 2.9 TOC removal rates of biodiesel in different water matrices under UV exposure. UP is ultra-pure, HA is humic acid, PY is pyrogallic acid. The HA and PY were used to mimic natural organic matter and a synthetic antioxidant [19].

2.3 Studies of Biodiesel Toxicity on the Aquatic Environment

Upon establishing that biodiesel does degrade in the environment, it now is important to understand whether this material and its degradation cause harm. Bluhm et al. wrote a comprehensive review of toxicological studies of biodiesel in 2012. They concluded that there are some contrasting results; however, studies on the toxicity of biodiesel remain difficult to compare due to the different testing mechanisms used [21]. Overall, they concluded that biodiesel is less toxic than regular petro diesel to aquatic organisms. However, the oil film on the surface of the water is a source of mortality for some organisms that is not accounted for through traditional toxicological measurements and should be taken into account when discussing biodiesel mortality to aquatic organisms [21].

Almost anything in excess can be toxic, but the level of toxicity depends on dosage and exposure. In a 2007 study, the 24-hour LC-50 on a freshwater fly population was found to be 4.65 ppm (compared to petro diesel's 1.78 ppm) [22]. LC-50 is a toxicological term used to indicate the point at which 50% of the studied population perishes. The same study found the

LC-50 value for juvenile trout was 1074 ppm for biodiesel (578 for petro diesel) [22]. These authors also discussed that some of the insect population became mired in the surface film of oil, causing mortality. The LC-50 value for the insect population is fairly low. Considering that the "safe" limit of regular petro oil allowed to be discharged into the sea is 15 ppm, an LC-50 for biodiesel of 4.7 ppm is fairly low. However, this study looked at two freshwater (e.g. lakes and streams) organisms with exposure to biodiesel fairly static and over a specific time. Biodiesel exposed to the marine environment from a ship's residual washing would be transported by physical oceanographic phenomena fairly quickly so a direct comparison is difficult.

In 2011, a research group from Brazil conducted a study of the toxicity of the water soluble fractions (WSFs) of biodiesels. That group used sea urchin larvae and microalgae. These saltwater species are more common across oceanic environments [23]. In using WSFs, the study uses a method developed by the US Environmental Protection Agency to obtain the WSFs from the original sample (in this case biodiesels from various feedstocks). Therefore, the organism is not directly exposed to the biodiesel per say, but to its water soluble fractions; in this case Leite et al. discuss that the most toxic WSF is methanol, which is formed by the reverse of the transesterification process due to hydrolysis with seawater [23]. In that research, the authors found that in as little as 4% concentration of the WSFs of one of the biodiesels, half of the sea urchin population showed negative effects, which in this research was abnormal offspring (this test is called EC-50) [23]. The microalgae fared stronger in that an almost 50% concentration of the WSFs showed negative effects on 50% of the population (this test was called IC-50) [23].

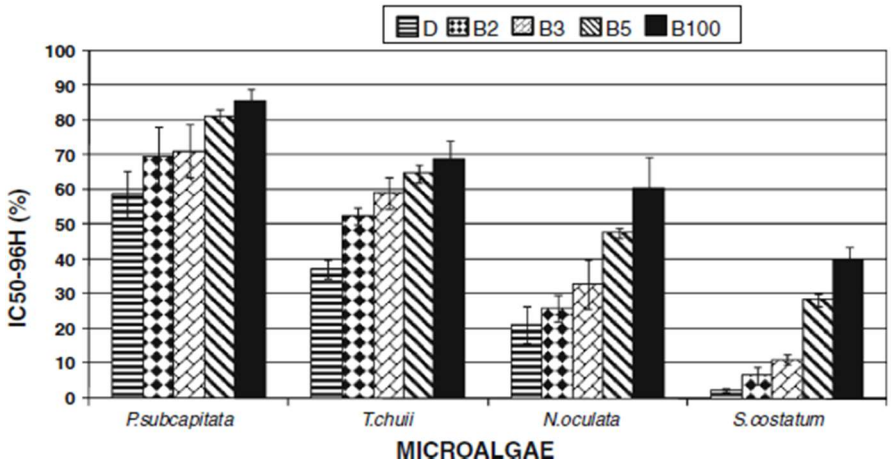

Figure 2.10 Toxicity results of biodiesel (B100), petro diesel (D) and blends of petro/biodiesel (B2, B3, & B5) on fresh and saltwater algae species. A high IC-50 value indicates that it took larger concentrations of the studied material to produce a 50% negative impact on the population (i.e. the smaller the IC-50 values, the greater the toxicity). [24]

Through GC, the authors found that over time (up to 120 days), methanol was the most abundant toxin found in the water soluble fractions over this storage or incubation time [23]. In this research, the sea urchin population was exposed to the biodiesel WSFs in a vial and left for 36 hours. It is not specified whether the vials were open to the environment or to any light source. Both exposure to air and exposure to a light source (especially sun or UV-light) may have caused the methanol to evaporate. Contrarily, if the vials were closed as is implied by the study, the methanol would not have an opportunity to evaporate, making the EC-50 values skewed to be lower (i.e. making the toxicity higher). The microalgae studied specifically were left in an open flask under continuous fluorescent illumination so that it could grow [23]. In this situation, methanol, the noted prominent contaminant from biodiesel, may have evaporated thence making the IC-50 values higher (or the toxicity of the biodiesel trend lower). Understandably, to determine the toxicity of a substance, variables such as evaporation must be controlled to indicate valid results. However in the natural environment, exposure to air and light would be available to a biodiesel spill and therefore, this must be taken into account when considering these results.

In a similar study, Brazilian researchers looked at the toxicity to fresh and saltwater algae to pure biodiesel compared with petro diesel and blends of petro/biodiesel. This research found that petro diesel was significantly more toxic to the microalgae than B100 as indicated in Figure 2.10 [24]. This study also concluded that even though B5 had the largest amount of methanol in it compared to the other biodiesel blends (B2 and B3), it was the lest toxic of the blends, indicating that the methanol present in the water soluble fractions did not "synergistically increase the toxic effects of the biodiesel" in the organisms studied [24]. Interestingly, Figure 2.10 shows that the freshwater algae species (*p. subcapitata*) showed the least sensitivity to all the fuels studied whereas the three saltwater algae species showed more sensitivity. This phenomenon could be due to the face that more methanol will degrade from the biodiesel faster into seawater than in freshwater [25]. Still, the most sensitive saltwater species, *s. costatum*, withstood biodiesel WSFs concentration of up to 40% before it reached the level at which half of the organisms were found to be negatively impacted (in this study the impact was chosen to be growth inhibition) [24]. Though 40% is 400,000 ppm – a high value - it is difficult to directly relate this to concentrations of direct biodiesel spill into the environment because the study used water soluble fractions of the biodiesel and not direct biodiesel exposure.

2.4 Conclusions

The most common form of instrumental evaluation of biodiesel and fuel, in general, is gas chromatography due to its specificity and extensive use in environmental forensics. However, the use of Raman spectroscopy to characterize fuels including biodiesels is increasing. Beattie et al., offered an excellent review of the use of Raman spectroscopy to characterize FAMEs, the building blocks of biodiesel. Their research identified functional groups, discussed the use of an internal standard, and compared temperature and phase differences in the Raman

spectra of many of the FAMEs that are the most common to biodiesel [13]. Miranda et al., published recent results that identified the line shape of the Raman spectra of biodiesels and the FAMEs common to them. Their results identified specific functional groups of the common FAMEs and discussed a mathematical method to identify an unknown biodiesel's FAME composition. It also showed some specific differences between the common FAMEs of biodiesel including the conformational differences [15].

The degradation of biodiesel, specifically in the marine environment, is becoming a research topic of more interest as biodiesel production and transport increases. Biodiesel is generally considered "biodegradable" and touted as one of the main reasons to switch from petro diesel. DeMello et al., offered an early study looking at the biodegradation of biodiesel and its blends through microorganism activity. That study showed that biodiesels degraded faster than petro diesel and that after 3 weeks the FAME constituents of biodiesel were 90% degraded [18]. Another study by Khoury et al. was conducted in 2011 by placing samples of biodiesel in seawater on the roof of a building in Australia and monitoring the degradation results for over 70 days. This study found that photo-oxidation was the strongest degradation method for unsaturated FAMEs whereas the saturated FAMEs were the most persistent [7]. After 20 days, 60% of oleic acid methyl ester (the most common FAME in biodiesel) had degraded [7]. A further study by Yang et al., looked specifically at the photo degradation of biodiesels using a very strong UV-lamp. That study found that under a UV lamp of an irradiance of 33.7 mW/cm^2, the samples had degraded to 60% within 3 hours, a significantly faster process than the Khoury experiment, likely due to the strength of the UV-lamp [19]. These studies indicate that biodiesel is degradable over time. Exposure to sunlight increases the degradation, especially of unsaturated components of biodiesel. Taking into account that oleic acid methyl ester (an unsaturated

FAME) makes up >70% of most biodiesel products, this shows that the stronger the exposure to sun, the faster the biodiesel will degrade [7, 19].

Finally the toxicity of biodiesel was reviewed. The University of Idaho studies in the 1990's conclude that biodiesel is significantly less toxic than petro diesel [17]. Biodiesel was toxic however, especially in freshwater insect populations, and to a lesser degree to juvenile trout [22]. Further studies from Brazilian researchers used water soluble fractions to measure toxicity of biodiesels in sea urchins and various microalgae. The sea urchins did show signs of distress when exposed to the biodiesel WSFs in concentrations as low as 4% [23]. The microalgae fared better, showing resistance to toxicity to fairly high WSF concentrations (>40%) [23, 24]. Importantly, these studies indicate that the most common and most toxic WSF of biodiesel is methanol that is formed through the reverse of transesterification by hydrolysis [23]. Though methanol was noted in larger amounts of biodiesel/petro blends, it still found not to be a contributing toxin in the biofuel/petro blends (i.e. petro diesel was less toxic with biodiesel blended into it even with the increase of methanol) [23]. Further study on the toxicity of biodiesel is necessary as there are different methods of measuring toxicity and not all research compares these measurements with predicted actual results in a complex biological ecosystem. In conclusion, though biodiesel is considered "readily biodegradable," a large influx of this product into a marine environment (e.g. in a large spill), could cause toxicity to some aquatic organisms, especially to those that may be mired in the upper layers of the oil/water interface.

Chapter 3. FAME Characterization and Evaluation Using Raman Spectroscopy

3.1 Methods and Procedures

Materials. In order to characterize biodiesel, the main FAMEs in biodiesel were identified and purchased for analysis. The research of Khoury et al. showed the FAME breakdown of four separate commercial biodiesel samples, shown in Table 3.1. From that, the five main FAMEs were identified as palmitic acid methyl ester (C16:0), stearic acid methyl ester (C18), oleic acid methyl ester (C18:1 *cis*-9), linoleic acid methyl ester (C18:2 *cis*-9,12), and linolenic acid methyl ester (C18:3 *cis*-9,12,15) [7].These five FAMEs were purchased from Sigma-Aldrich, USA, ≥98.5% purity. When not in use, the FAMEs were stored as indicated by the manufacturer.

Instrument. The Raman spectrometer is a Renishaw inVia Raman Spectrometer with a Leica microscope (10x, 50x, and 100x objectives). Both a 514 nm (1800 l/mm grating, 150 mW Ar-ion) and 785 nm (1200 l/mm grating, 300 mW, diode) laser was used. The Renishaw Wire™ 2.0 software was used to document the initial spectra obtained. The Raman spectra were optimized using a 20 second exposure time with 3 accumulations. The laser power for the solid

Table 3.1 Mass fractions (%) of FAMEs detected using chromatography in four pure biodiesels used in a study by Khoury et al. [7]

Compound	Abbreviation	Oil 1	Oil 2	Oil 3	Oil 4
Lauric acid methyl ester	C12:0	0.03 (0.02)	0.06 (0.01)	0.03 (0.01)	0.01 (0.01)
Myristic acid methyl ester	C14:0	0.8 (0.1)	0.7 (0.1)	0.3 (0.0)	0.02 (0.01)
Myristoleic acid methyl ester	C14:1 *cis*-9	0.2 (0.0)	0.1 (0.0)	ND	ND
Pentadecanoic acid methyl ester	C15:0	0.1 (0.0)	0.1 (0.0)	ND	ND
Palmitic acid methyl ester	C16:0	10.4 (1.1)	9.2 (1.0)	8.8 (0.9)	1.4 (0.1)
Palmitoleic acid methyl ester	C16:1 *cis*-9	1.4 (0.2)	1.3 (0.1)	1.0 (0.1)	0.09 (0.01)
Heptadecanoic acid methyl ester	C17:0	0.41 (0.05)	0.40 (0.05)	0.14 (0.02)	0.09 (0.01)
cis-10-heptadecenoic acid methyl ester	C17:1 *cis*-10	0.5 (0.1)	0.36 (0.04)	0.11 (0.02)	0.04 (0.01)
Stearic acid methyl ester	C18:0	7.5 (0.8)	8.8 (0.9)	2.9 (0.3)	0.9 (0.1)
Oleic acid methyl ester	C18:1 *cis*-9	66.7 (6.9)	70.3 (7.3)	67.4 (7.0)	81.7 (8.5)
Elaidic acid methyl ester	C18:1 *trans*-9	0.89 (0.10)	0.18 (0.03)	ND	ND
Linoleic acid methyl ester	C18:2 *cis*-9,12	10.2 (1.1)	6.9 (0.7)	18.1 (1.9)	10.9 (1.1)
Linolenic acid methyl ester	C18:3 *cis*-9,12,15	0.8 (0.1)	1.3 (0.1)	1.0 (0.1)	4.1 (0.4)
γ-Linolenic acid methyl ester	C18:3 *cis*-6,9,12	ND	ND	ND	0.22 (0.03)
cis-11-eicosenoic acid methyl ester	C20:1 *cis*-11	ND	0.22 (0.03)	0.24 (0.03)	0.58 (0.06)
Behenic acid methyl ester	C22:0	ND	ND	0.1 (0.0)	ND

samples is noted on their results and the laser power for the liquid samples was 100%.

Data analysis. Data analysis was completed with the WIRE 2.0 software and Microsoft Excel. Normalization was applied to the spectra in order to compare different laser powers and to compare solid and liquid samples. The standard normal variate normalization technique was used to normalize the spectra. This is a weighted normalization technique that accounts for the effects of sample differences and scales the spectra so that they can be compared [26]. It is a good tool for spectra that are expected to be similar from measurement to

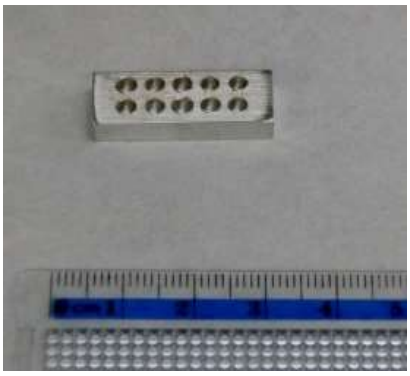

Figure 3.1 Aluminum sample holder used for FAME and biodiesel Raman spectroscopical analysis.

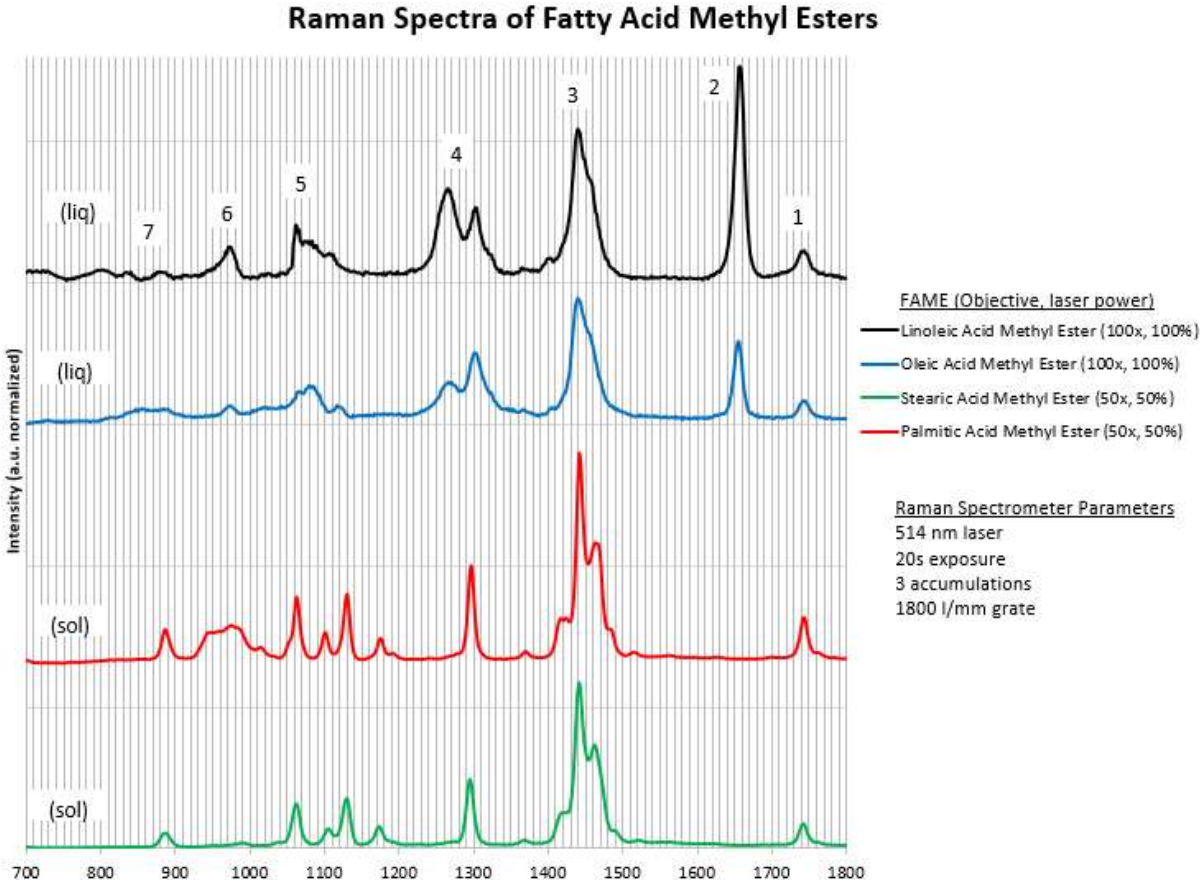

Figure 3.2 Raman spectra of four common FAMEs found in biodiesel. The numbered peaks are discussed in more detail in the text.

measurement [26].

Methods. The liquid samples (oleic, linoleic, and linolenic acid methyl esters) were placed in an aluminum sample holder, shown in Figure 3.1, which contained 10 cylindrical shaped openings. Each opening was 2 mm wide by 5 mm deep making the volume of each sampling port approximately 15 μL. Each FAME was placed into the sampler using a micropipette. The two solid samples (palmitic and stearic acid methyl esters) were placed on a clean flat silicon wafer and measured directly in the solid state.

3.2 Results and Discussion

3.2.1 Sample Phase Differences

The Raman spectra of four of the FAMEs are displayed in Figure 3.2. It is first apparent that the liquid samples (the two top spectra) have less defined peaks than the two solid samples. In fact Miranda et al., also discussed that the liquid samples had broader and mixed bands than the solid samples. This is likely due to the increased molecular movement (or lack thereof) in the liquid versus solid samples [15].

3.2.2 Identification of Vibrational Modes

Peak group "1", carbonyl stretch. The peak labeled "1" is the carbonyl stretch at approximately 1744 cm^{-1}. This peak is apparent on all of the FAMEs and is one characteristic that will be the same in any FAME studied. Due to this, it makes a good internal standard for comparing different FAMEs and could be used for normalization if studying multiple FAMEs. However, carbon chain length can cause a frequency shift in the carbonyl peak noticeable over a large range of chain lengths [13]. This is illustrated by Beattie et al. in Figure 3.3. Though this frequency shift could be a reason not to use the carbonyl group as in internal standard, it is only relevant over larger carbon chain length differences [13]. As Table 3.1 indicates, most biodiesels

are made up of a core group of FAMEs ranging from carbon chains of 12-22, with the 16-18 chain lengths making up the most predominant portion of biodiesels; therefore if an internal standard is used to study the FAMEs that make up biodiesel, the C=O stretch remains a good candidate [7, 13]. The carbonyl band can also be affected by the unsaturated C=C stretch, discussed individually in more detail in the next section. Similar to carbon chain length, large amounts of unsaturation can cause greater changes in the C=O peak [13]. However, again noting Table 3.1, most biodiesels are made up of one to three carbon double bonds and this is unlikely to affect the C=O peak significantly.

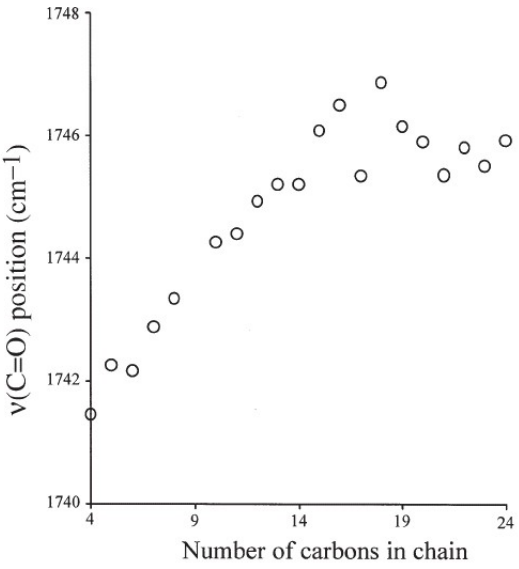

Figure 3.3 From Beattie et al., the frequency shift of the carbonyl peak due to carbon chain length. [13]

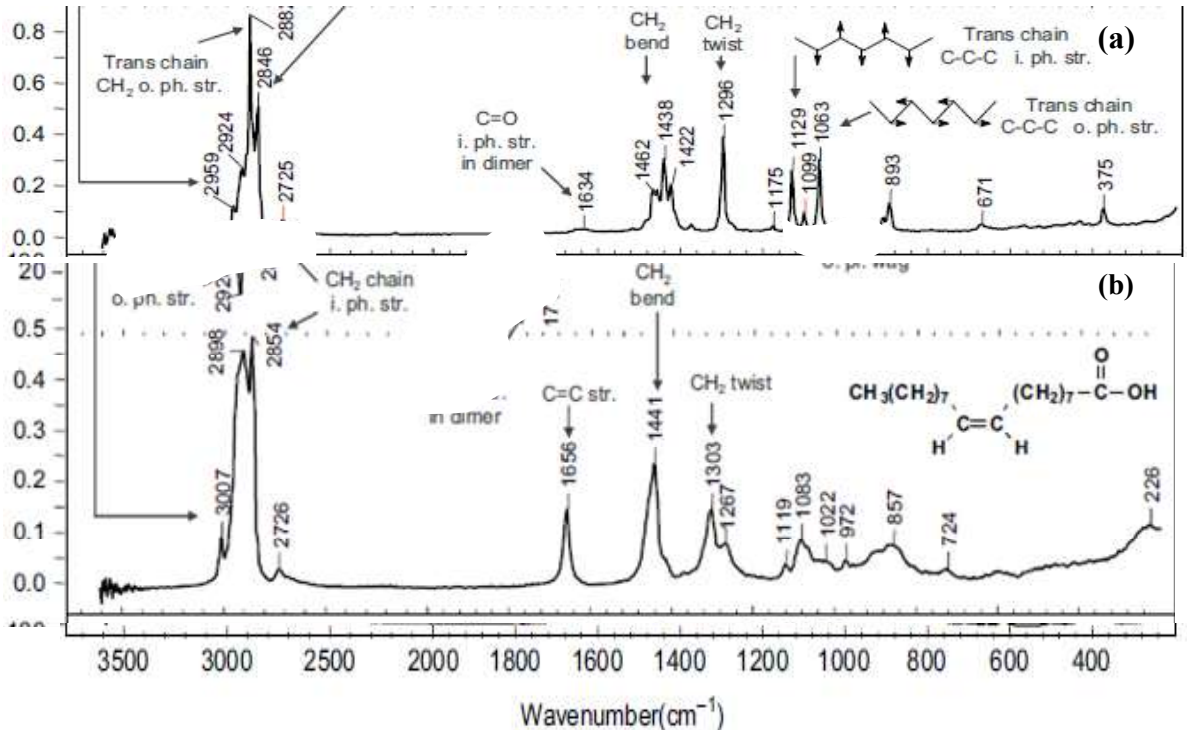

Figure 3.4 Raman spectra of free fatty acids, (a) palmitic acid and (b) oleic acid). The C=O stretch is weak in (a) and indiscernible in (b) due to it coinciding with the unsaturated C=C stretch. [28]

It is useful to note that the carbonyl stretch is not necessarily unique to fatty acid methyl esters. Free fatty acids (FFAs) also have a carbonyl group. However, the peak of the carbonyl group in the FFAs is weakened and shifted to a lower frequency due to the difference in the functional group on the ends of the fatty acid chain. Therefore the C=O stretch is either almost undetectable in saturated FFAs, or it coincides with the C=C unsaturated stretch and is therefore masked [27]. This is illustrated in Figure 3.4 which shows the Raman spectra of palmitic acid (top) and oleic acid (bottom) [28]. Since palmitic acid has no unsaturation, the C=O is noted as a weak peak around 1634 cm^{-1}. In the oleic acid, the C=O peak is indiscernible due to the strength of the C=C vibration at 1656 cm^{-1}.

Peak group "2", C=C stretch (unsaturation). Both linoleic and oleic acid methyl esters exhibit a peak around 1657 cm^{-1} in Figure 3.2. This peak is associated with the unsaturated C=C

stretch [13]. It is clear that linoleic acid methyl ester has greater peak intensity than oleic acid methyl ester. This is due to the fact that linoleic acid methyl ester had two C=C bonds to oleic acid methyl ester's one. Clearly the palmitic and stearic acid methyl esters have no peak in this region because these are saturated FAMEs.

Peak group "3", CH_2 bend and CH_3 symmetry. It is clear from studying the solid FAMEs in Figure 3.2 (stearic and palmitic acid methyl esters), that there are 3 peaks in this area of the spectra. These three peaks morph into one large somewhat crooked peak in the liquid FAMEs' (oleic and linoleic acid methyl esters) spectra due to spectral differences between liquid and solid phases. The first peak in the solids, noticeable around 1464 cm^{-1} is due to the CH_3 asymmetric deformation illustrated in Figure 3.5 (a) [15]. The second peak in the solids, and the clear, broad peak in the liquids, around 1443 cm^{-1} is due to the CH_2 scissor bend (meaning a change in the angle between two bonds), shown in Figure 3.5 (c) [15, 28]. This is a strong intensity band due to the large number of CH_2 groups that exist in these FAMEs (due to the carbon chain length). The last peak in this group, clear in the solid FAMEs around 1422 cm^{-1} is due to the CH_3 symmetric stretch, illustrated in Figure 3.5 (b) [15].

Peak group "4", CH_2 bend and olefinic bend. The first peak in this group around 1303 cm^{-1} is visible in all the FAMEs and is due to the CH_2 twist bend, a bend indicating a change in

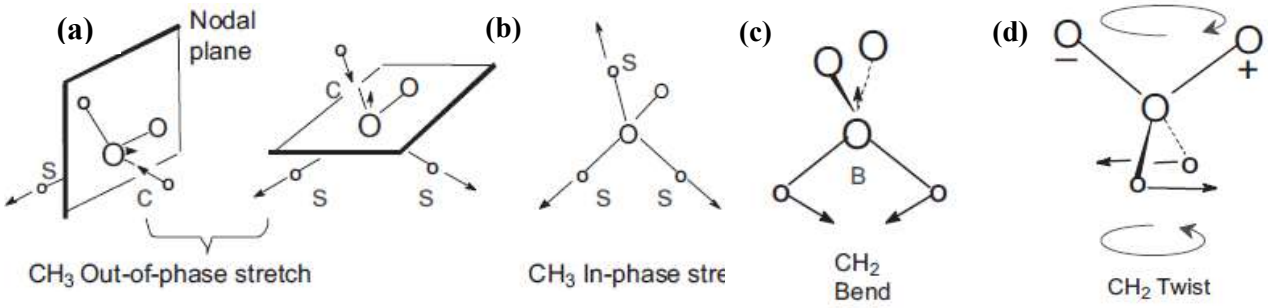

Figure 3.5 Illustration of: CH_3 symmetry vibrational modes (a) antisymmetric, (b) symmetric, (c) the CH_2 bend (scissor) mode and (d) the CH_2 bend (twist). C and S stand for contract and stretch. B and O stand for bend and open. [28]

angle between planes of two groups of atoms [13]. Similar to the scissor bend, it is a strong peak due to the large number of CH_2 groups that exist in these FAMEs and the motion is depicted in Figure 3.5(d) [28]. The second peak in this group is only visible in the unsaturated FAMEs because the vibration has to do with the unsaturation; it is the =CH scissor bend around 1267cm^{-1} [13]. Again this peak shows a higher intensity in the linoleic acid methyl ester because it has two double bonded carbon groups.

Peak group "5", carbon backbone vibrations. The peaks from approximately 1065-1180 cm^{-1} are all assigned to the main carbon chain stretching modes. The saturated FAMEs exhibit a peak around 1176 cm^{-1} that does not occur in the unsaturated FAMEs. This peak is likely attributable to the carbon backbone stretching in the *trans* conformation of the two saturated FAMEs [28]. Further broad bands are visible in the two liquid samples, and the sharper peaks visible in the solid samples from 1030-1130 cm^{-1} are characteristic of the carbon backbone in (symmetric) and out of phase (antisymmetric) stretching in both the *cis* and *trans* formations of the FAMEs [13]. Figure 3.6 (a)-(b) shows the carbon chain backbone movement of the *trans* conformations.

Peak group "6", =CH twist bend, cis-conformation. A peak especially noticeable in the oleic and linoleic acid methyl esters occurs around 975 cm^{-1} and is associated with the =CH twist

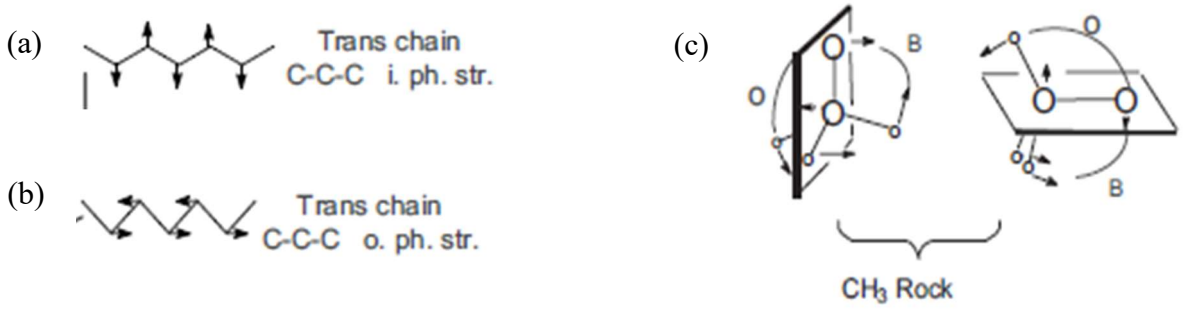

Figure 3.6 Carbon backbone (a) in phase (symmetric), (b) out of phase (anti-symmetric) stretches in the *trans* conformation, and (c) the CH_3 rock; B stands for "bend" and O stands for "open". [28]

bend [15]. This is a vibration that is made stronger due to the *cis* formation of these two FAMEs. The bend-twist vibration occurs when there is change to the angle between configurations of two groups of atoms and so this peak is more apparent in the top two FAMEs of Figure 3.2 [28]. There is a broad peak in the solid palmitic acid methyl ester in this region. This is not due to the =CH bend as there is no double bond in that FAME; the broad peak in that location is likely due to the end group vibrations discussed in the next section.

Peak group "7", end group vibrations. At the lower frequency of this studied fingerprint region, there are broad peaks that are indicative of the end groups of the FAMEs. These vibrations include the C_1-C_2 acyl stretch, the C-O stretch, and the CH_3 rock [13]. The C_1-C_2 acyl group is proposed to be apparent at 890 cm^{-1} [29]. However the literature on this is contradictory with some indicating that this vibration can move depending on the chain length [30]. The CH_3 rock, depicted in Figure 3.6 (c), and C-O stretch are also located in this region, which makes them difficult to individually identify.

3.2.3 Spectral Analysis of FAME Mix

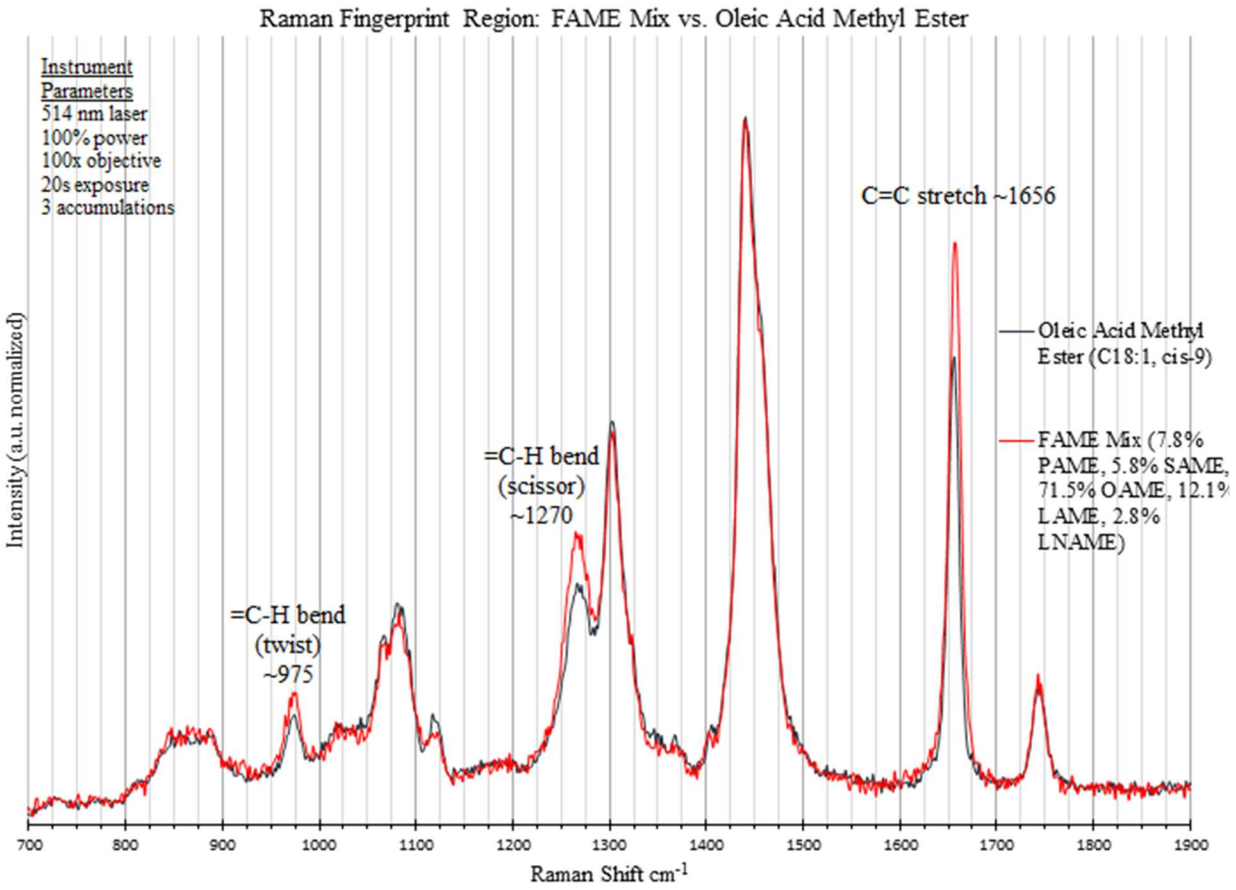

Figure 3.7 Raman spectra of lab-made FAME mix (red) and its main component, oleic acid methyl ester (black). The major differences in the C=C and =CH bends are noted in their respective locations on the spectra.

Biodiesel is a mix of numerous different FAMEs and so the Raman spectrum of biodiesel will be unique compared with any single FAME. In order to study commercial biofuels, a laboratory made replica using a FAME mix was made. The percentages of the FAMEs used were taken from the GC analysis of Khoury et al. of four commercial biodiesels show in Table 3.1. The percentage breakdown of the lab-made FAME mix is indicated in Table 3.2. Figure 3.7 shows the Raman spectra of the lab-made FAME mix compared to its main component, oleic acid methyl ester. Some immediate differences are apparent and those are noted on the spectra in Figure 3.7. First, the peak at 1656 cm^{-1} that indicates the C=C stretch is of a higher intensity in the FAME Mix than in pure oleic acid methyl ester. This is due to the fact that the FAME mix

Table 3.2 Percentage of fatty acid methyl esters in a lab-made FAME mix.

Component	Percentage
Palmitic Acid Methyl Ester (C16:0)	7.8%
Stearic Acid Methyl Ester (C18:0)	5.8%
Oleic Acid Methyl Ester (C18:1 *cis* -9)	71.5%
Linoleic Acid Methyl Ester (C18:2 *cis* -9,12)	12.1%
Linolenic Acid Methyl Ester (C18:3 *cis*- 9,12,15)	2.8%

has more unsaturated FAMEs in it. With the addition of linolenic and linoleic acid methyl esters (having three and two double bonds respectively), the FAME mix has a greater peak for this vibrational mode. The peaks associated with the =CH bends (scissor at 1270 cm^{-1} and twist at 975cm^{-1}) are also at a higher intensity than the oleic acid methyl ester. This is again due to the fact that the FAME Mix has some additional components with unsaturated bonds, and also because these additional FAMEs are in the *cis* conformation, making these vibrational modes more prominent.

3.3 Conclusion

Biodiesel is made up of mixtures of fatty acid methyl esters. In order to characterize biodiesel, the main FAMEs that make up most biodiesels were identified from previous literature research and characterized using Raman spectroscopy. A noted difference between the spectra of solid and liquid samples was the liquid samples exhibited more broad and mixed peaks than the solids. Main vibrational modes common to all the FAMEs included the C=O stretch, the CH_2 vibrations, the CH_3 symmetry vibrations, and the C-C skeletal vibrations. Some major differences between the FAMEs included the presence of double bonds (C=C) indicating unsaturation, and the *cis* conformation indicated through the =CH bends.

FAMEs were mixed in a percentage relative to those biodiesels studied in the literature and that spectrum was characterized in preparation for obtaining a commercial biodiesel sample.

The FAME mix was compared to its main component, oleic acid methyl ester, and some major differences include the intensity of the peaks indicative of double bonds (C=C stretch and =CH bends). Those peaks associated with the =CH bends also indicate components with the *cis* conformation and therefore were more intense in the FAME mix due to the addition of linoleic and linolenic acid methyl esters.

Chapter 4. Characterization of a Biodiesel Sample

4.1 Methods and Procedures

Materials. The biodiesel used in this experiment was obtained from a commercial biodiesel pump in Ballard, Washington, USA. The sample was B100 or pure biodiesel. A specification sheet was unavailable so the main feed source is unknown. The biodiesel was gold in color, similar to the color of petro diesel. FAMEs in their pure form are clear and so the coloring of the commercial biodiesel is due to dyes and additives [2]. The biodiesel was purchased in April 2016 and used immediately. When not in use, it was stored at room temperature in a dark environment. The oleic acid methyl ester was the same sample as used in chapter 3.

Instrument. The Raman spectrometer is a Renishaw inVia Raman Spectrometer with a Leica microscope (10x, 50x, and 100x objectives) and CCD camera. The biodiesel exhibited a large amount of fluorescence likely due to the dyes used; therefore, a 785 nm (1200 l/mm grating, 100 mW power) laser was used [2]. The 10x objective of the microscope was used due to the working distance from the liquid sample being more manageable than other objectives.

Data analysis. Data analysis was completed with the Renishaw Wire™ 2.0 software, Microsoft Excel™, and MatLab™. Due to a high level of fluorescence, a baseline subtraction was necessary to clearly resolve the vibrational peaks. A piecewise cubic spline interpolation baseline subtraction function was used in the mathematics program MatLab™ [31]. This piecewise method is good for samples with high fluorescence which causes a drifted baseline [32]. For this experiment, at least 9 points were chosen on the spectra and all points were the same for each spectrum to yield accuracy between sample analyses. Figure 4.1 illustrates the fluorescence of the biodiesel and the difference between the raw biodiesel spectrum (a) and the

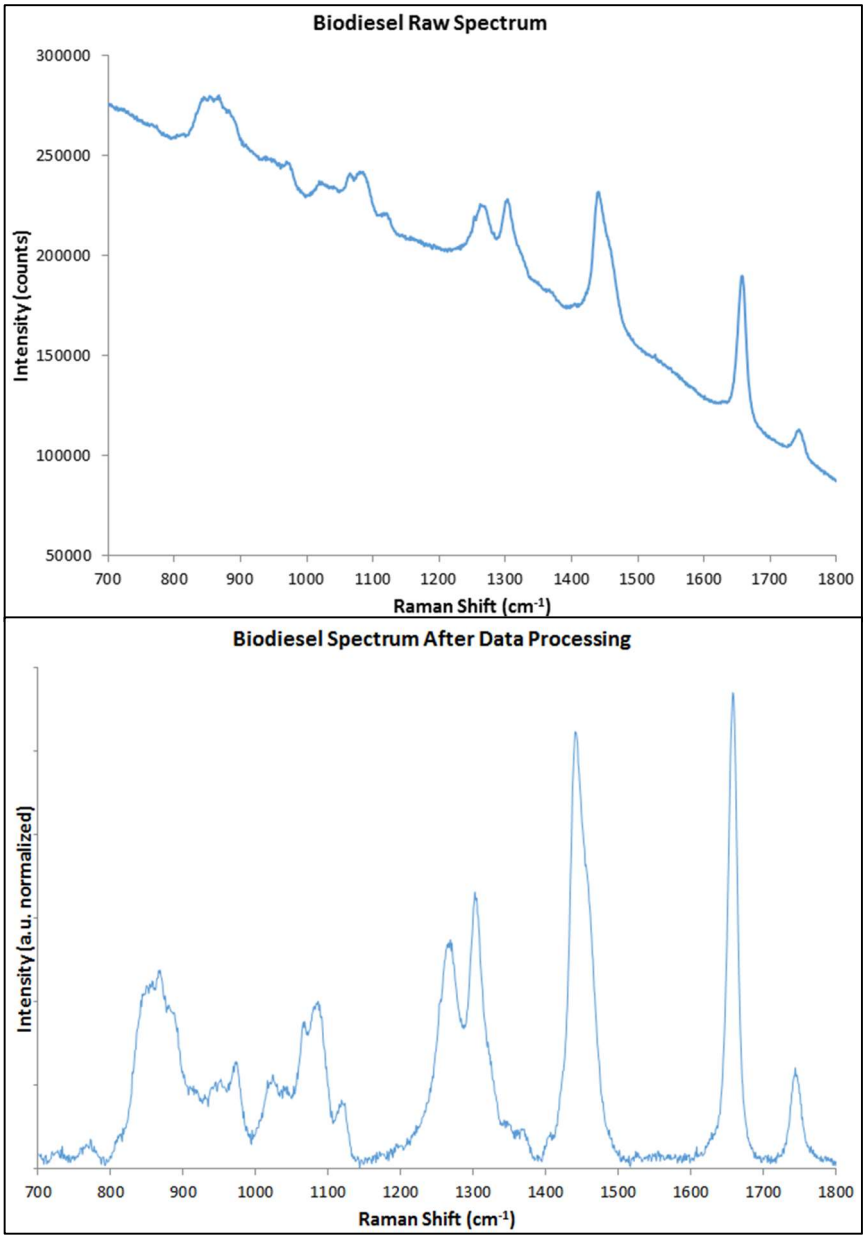

Figure 4.1 The Raman spectra of commercial biodiesel (a) before data processing and (b) after data processing. The fluorescence of the biodiesel is clear in (a) as the spectrum's baseline drift is clearly increasing from higher frequency (right) to lower frequency (left). After the baseline correction (b) the spectrum is clear and yields more resolved peaks.

processed biodiesel spectrum (b) after baseline subtraction and normalization. After baseline subtraction, normalization was applied to the spectra in order to compare different samples. As in the previous chapter, the standard normal variate normalization technique was used to normalize the spectra.

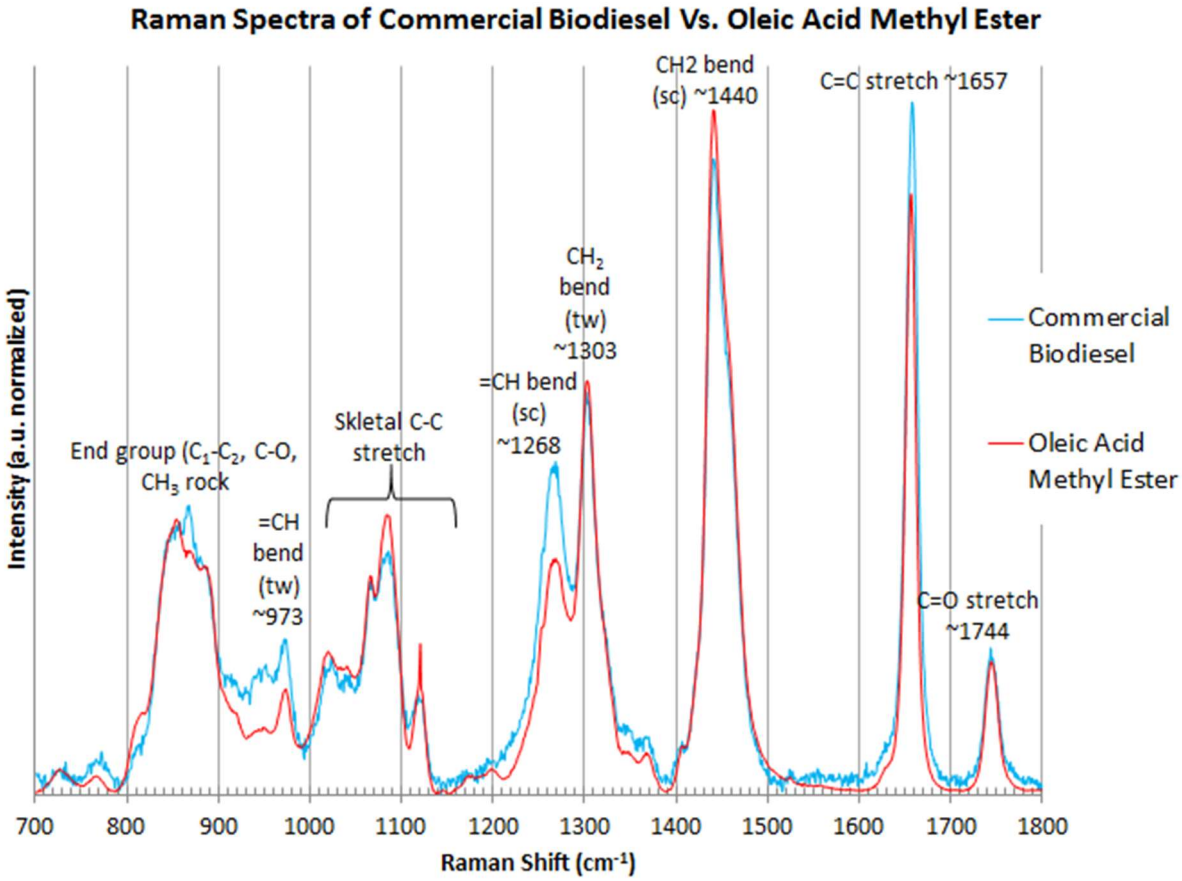

Figure 4.2 Raman spectra of commercial biodiesel compared with its main FAME, oleic acid methyl ester. Some of the major vibrational modes are noted on the graph above their representative peaks. The commercial biodiesel shows less saturation with stronger peaks at 1657, 1268, and 973 cm^{-1}.

Methods. The biodiesel sample is a liquid at room temperature; the samples were placed in the same aluminum sample holder described in section 3.1. The biodiesel sample was placed into the sampler using a micropipette. The Renishaw Wire™ 2.0 software was used to document the initial spectra obtained. The Raman spectra were optimized using a 20 second exposure time with 3 accumulations. Data processing occurred after collection of the spectra.

4.2 Results and Discussion

4.2.1 Spectral Analysis of Biodiesel Compared With Oleic Acid Methyl Ester

Biodiesel's main component is oleic acid methyl ester and this FAME is a useful comparison to commercial biodiesel [7]. Figure 4.2 shows the Raman spectra of the commercial

biodiesel compared with the oleic acid methyl ester. As expected, the commercial biodiesel shows stronger peaks at 1657, 1268, and 973 cm^{-1} indicating that this sample has more unsaturated components than just oleic acid methyl ester. This is expected as the biodiesel is made up of additional FAMEs than oleic acid methyl ester which have higher degrees of unsaturation such as linoleic and linolenic acid methyl ester.

Additionally, the spectrum of the commercial biodiesel does not indicate any new peaks from the oleic acid methyl ester. New peaks would indicate that the B100 was not pure; impurities such as petro diesel, heavy metals, or others could show up as new peaks if it existed in great enough amounts to show a vibrational mode. Figure 4.1 illustrates that the commercial biodiesel sample has florescent properties. Most commercial biodiesels are treated with antioxidants to avoid degradation [2]. Miranda et al. observed the fluorescence in their biodiesel sample and noted that the dyes and additives used in biodiesel did not have a Raman spectrum contribution [15]. The findings of Miranda et al. with this respect are further supported in Figures 4.1 and 4.2 where fluorescence is clear in Figure 4.1(a) but no additional peaks indicating dyes or additives are present in Figure 4.2.

4.2.2 Spectral Analysis of Biodiesel Compared With Petro Diesel

Figure 4.3 shows the Raman spectrum of biodiesel with a spectrum of petro diesel inset in the graph. An obvious difference between petro and biodiesel is the presence of unsaturated vibrations in the biodiesel, notably at the C=C stretch (1657 cm^{-1}), and the =CH bends (scissor at 1268 cm^{-1} and twist at 973 cm^{-1}). Additionally, there is no carbonyl stretch in the petro diesel around 1744 cm^{-1} indicating the absence of the esters that make up biodiesel. The end group vibrations from 800-900 cm^{-1} are different in these samples. The C-O stretch present in biodiesel enhances the peaks in that range, whereas petro diesel does not have a C-O stretch and those

peaks are not prominent.

Petro diesel possesses some additional peaks that biodiesel does not. The double peak in the petro at 1583 and 1609 cm^{-1} is indicative of a benzene ring stretch [33]. Also, the peak indicated on the petro diesel inset at 1378 cm^{-1} is attributed to the bicyclic aromatic stretch [33]. Lastly, according to Marinović et al., the peak indicated at 1002 cm^{-1} is due to the "symmetrical ring-breathing mode of monocyclic aromatic components" and is not present in biodiesel [33]. The absence of these peaks in the commercial biodiesel shows that this sample is pure biodiesel (B100) and was not blended with petro.

There are some similarities between petro and biodiesel that are apparent when comparing the Raman spectra in Figure 4.3. Mostly, the CH_2 vibrations that occur along the

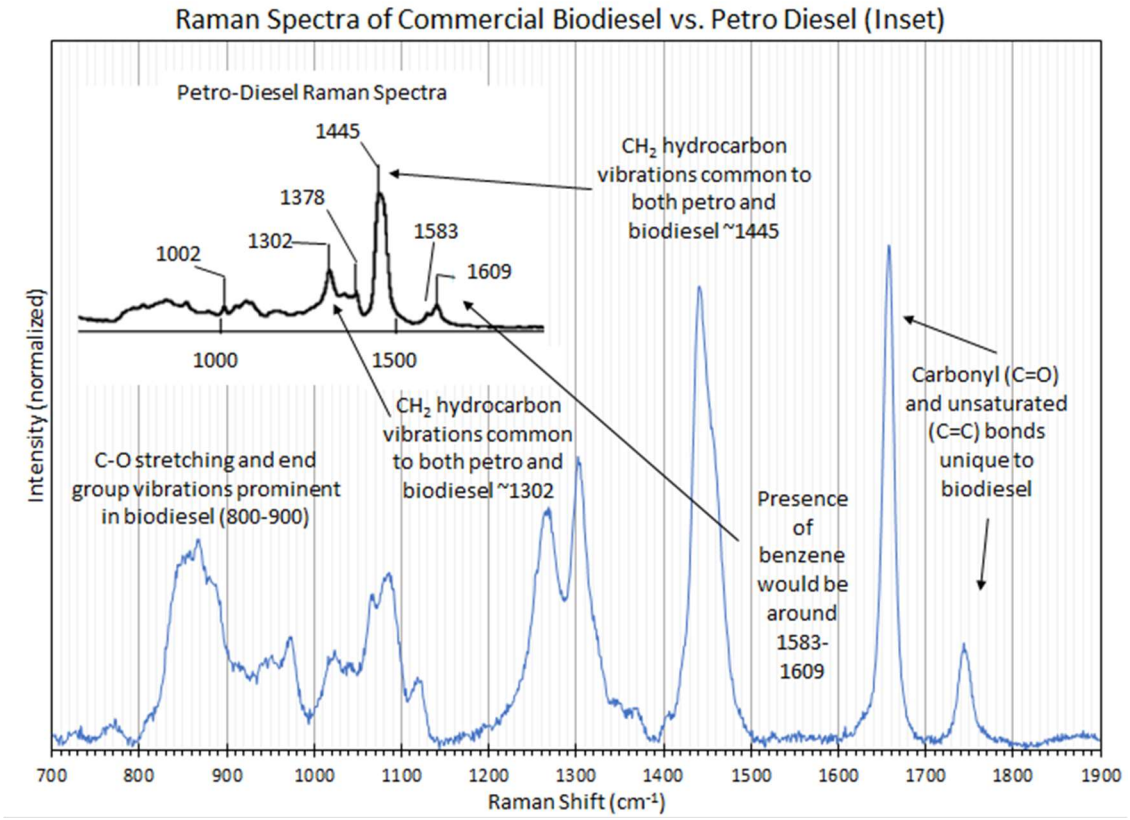

Figure 4.3 Raman spectra of commercial biodiesel compared to petro diesel (inset). Some of the obvious differences and similarities are indicated on the diagram. [33]

carbon backbone are prominent in both spectra. These occur at the CH_2 scissor (1445 cm^{-1}) and twist (1302 cm^{-1}) vibrations. Though not annotated in Figure 4.3, the skeletal carbon backbone stretching from ~1000-1140 cm^{-1} is present in both petro and biodiesel.

4.3 Conclusions

A commercial biodiesel sample was obtained at a biodiesel pump in Ballard, Washington, USA and characterized using Raman spectroscopy. Since commercial biodiesel has additives and dyes, a significant fluorescence was exhibited requiring additional data analysis. A cubic spline interpolation program in MatLab™ was used to subtract the drifted baseline caused by this fluorescence. Additionally, the data was normalized to compare it with other samples such as a pure FAME and petro diesel.

The characteristic vibrational modes of biodiesel were highly comparable to its main component FAME, oleic acid methyl ester. Notable characteristic vibrational modes are the carbonyl group, the unsaturated stretches (C=C and =CH bends), the CH_2 bends, the skeletal C-C stretches, and the end group (C-O, acyl, and CH_3 rock) stretches. From the relative intensity of the double bond vibrations, the biodiesel clearly possessed more unsaturated components than oleic acid methyl ester alone. No anomalous peaks were noted in the commercial biodiesel that would indicate impurity and the presence of the dyes and additives do not contribute to the Raman spectrum of biodiesel, as also shown by Miranda et al.

The Raman spectrum of commercial biodiesel had identifiable differences from petro diesel including the carbonyl group and the unsaturated vibrational modes. Further, petro biodiesel had characteristic peaks not present in biodiesel mainly attributable to aromatic compounds [33]. Some similarities between these two substances included the CH_2 bends and some of the skeletal C-C backbone stretching. Overall, the difference between the petro and

biodiesel spectra supported that the commercial biodiesel was pure (B100) and was not blended with any traceable amounts of petro diesel.

Chapter 5. Characterization and Evaluation of FAMEs and Biodiesel in Water Mixtures

In order to study the degradation of biodiesel in saltwater under UV or sunlight conditions, it first is necessary to determine how biodiesel reacts in water and how sensitive the Raman spectrometer is to this specimen. FAMEs were first used in deionized water to study this oil-water interaction and to determine the concentration sensitivity of the instrument. Then the same goal was applied to FAMEs mixed in artificial seawater. Since biodiesel is a mix of FAMEs, and its main component is oleic acid methyl ester, this initial FAME/water mix acted as a foundation for the study of commercial biodiesel in artificial seawater and the set-up of the photolytic degradation experiment discussed in section 6.

5.1 Methods and Procedures

Materials. The FAMEs used in this section of the study are the same as described in section 3.1. The biodiesel used is the same as described in section 4.1. Deionized water was further purified using a Millipore filter (Simplicity UV™) yielding ultra-pure water. The artificial seawater (ASW) was obtained from the National Oceanic and Atmospheric Administration's Northwest Fisheries Science Center in Seattle, WA, USA. The ASW contained the following salt solutions: sodium chloride, sodium sulfate, potassium chloride, sodium bicarbonate, potassium bromide, borate, sodium fluoride, magnesium chloride, calcium chloride, and strontium chloride. Oleic acid methyl ester was combined with UP in concentrations from 0.01% to 90%. Then a FAME mix was combined with ASW in concentrations of 10%, 15%, 25%, and 35%. Lastly, B100 was combined with ASW in concentrations of 10%, 20%, and 30% for comparison.

Instrument and data analysis. The same Raman spectrometer that was described in 3.1 was used in this section of the study. Both the 514 nm and 785 nm lasers were used. Data

analysis was conducted as described in section 3.1.

Methods. The water/oil mixtures were prepared with micropipettes in a 500 µL total volume working sample. For example if the concentration was 40% FAME and 60% water, 200 µL of FAME was mixed with 300 µL of water to yield a 500 µL working sample. The samples were mixed with a vortex spinner and by hand prior to sampling. The samples were then placed in the liquid sampler described in section 3.1 using a micropipette.

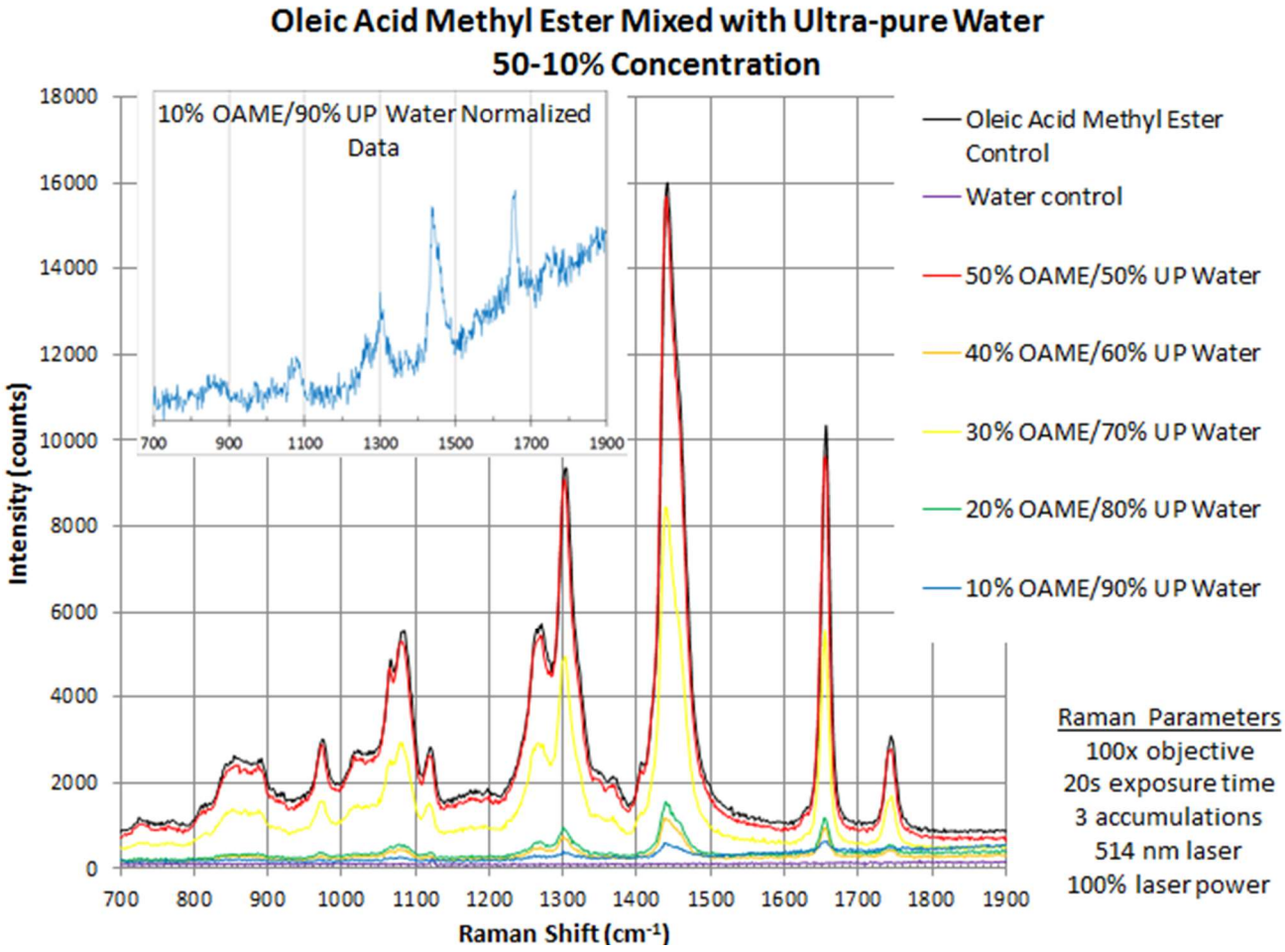

Figure 5.1 Raman spectra of oleic acid methyl ester (OAME) mixed with ultra-pure (UP) water in concentrations ranging from 50% to 10%. The 10% concentration normalized spectrum is also inset into the top left of the Figure to better indicate the resolution obtained. Clearly for concentrations down to approximately 20% the resolution of the Raman fingerprint region remains good.

5.2. Results and Discussion

5.2.1 FAMEs in Ultra-pure Water Concentration Analysis

Oleic acid methyl ester makes up the main component of biodiesel and therefore it was used as the representative FAME in studying the concentration resolution in ultra-pure water [7]. Figure 5.1 shows the results of mixing oleic acid methyl ester (OAME) in ultra-pure (UP) water in concentrations as high as 50% OAME to as low as 10% OAME water. The inset to Figure 5.1 shows a clearer representation of the 10% OAME concentration data on a normalized intensity axis to evaluate whether the fingerprint region is still accessible. It is clear from Figure 5.1 that concentrations down to approximately 20% still maintain a good resolution of the Raman fingerprint region. The 10% concentration still exhibits the same vibrational modes; however, some characteristic peaks such as the C=O at 1744 cm^{-1} and most of the peaks lower than 1000 cm^{-1} have poor resolution. The increase of the 10% concentration spectrum as the frequency increases (inset to Figure 5.1) is due to the UP water background. Water generally has a weak Raman signal which is one reason why Raman spectroscopy is a good measurement tool for water or biological samples. However, there is an O-H stretch peak at 3420 cm^{-1} and this peak is a large, broad peak having a gradual slope increase that interrupts the high frequency end of the fingerprint region of the 10% concentration [34].

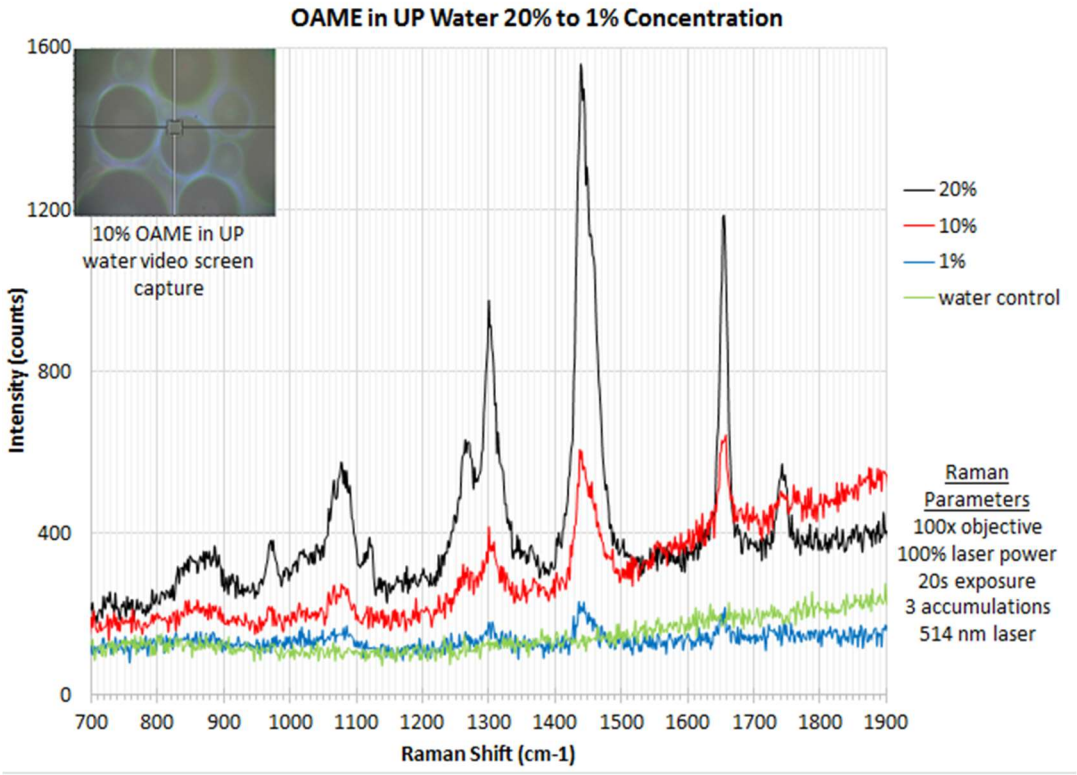

Figure 5.2 Raman spectra of OAME in UP water in concentrations from 20% to 1%. The inset at the top left of the Figure shows a screen capture of the CCD video of the 10% OAME in UP water indicating the coalescence of the oil droplets at the top of the sampler.

Concentrations lower than 10% were detectable. Figure 5.2 is the Raman spectra of oleic acid methyl ester in ultra-pure water in concentrations from 20% down to 1%. As in Figure 5.1, the spectrum of the 20% OAME in UP water shows good resolution in the Raman fingerprint region; all the characteristic peaks discussed in section 3 are well resolved. At 10% concentration, the peaks are present but are not well resolved. The inset to the Figure shows a video screen capture of the 10% OAME in UP water concentration. The image shows that the oil bubbles remained at the top of the sample and coalesced, likely contributing to the detectability of the Raman signal. The 1% OAME in UP water Raman spectrum is detectable, but without knowing the substance of study, the resolution is too poor to properly identify the sample. The detectable peaks in the 1% spectrum include the C=C stretch around 1657 cm^{-1}, the CH_2 bends around 1445 and 1303 cm^{-1}, and some of the broad peak indicating the skeletal C-C stretch in the

1000-1140 cm^{-1} region.

Concentrations lower than 1% were studied; however the only identifiable peaks were mostly outside of the fingerprint region in the 2700-3100 cm^{-1} range. This area is indicative of hydrocarbon stretches (CH_2 bends/stretches and CH_3 vibrations) [15]. Figure 5.3 is the Raman spectra of OAME in UP water from concentrations of 1% down to 0.01%. Inset to Figure 5.3 is a screen capture of the video image of the 1% concentration showing a single oil bubble drifting across the camera lens. In this small concentration, oil bubbles were not coalesced due to the low concentration. From these results, though a Raman signal is detectable in concentrations lower

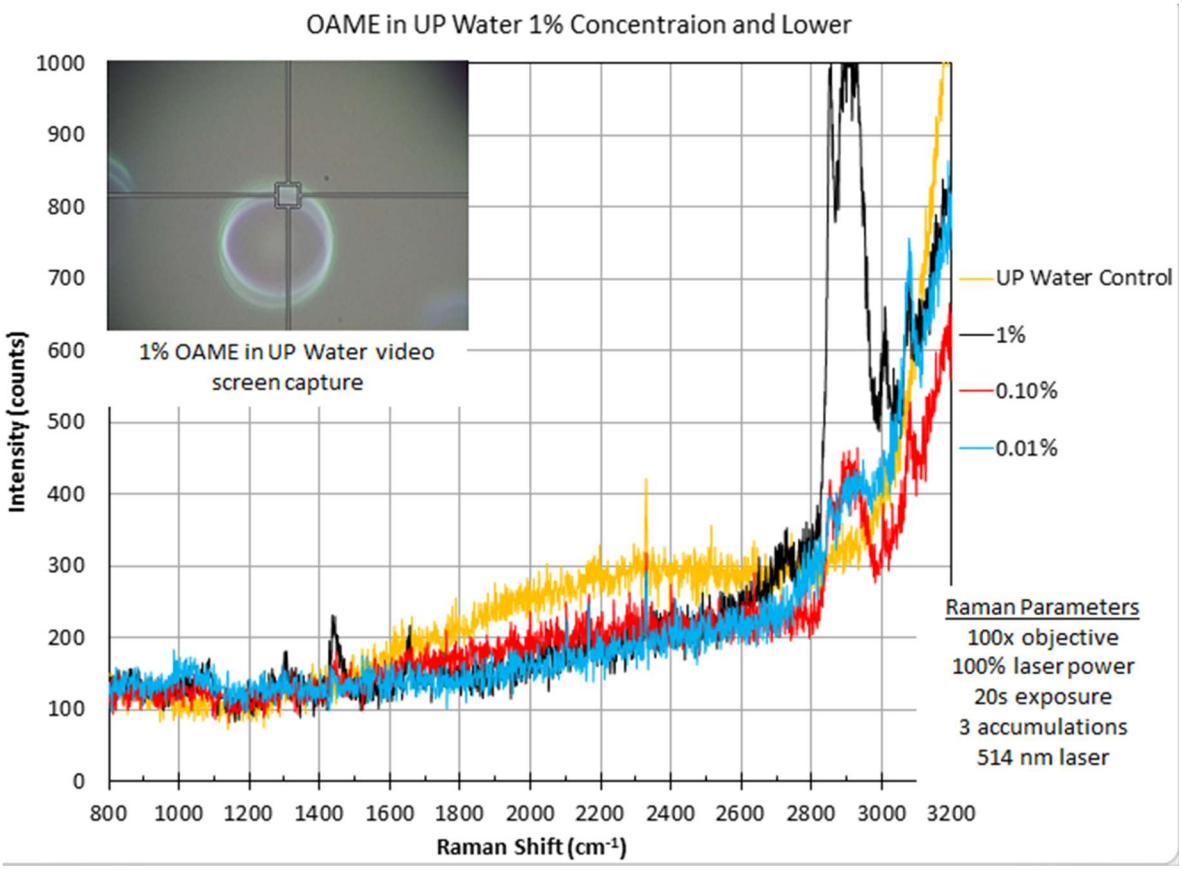

Figure 5.3 Raman spectra of OAME in UP water in concentrations of 1% and lower. The full spectrum of 800-3200 cm^{-1} is shown. Only the 1% concentration exhibits any signal in the fingerprint region, but it is too weak to yield a positive sample match without previous knowledge of the sample. All of the concentrations show a weak signal between 2800-3000 cm^{-1} indicating the hydrocarbon vibrations (CH_2 and CH_3 stretches/bends).

than 10%, the fingerprint region of approximately 700-1900 cm^{-1} is best resolved in concentrations higher than 10%.

5.2.2 FAMEs in Artificial Seawater Concentration Analysis

To mimic commercial biodiesel concentration in artificial seawater, the FAME mix discussed in section 3.3.3 was mixed with the artificial seawater (ASW). From the results obtained by using ultra-pure water, similar peak resolution was expected at the same concentration for the ASW/FAME mix. Figure 5.4 shows the results of a 10% and 35% FAME to ASW mix compared with its pure components. The Figure indicates that the concentration at 10% does show some of the characteristic peaks in the fingerprint region, but at a poor

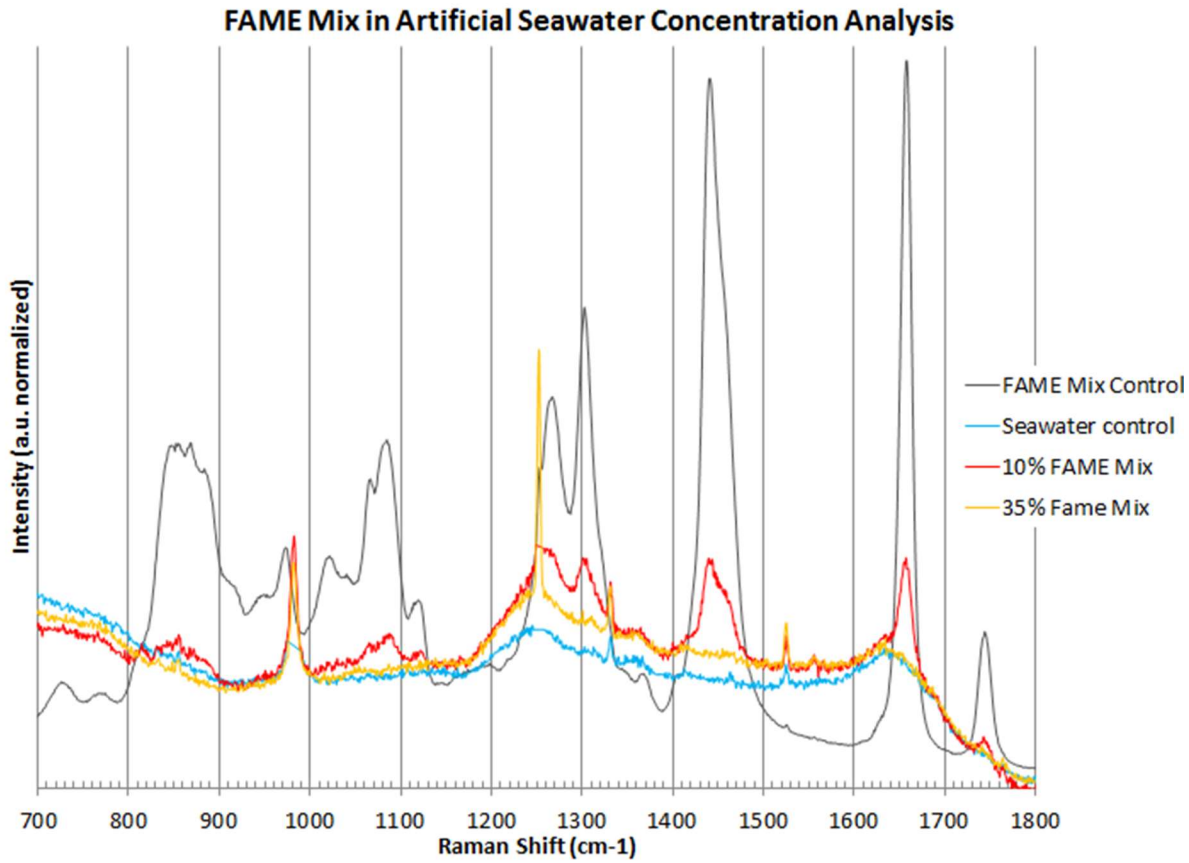

Figure 5.4 The Raman spectra of 10% and 35% FAME mix in ASW compared with the FAME and ASW controls. Neither the 10% nor 35% concentration yielded good resolution in the fingerprint region.

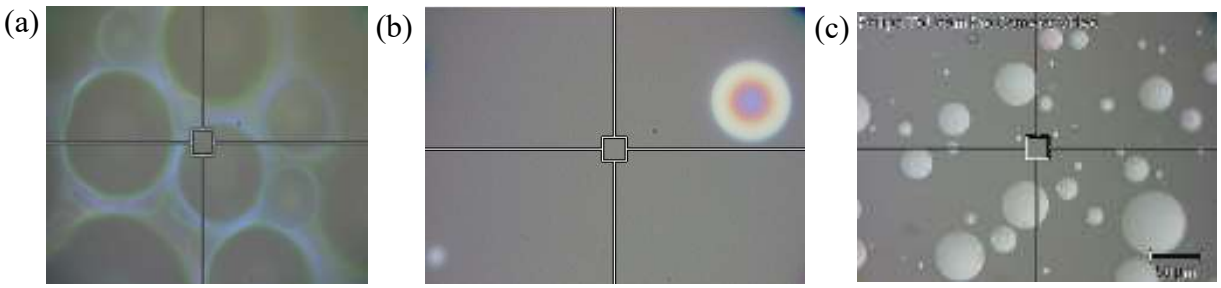

Figure 5.5 CCD video screen capture of (a) 10% OAME mixed with UP Water, (b) 15% FAMEs mixed with ASW and (c) 25% FAMEs mixed with ASW. The OAME coalesced into firm, grouped bubbles in the UP water but did not coalesce well in the ASW even at higher concentrations of 25%.

resolution. This resolution was very poor compared to that obtained by the OAME in UP water at the same concentration, shown in Figure 5.2. Oddly, the concentration at 35% shows poorer resolution than the 10%; this was likely due to poor mixing or sampling.

Figure 5.5 shows the screen capture of the CCD video of 10% OAME in UP water (a) versus 15% FAME in ASW (b) and 25% FAME in ASW (c). It is clear that in UP water the sample coalesced at the top of the water, forming solid, firm oil bubbles that took up a large portion of the upper layer of the liquid, making Raman sampling at the top yield a more resolved signal. In the ASW, the sample dispersed in the water, poorly coalescing and creating a problem for the Raman sampling as not enough oil sample coalesced at the top to be detectable.

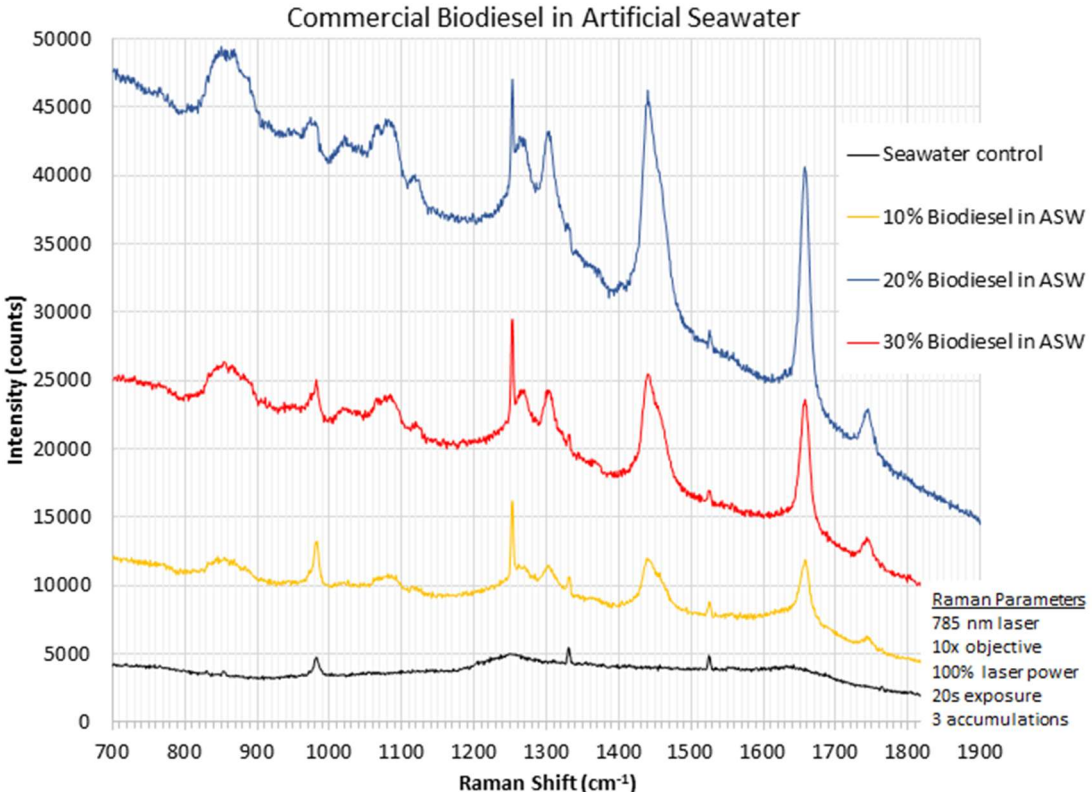

Figure 5.6 Raman spectra of commercial biodiesel in ASW in concentrations of 30% (red), 20% (blue) and 10% (yellow). Though vibrational characteristics are apparent at 10%, better resolution occurred at 20% and 30%.

This phenomenon is due in part to the electrostatic properties of water. Freshwater - especially ultra-pure water - is a poor conductor of electricity and so poorly conducts any electric fields that may develop due to the polarity of molecules [35]. Because of this, the oil (OAME or FAME) droplets coalesce into large bubbles on the surface since the density of FAMEs is also less than that of water as indicated in Figure 5.5(a). Contrarily, saltwater is a reasonable conductor of electricity so an electrostatic potential that may become present is conducted away, preventing natural coalescence as is seen in Figure 5.5(b) and (c) [35]. From these results, when mixing biodiesel into ASW for experimental purposes, concentrations higher than 35% likely are necessary for Raman spectroscopy.

5.2.3. Biodiesel in Artificial Seawater Concentration Analysis

Figure 5.7 Screen capture images of video images of commercial biodiesel in ASW in (a) 10%, (b) 20%, and (c) 30% concentrations. Commercial biodiesel coalesced better than the FAME mix in ASW. The larger bubble appearing in (b) and (c) show a large oil formation used to focus the laser for spectroscopic measurement.

From the results discussed in 5.2.2, it was determined that a higher concentration of biodiesel in ASW would be necessary in moving into a full experimental phase. However biodiesel does contain additives and dyes not present in the lab-made FAME mix that could alter its properties, making it behave different from the FAME mix. Figure 5.6 shows the results of mixing commercial biodiesel in ASW. The commercial biodiesel in ASW exhibited better spectral resolution than the FAME mix in ASW as illustrated in comparing Figures 5.5 and 5.6. Spectral resolution was not obtainable in the FAME mix even at 35% concentration whereas Figure 5.6 shows the biodiesel in ASW obtaining characteristic peaks in good resolution at 20% and 30%. This could be due to the additives and dyes added to commercial biodiesel to prevent oxidation and degradation [2]. Additionally, the FAMEs were purchased approximately four months prior to the commercial biodiesel and could have deteriorated some in that time. They were mixed in the laboratory and could therefore have been mixed poorly compared to the FAMEs in biodiesel further attributing to their inability to coalesce in the saltwater.

The biodiesel coalesced better than the FAME mix, as indicated in Figure 5.7 showing the video screen capture of the biodiesel in ASW at (a) 10%, (b) 20%, and (c) 30% concentration. From these results, the Raman analysis of biodiesel mixed in ASW should occur in concentration levels over 20% in order to maintain spectral resolution of characteristic peaks

in the fingerprint region.

5.3. Conclusions

In order to research biodiesel in artificial seawater, it was necessary to study the concentration sensitivity of these samples in the Raman spectrometer. Biodiesel's main component, oleic acid methyl ester was mixed with ultra-pure water to determine this initial sensitivity. Concentrations as low as 10% still showed the characteristic peaks in the Raman fingerprint region, though higher concentrations were better resolved. Concentrations of OAME in UP water were tested as low as .01%. At levels below 1% only the peaks outside of the fingerprint region where hydrocarbon stretching occurred (2900-3100 cm^{-1}) yielded any resolution. The samples in UP water coalesced at the top of the sampler making for good detection by the instrument.

The FAME mix described in 3.3.3 was mixed with artificial seawater (ASW) to mimic biodiesel in ASW. FAME mixed in ASW yielded poor concentration sensitivity compared to the OAME in UP water. Even in concentrations as high as 35%, spectral resolution of characteristic peaks in the fingerprint region was poor. The sample did not coalesce well at the top of the liquid. This phenomenon is due to the electrostatic properties of water as freshwater is a poor conductor and saltwater is a reasonable conductor of electricity allowing for natural coalescence in the freshwater sample, but poor coalescence in the ASW. Further contributing to the poor resolution is the age and lab mixing procedures of the FAME mix.

Commercial biodiesel contains additives and dyes to resist oxidation and degradation and therefore, its concentration sensitivity in ASW was also tested. Commercial biodiesel had greater concentration sensitivity in ASW than the FAME mix, showing similar sensitivity to the OAME in UP water. However, the best spectral resolution of characteristic peaks in the Raman

fingerprint region was obtained at concentrations higher than 20% for biodiesel in ASW.

In terms of environmental forensics, this indicates if a biodiesel sample exists in a strong concentration (i.e. a large amount of oil is present on top of the water and can be recovered), it could be possible to take a Raman spectrum of the sample and obtain an interpretable result. However, if the oil was well mixed with the water seemingly in very low concentrations, Raman spectroscopy would not be able to detect the sample with interpretable results and therefore another mode of measurement such as chromatography would be the best course of study unless enhanced Raman tactics are used such as micro-extraction or surface enhanced Raman spectroscopy, both discussed briefly in section 7.

6. Degradation of FAMEs and Biodiesel in Artificial Seawater Under UV Exposure

6.1 Literature Review and Expected Changes in Raman Spectra

6.1.1 Literature Review of Degradation Mechanisms of Biodiesel

Two studies occurred within the past five years that specifically addressed the degradation of biodiesel under sunlight and UV conditions. In 2011, Khoury et al. extensively studied the weathering of biodiesel samples by placing them in direct environmental stimulus [7]. Their research into the photo-oxidation of biodiesel used a pure biodiesel sample placed in direct sunlight on the roof of a building for 10 days. They showed that photolytic degradation was responsible for faster break-down of unsaturated FAMEs than biodegradation (via microbial activities) [7]. Also compounds containing one double bond (e.g. oleic acid methyl ester)

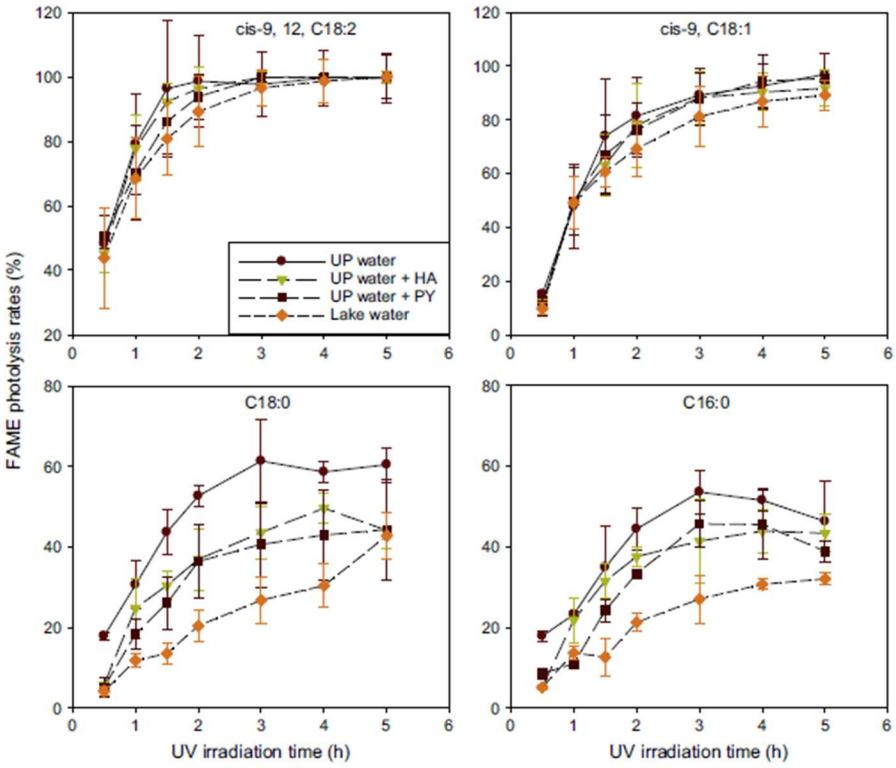

Figure 6.1 Degradation rates of different FAMEs indicated by their nomenclature in each chart title over 5 hours of strong UV exposure. Clearly the degradation rate of palmitic acid methyl ester (C16:0) is slower than that of linoleic acid methyl ester (C18:2 *cis*-9, 12) showing that unsaturated FAMEs degrade faster than saturated ones under photolytic conditions. [19]

degraded 60% under sunlight conditions after 10 days [7]. It was evident from this study that the unsaturated bonds of the FAMEs were the most vulnerable to degradation.

Similarly, Yang et al. published a study in 2015 specifically aimed at researching the photolytic degradation of biodiesel under UV conditions using a strong UV source. Figure 6.1 is from that study showing the results of individual FAMEs under a 33.7 mW/cm^2 intensity UV light for up to five hours. Like the findings of Khoury et al, this Figure shows that the unsaturated FAMEs broke down faster than the saturated FAMEs; after five hours 40% of palmitic acid methyl ester was degraded compared with 100% degradation of linoleic acid methyl ester in the same water matrix [19].

Both DeMello et al. and Khoury et al. indicated that biodiesel "easily" breaks down into its relative free fatty acids (FFAs) and methanol during degradation [18, 7]. In terms of relative FFAs, for instance oleic acid methyl ester's FFA is simply oleic acid. Toxicity studies of biodiesel on various marine organisms from Brazilian researchers studied the components of the degradation of water soluble fractions of biodiesel. In this study, Leite et al., found that the most prominent component in these water soluble fractions of degraded biodiesel was methanol, affirming the indications of Khoury and DeMello [23]. Leite et al., suggested that the formation of methanol was due to the reverse transesterification of the biodiesel [23].

Another degradation study unrelated to bio- or photolytic degradation occurred in 2013 from researchers of Syracuse University that looked into the degradation mechanism under high temperature conditions. Similar to Khoury et al., this research indicated the following order of biodiesel FAME stability under high thermal conditions from highest stability to lowest stability: palmitic (C16:0), stearic (C18:0), oleic (C18:1), linoleic (C18:2) and linolenic (C18:3) acid methyl esters [36]. That research also demonstrates saturated FAMEs are more stable than

unsaturated FAMEs. In that study at 275ºC the first sign of degradation was isomerization of the *cis-trans* configurations [36]. As temperatures were increased further, dimers formed through a Diels-Alder reaction and finally pyrolysis led to lower weight FAMEs, hydrocarbons, and gas products [36].

6.1.2 Hypothesized Changes in Raman Spectra of Biodiesel Exposed to UV Light

The research reviewed in 6.1.1 yields good predictions for the expected changes to the Raman spectra of biodiesel in artificial seawater as it degrades under UV conditions. The unsaturated FAMEs are expected to degrade first and fairly quickly. Therefore, the C=C stretches at 1657 cm^{-1}, and the =CH bends at 1268 cm^{-1} (scissor) and 973 cm^{-1} (twist) should become less intense over time indicating there are less of these bond vibrations in the sample.

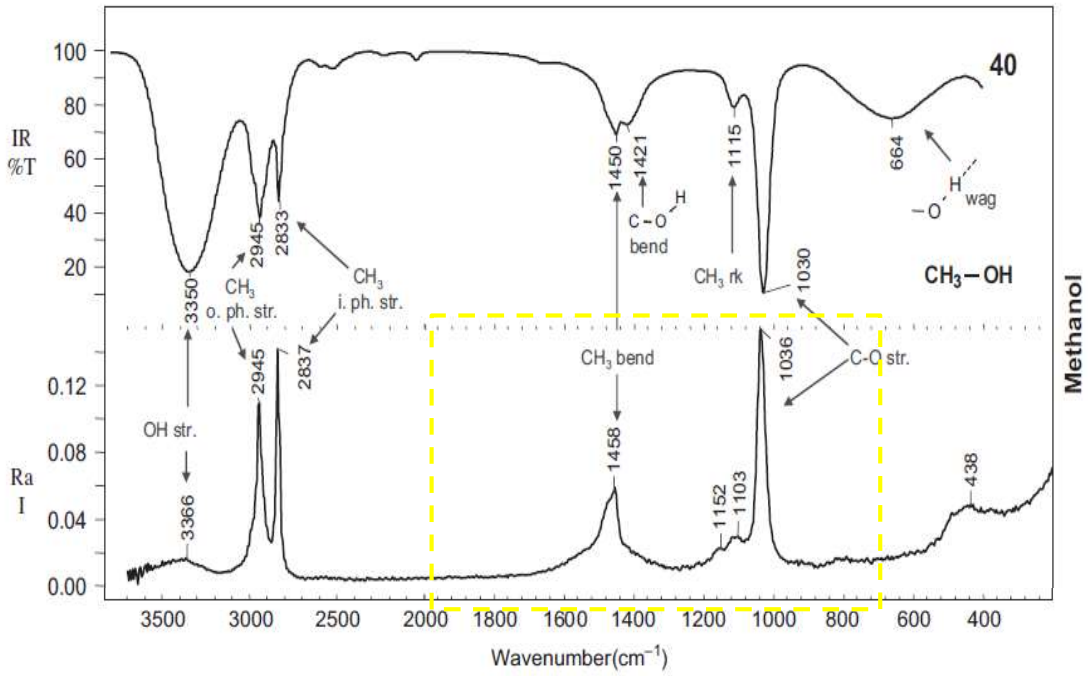

Figure 6.2 Infrared (top) and Raman (bottom) spectrum of methanol (CH_3OH). The yellow dashed box shows the Raman fingerprint region used for comparison in this research. notable in the Raman spectrum is the large peak at 1036 cm-1 indicating the C-O stretch. [28]

New components that may form in this degradation are FFAs and methanol. In comparing relative free fatty acids with their fatty acid methyl esters, it was noted in section

3.3.2 that the C=O (carbonyl) stretch in the free fatty acid is undetectable because this peak occurs around the same frequency as the C=C stretch at 1657 cm^{-1}. If FFAs are forming, the C=O peak may become weakened over time. Additionally, the end-groups of the FAMEs and their respective FFAs are different in that the FAMEs have an ester group on the non-acyl end. From this, the end-group vibrations visible in the 800-900 cm^{-1} range could change. Unfortunately, as discussed in section 3.3.2 the end group vibrations in that region of the spectrum of biodiesel and/or a FAME are somewhat undistinguishable as it simply forms a broad peak combining the C-O stretch, CH_3 rock, and C_1-C_2 acyl stretch. However, since the ester group is not present in the FFA, there should be a difference in that region of the spectrum.

Methanol is also expected to form and its Raman spectrum is shown in Figure 6.2 (bottom spectrum). The CH_3 bend at 1458 cm^{-1} will not present itself with FAMEs or FFAs in the same solution due to the strong CH_2 bend present in those spectra around1440 cm^{-1}. However, the C-O stretch noted at 1036 cm^{-1} and the two unidentified peaks at 1152 and 1103 cm^{-1} are unique to methanol and may become present if enough methanol forms in the degraded biodiesel/water samples. From previous literature regarding degradation of biodiesel and FAMEs and through comparison of predicted components degraded from biodiesel, the change to the Raman spectrum of biodiesel in artificial seawater is predicted and those changes are summarized in Table 6.1.

Table 6.1 Expected changes of Raman spectrum of biodiesel in ASW over time under UV exposure.

Vibrational Mode	Frequency (cm^{-1})	Expected Change	Indication
C=C stretch	1657	Intensity decrease	Break down of unsaturated components
=CH bend (scissor)	1268	Intensity decrease	Break down of unsaturated components; isomerization
=CH bend (twist)	973	Intensity decrease	Break down of unsaturated components; isomerization
C=O stretch	1744	Intensity decrease/frequency blue shift	Free fatty acid formation
End groups	800-900	Intensity change/shift	Free fatty acid formation
C-O stretch	1036	New peak formation	Methanol formation
Unidentified	1152, 1103	New peak formation	Methanol formation

6.2 Methods and Procedure

Materials. The FAMEs, biodiesel, and artificial seawater used for this experiment are as described in section 3.1, 4.1, and 5.1 respectively. The UV lamp used is a UVP, model UVM-225D lamp of 50W with a monochromatic light at 302 nm with a light intensity of 3.6 mW/cm^2 at a sample distance of 3 inches.

Instrument and data analysis. The Raman instrument is the same as described in section 3.1. Only the 785 nm laser was used due to biodiesel fluorescence as described in section 4.1 and the 10x objective was used to allow for the largest volume Raman sampling. The same data analysis technique was used as described in section 4.1 including normalization and baseline subtraction.

Methods. For the biodiesel in ASW degradation, four samples were prepared: two 100% biodiesel and two 40% biodiesel in 60% ASW. These samples were prepared in 20 mL glass jars with tops. The total sample volume was 15 mL. The samples were measured with a graduated

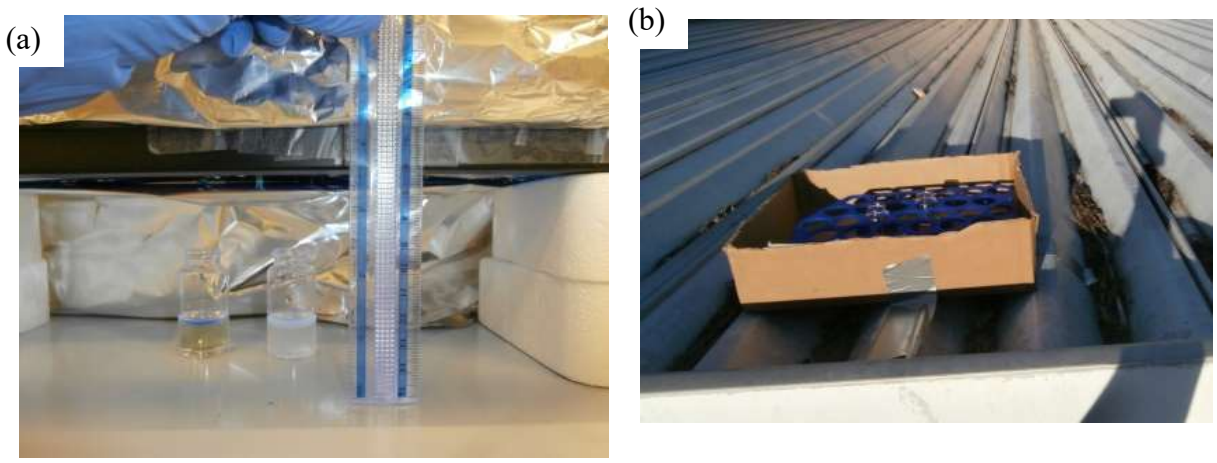

Figure 6.3 Experimental set-up for (a) biodiesel and FAMEs under UV exposure and (b) biodiesel under sunlight (photo taken in the early morning).

cylinder and micropipette. The sample jars were cleaned and dried prior to preparing the experimental specimen. The baseline spectra of each sample was taken prior to placing one 100% biodiesel and one 40% biodiesel in ASW sample under the UV lamp, approximately 3 inches from the light source. This set-up is illustrated in Figure 6.3 (a).The other 100% biodiesel and 40% biodiesel in ASW specimen were kept wrapped in aluminum foil (dark conditions) at room temperature. For the first, 10 days, small samples were pulled from the main specimen every 12 hours to be measured with the Raman spectrometer using the sampler described in section 3.1. After 10 days, the specimens were pulled every 24 hours around 8 a.m. for instrumental analysis. The experiment lasted 23 days. Prior to each analysis, the samples were shaken with a vortex spinner for approximately 15 seconds to mix the specimens. Prior to mixing, the four samples were photographed and any visual changes noted.

For the FAMEs in ASW experiment under UV exposure, a new FAME mix was developed due to the necessity to purchase new oleic acid methyl ester. The FAME mix used in this portion of the experiment had the following mixture: 6% palmitic acid methyl ester, 10% stearic acid methyl ester, 70% oleic acid methyl ester, 8% linoleic acid methyl ester, and 6%

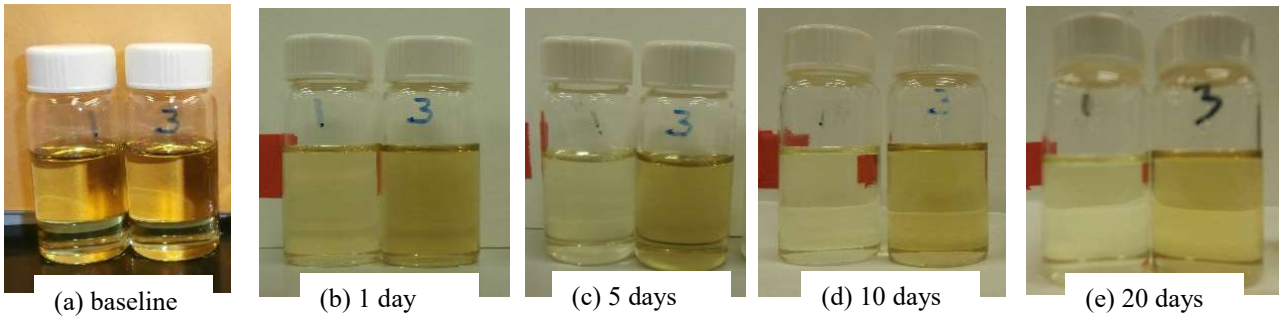

Figure 6.4 Photographs of 100% biodiesel under UV (left sample, labeled 1) and in the dark (right sample, labeled 3) for a selection of times during the 23 day experiment. The original color of the biodiesel seen in (a) begins to lighten after time (b)-(e) due to photo bleaching.

linolenic acid methyl ester. Only two samples were prepared: two 40% FAMEs in 60% ASW samples with a total specimen volume of 5 mL. One specimen was placed under the UV lamp 3 inches from the light and the other was placed in the foil at room temperature. The same sampling procedures were followed as described above except that the samples were checked every 24 hours for 7 days.

A brief experiment of biodiesel mixed in ASW under actual sunlight conditions occurred for 3 days from April 29 – May 2, 2016 in Seattle, WA. In this short experiment four specimens were prepared the same as for the biodiesel under UV experiment. Two of these specimens were placed on a carport roof from 7 a.m. to 7 p.m. for 3 days of full sunlight exposure on April 30th, and May 1st-2nd. During this time the daylight length was approximately 14.5 hours per day. The other two specimens were placed in foil (dark). Samples were taken every 24 hours in the evening (after a day of sun exposure). The length of this experiment was short due to the weather conditions; after three days the weather was cloudy and the experiment was discontinued. The set-up of the specimens in the sunlight is shown in Figure 6.3 (b). The same Raman analysis occurred on these samples as described for the biodiesel in ASW experiment.

6.3 Results

6.3.1 Biodiesel Exposed to UV Light

100% Biodiesel exposed to UV light. An initial result of this UV exposure that was visually observed and scientifically confirmed was the photo bleaching of the dyes in the commercial biodiesel. Visually, the sample under UV exposure started out the same color as the sample placed in the dark as illustrated in Figure 6.4 (a). After just one day, the 100% biodiesel under UV conditions was visibly lighter in color. After a few days, the photo bleaching visibly stabilized (Figure 6.4 (c)-(e)). This visual observation is confirmed by examining the unaltered (raw) Raman spectra of the 100% biodiesel under UV conditions presented in Figure 6.5. The baseline (initial) spectrum shows the spectral baseline drift indicative of fluorescence due to the dyes in the biodiesel. After only one day, the photo bleaching reduces the baseline shift. After 5

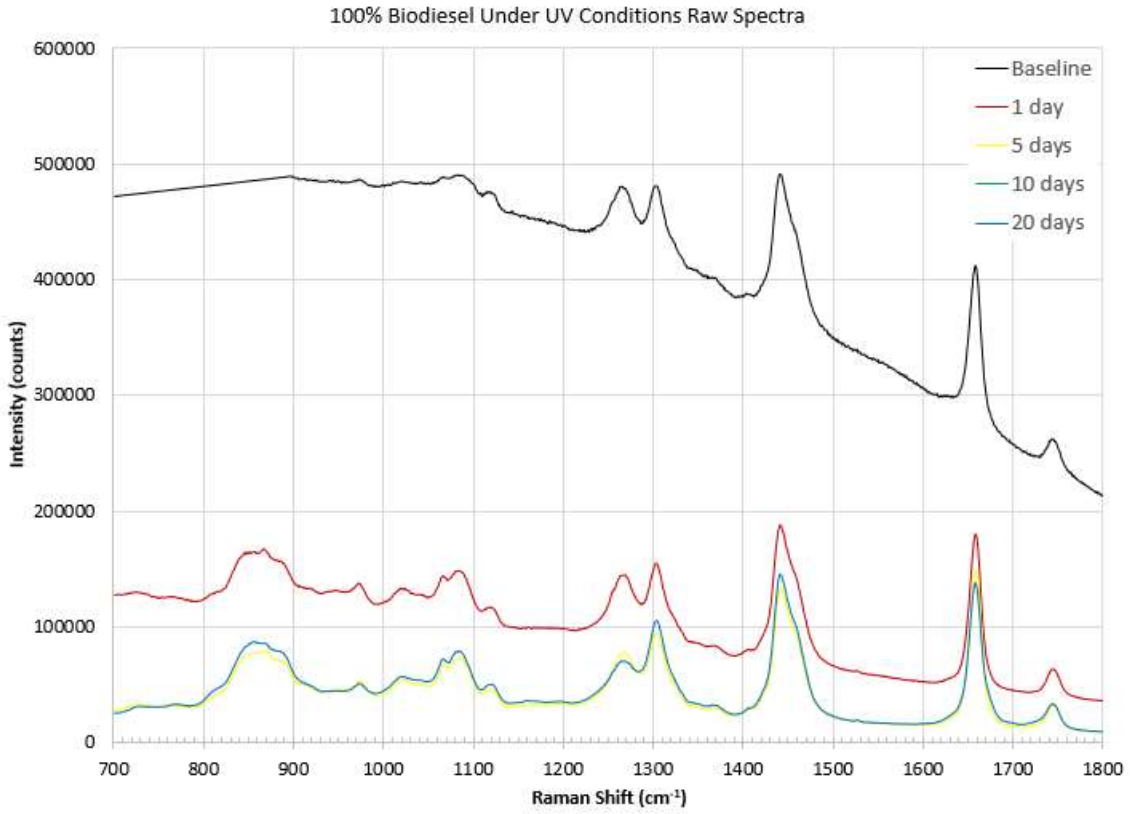

Figure 6.5 Unaltered (raw) Raman spectra of 100% biodiesel under UV exposure for a selection of times. The fluorescence visible in the baseline decreases with time; after the fifth day, the extent of photo bleaching is complete.

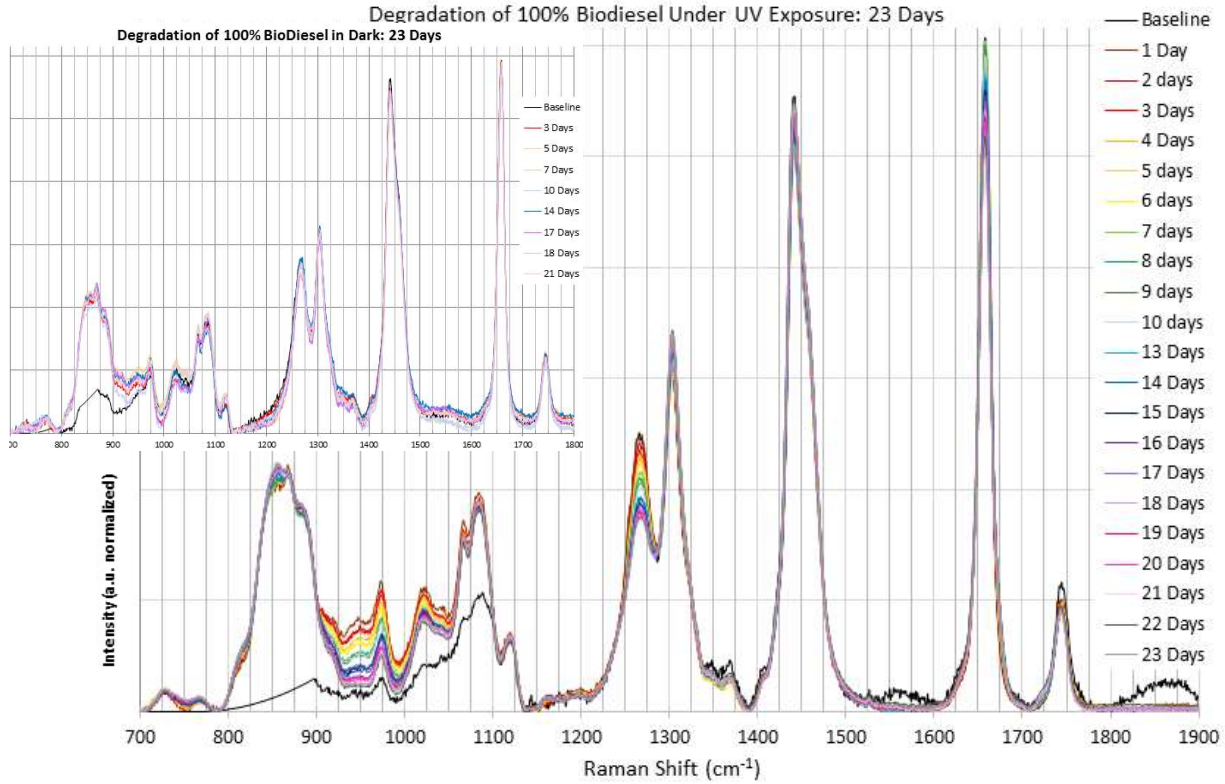

Figure 6.6 Raman spectra of 100% biodiesel under UV exposure for 23 days. The inset at the top left shows the 100% biodiesel control (dark) spectra for a selection of days. Obvious changes to the spectra include declining peak intensity at 1657, 1267, 1023 and 973 cm^{-1}.

days, the photo bleaching is mostly complete as the spectra do not change their baseline any further.

Figure 6.6 shows the analyzed Raman spectra of the 100% biodiesel under UV exposure for 23 days. The inset to the Figure shows a sample of the 100% biodiesel control left in the dark for the same period of time. The initial baseline (black lined spectrum) in the Figure shows problems with the baseline fit, especially below 1150 cm^{-1}. This was due in part to the high fluorescence of the sample. The instrument failed to recognize a good signal below approximately 900 cm^{-1} making the baseline fit for this sample difficult; therefore the baseline spectrum displayed in the Figure is only useful as a reference from 1150-1800 cm^{-1}.

There are some obvious changes to the Raman spectrum of the biodiesel exposed to UV light. The peaks at 1657, 1267, 1023 and 973 cm^{-1} decreased in intensity over the 23 day period

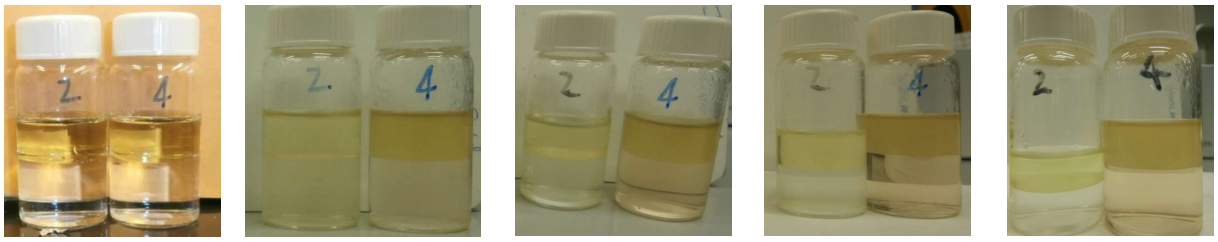

(a) Baseline (b) 1 day (c) 5 days (d) 10 days (e) 20 days

Figure 6.7 Photographs of 40% biodiesel under UV exposure (left sample, labeled 2) and in the dark (right sample, labeled 4) for a selection of times during the 23 day experiment. The original color of the biodiesel seen in (a) begins to lighten after time (b)-(e) due to photo bleaching. Evaporation of the sample placed under the UV light becomes clear in (d) and (e).

studied. The inset to Figure 6.6 showing the spectra of 100% biodiesel control in the dark is colored the same as the UV sample but with less selection and it shows that there is no identifiable change to the spectra of the times selected. Some of the spectra in the inset to Figure 6.6 shift in the 900-1000 cm^{-1}region. This is due to problems with the baseline fit as observed and discussed in the original baseline (time zero) spectrum. Notably, these visual shifts in the dark control between 900-1000 cm^{-1} have no pattern with regards to change over time and so they are attributable to the baseline errors due to continued fluorescence of the dark sample.

40% Biodiesel in ASW exposed to UV light. The biodiesel in the artificial seawater visibly changed. The biodiesel is visible on top of the water due to its lower density and its florescence became lighter in color as photo bleaching occurred just as in the 100% biodiesel sample. However, another visual change to the 40% biodiesel in ASW under UV conditions that occurred over time was evaporation. Evaporation did not occur to any notable degree in the 100% biodiesel sample under UV conditions as indicated in Figure 6.4. Figure 6.7 shows the photographs of the 40% biodiesel in ASW compared to its dark control.

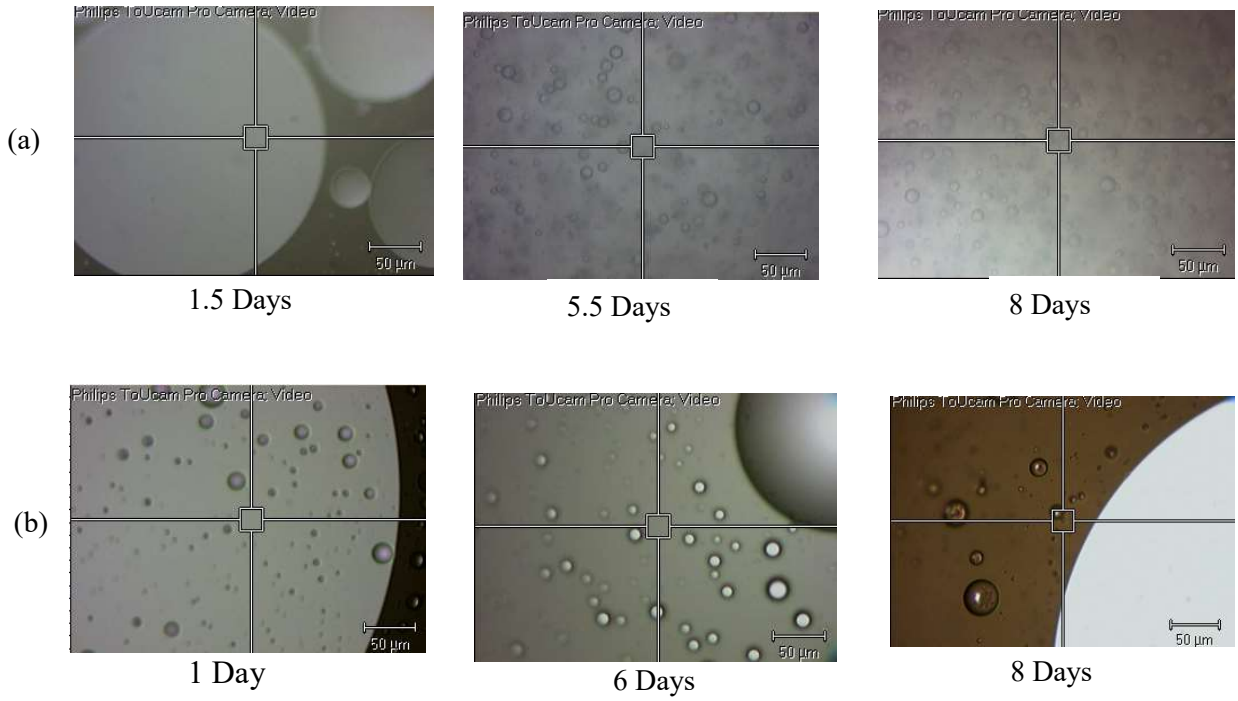

Figure 6.8 Video screen captures of (a) 40% biodiesel in ASW under UV exposure and (b) 40% biodiesel in ASW in dark conditions after a selection of time. The biodiesel in ASW under UV conditions emulsified some over time whereas the dark sample maintained some oil/water separation.

Another difference in the biodiesel/ASW mixture observed visually under UV exposure is illustrated through the video screen captures of some selected times located in Figure 6.8. The 40% biodiesel in ASW under UV conditions (Figure 6.8 (a)) showed some visual emulsification over time. This is in contrast to the 40% biodiesel in ASW in dark conditions which continued to show oil/water separation throughout the experiment (Figure 6.8 (b)).

The spectra of the 40% biodiesel under UV conditions are illustrated in Figure 6.9 and numerous differences in the original spectrum are observed over time. The C=O stretch at 1744 cm^{-1} becomes wider at the base on the lower frequency side (blue shift). The C=C stretch at 1657 cm^{-1} reduces in intensity significantly. The CH_2 bends at 1440 and 1303 cm^{-1} increase in intensity. The =CH bends at 1267 and 973 cm^{-1} decrease in intensity. The skeletal C-C backbone stretches from 1050-1150 cm^{-1} increase a small amount in intensity. Finally, the end group stretches from 800-900 cm^{-1} change. The inset to Figure 6.9 illustrates the 40% biodiesel in ASW kept in the dark, or the control to the UV sample. The dark sample has the same color scheme as the main Figure but only a selection of sample times. Though the spectra on the dark

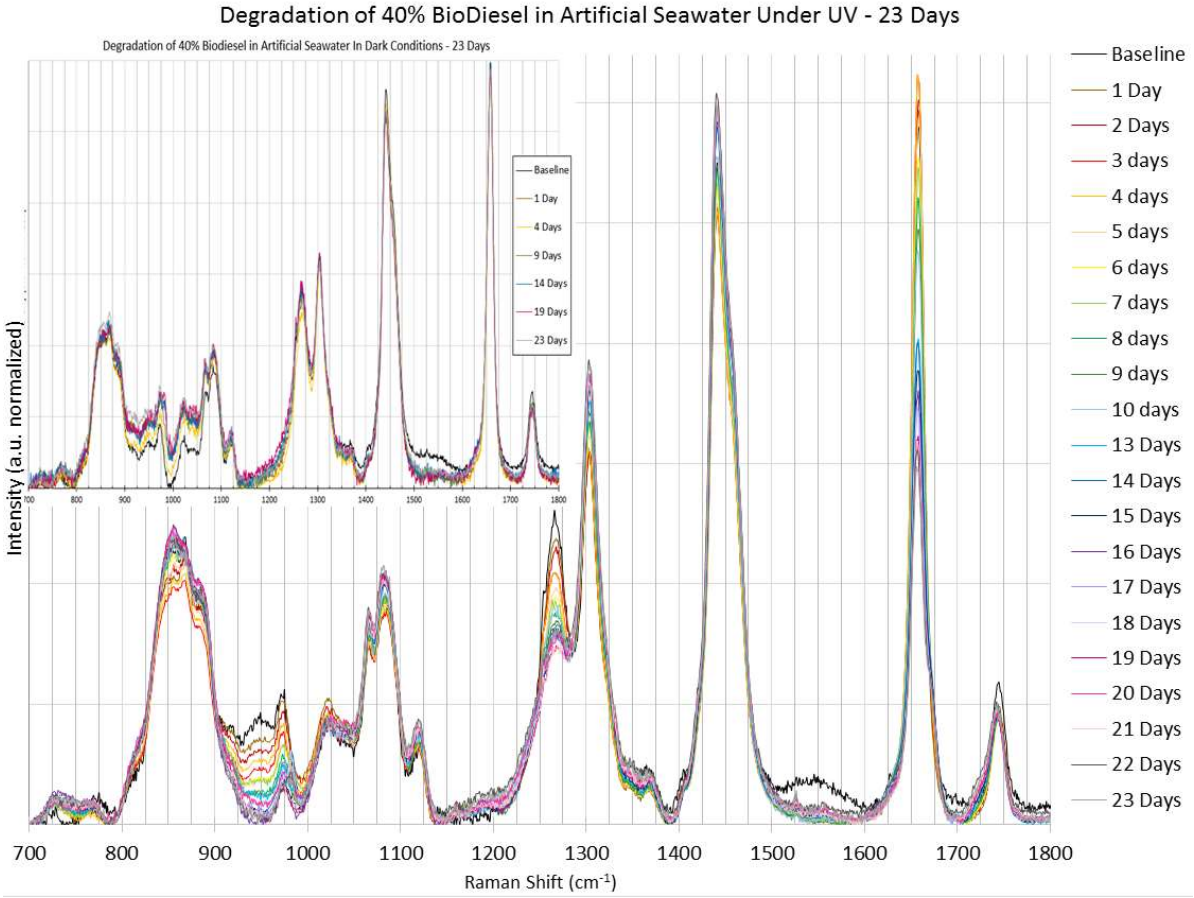

Figure 6.9 Raman spectra of 40% biodiesel in ASW under UV exposure for 23 days. The inset at the top left shows the 40% biodiesel/ASW control (dark) spectra for a selection of days. Changes to the 40% biodiesel under UV are apparent throughout the spectrum and discussed in the text.

control do not align at all times, their differences show no pattern with time. Therefore, there were no notable changes to the dark sample. Any differences between spectra are attributable to the data analyses techniques or sampling as these samples still showed fluorescence and the ASW signal occasionally interfered with good measurements.

6.3.2 FAMEs Exposed to UV Light

Only a 40% FAME mix with 60% ASW was studied under UV and dark conditions due to the amount of FAME available and timeframe required for the experiment. Figure 6.10 shows the photographs of the 40% FAMEs in ASW under UV conditions compared with its dark control over a selection of time. Two visual differences are illustrated. First, the FAMEs under UV exposure darken slightly in color from clear to a light greyish-yellow. Secondly, evaporation occurs in the FAMEs in ASW that were placed under UV exposure.

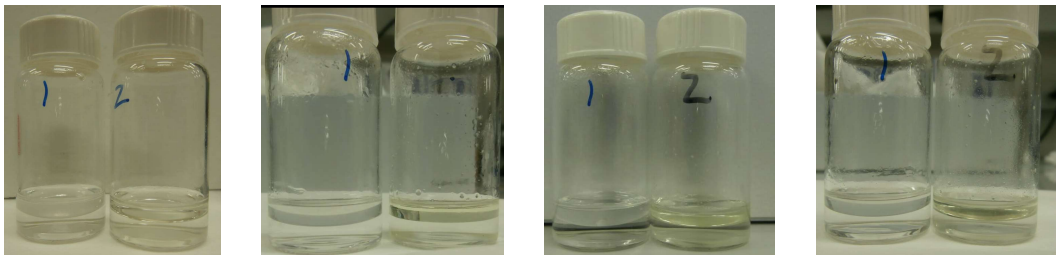

(a) 1 Day (b) 3 Days (c) 5 Days (d) 7 Days

Figure 6.10 Photographs of 40% FAMEs in ASW under UV exposure (right sample, labeled 2) and in the dark (left sample, labeled 1) for a selection of times during the 7 day experiment. The original color of the FAME was clear and it darkens slightly after time (b)-(d). Evaporation of the sample placed under the UV light is apparent in (c) and (d).

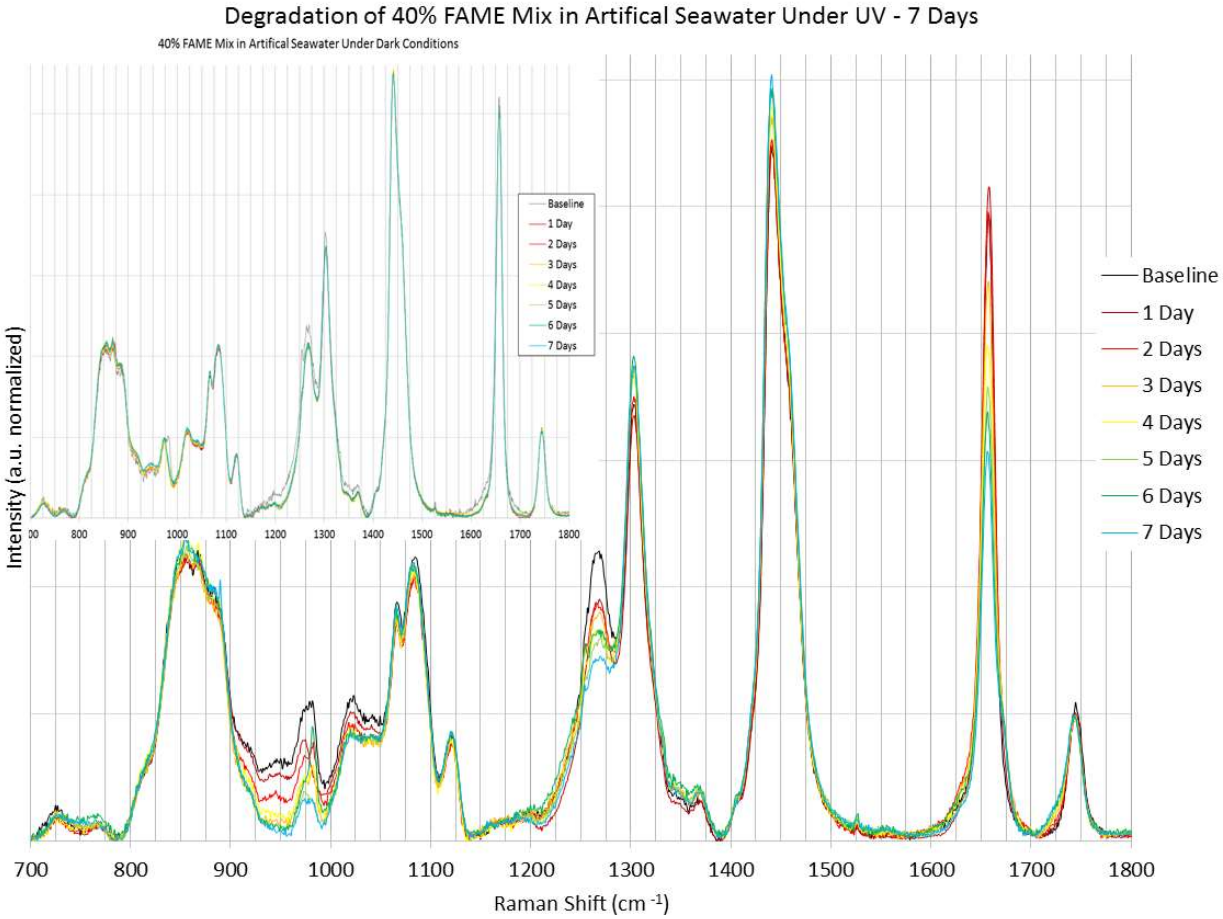

Figure 6.11 Raman spectra of 40% FAMEs in ASW under UV exposure. The inset at the top left is the same sample under dark conditions (control). Similar spectral changes occurred to this sample as to the 40% biodiesel/ASW in UV exposure except that the 40% FAME/ASW sample changed more drastically over 7 days.

Similar spectral differences that were observed in the 40% biodiesel/ASW under UV conditions occurred in the 40% FAMEs/ASW under UV condition. The only difference is that after 7 days, the spectral changes to the FAMEs/ASW sample are more extreme than after 7 days of biodiesel/ASW UV exposure. This is apparent in Figure 6.11 which illustrates the spectral changes of the 40% FAMEs in ASW under UV conditions. The inset to Figure 6.11 is the FAMEs in ASW dark control which exhibited no discernable difference during the 7 days.

6.3.3 Biodiesel Exposed to Sunlight

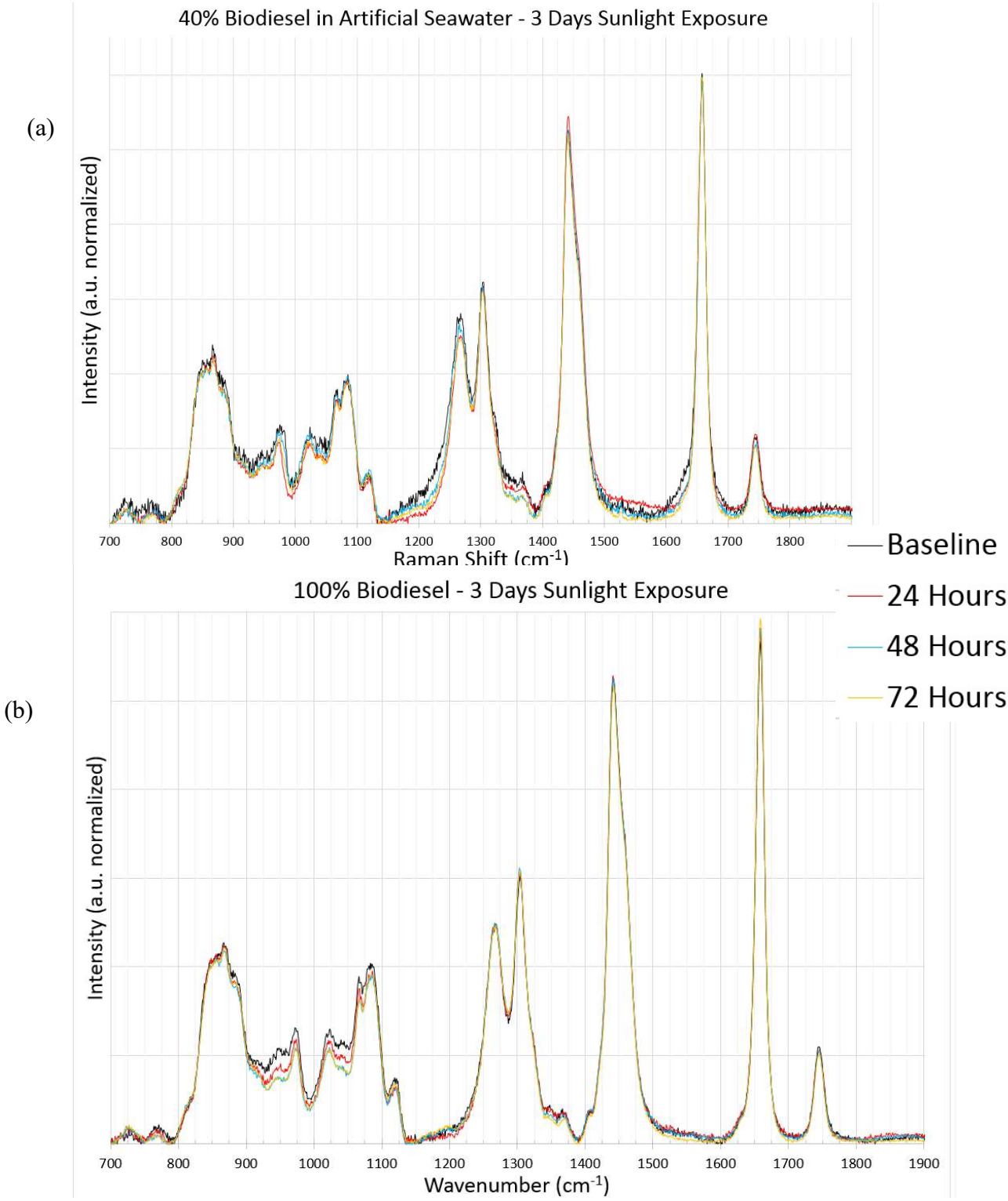

Figure 6.12 Raman spectra of (a) 40% biodiesel in ASW and (b) 100% biodiesel under sunlight exposure for 3 days.

To compare the effects of natural sunlight to the UV lamp used in section 6.3.1, biodiesel was place on the roof of a carport during sunny conditions for three days. The spectra of the 40%

biodiesel in ASW under sunlight and 100% biodiesel under sunlight are illustrated in Figure 6.12 (a) and (b) respectively. Their controls are not shown for the sake of space, but indicated no changes. These samples presented some similar spectral changes as noted for the biodiesel samples under UV conditions. However, it is evident that with only 3 days of 12-hour actual sunlight exposure that the changes are minor and without additional time, the results are only preliminary.

6.4. Discussion

6.4.1 Degradation Mechanisms of Biodiesel

Isomerization. The first stage of degradation observed in the Raman spectra is the isomerization of the FAMEs from the *cis* to the *trans* configuration. It is evident in all the spectra of biodiesel exposed to UV and sunlight and whether it was in ASW or not; the =CH bends at 973 and 1268 cm^{-1} decrease in intensity over time. This was not observed in the specimens left in

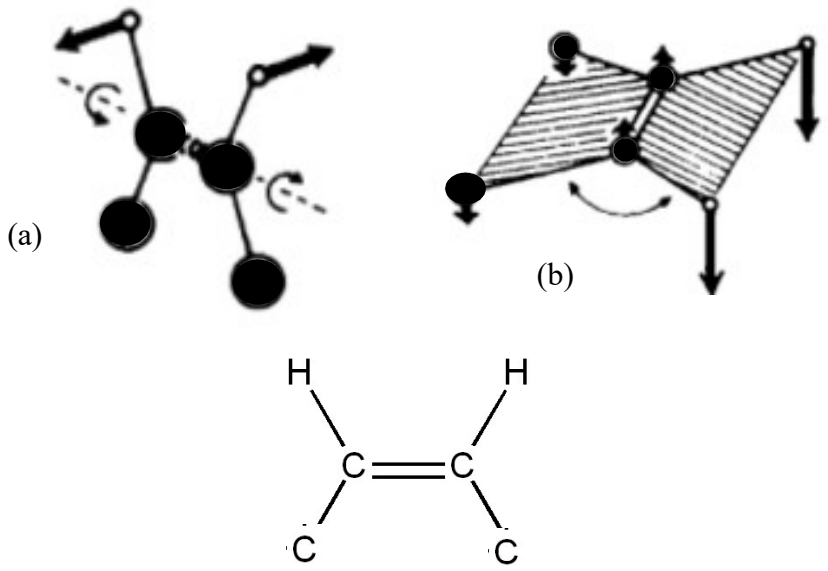

Figure 6.13 Olefin bends in the *cis* conformation. The carbon atoms in the (a) twist and (b) scissor are large black circles; the two hydrogen atoms are small open circles. [44]

the dark. These two bends are associated with changes to bond angles in the *cis* formation as illustrated in Figure 6.13. When *cis* configured molecules change to *trans* configured molecules

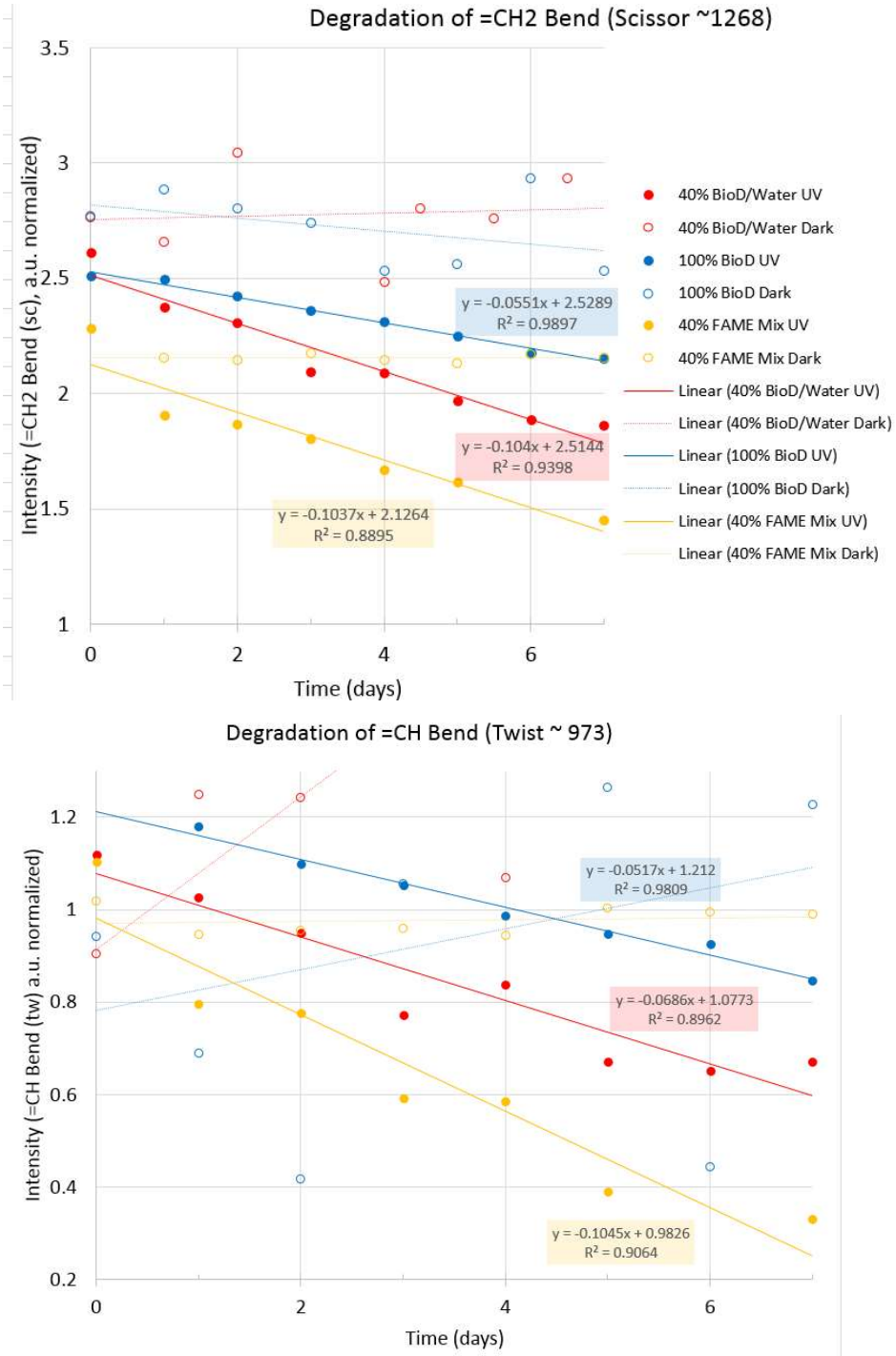

Figure 6.14 Degradation of =CH bends in FAMEs and B100 over 7 days: scissor (top) and twist (bottom). The linear fits are displayed on the graphs

during isomerization, these two bends are no longer detectable. This was the first type of degradation noted by Lin, Zhu and Tavlarides in their study of thermal degradation of biodiesel [36]. Though these samples warmed slightly under the UV or sunlight exposure, they never reached temperatures that were too hot to touch with the bare skin; Lin, Zhu, and Tavlarides noted the isomerization under thermal degradation occurred around 275ºC [36]. The radiative properties of the UV light caused the same degradation but at much lower temperatures. Further, the rate of the isomerization was faster for the biodiesel and FAMEs in ASW than the pure biodiesel, during the first week of degradation. This is illustrated in Figure 6.14 which shows the normalized intensity of the =CH bends over the first 7 days. The linear fit is shown on the graph along with its equation. In the first 7 days, the 100% biodiesel showed the slowest isomerization degradation (indicated by the greater absolute value of the slope of the line) but the difference between the samples is quite small. After 7 days the isomerization steadies, as there are less *cis* configured FAMEs left to degrade into the *trans* formation. This is illustrated in Figure 6.15. After the full 23 days the rate of the degradation of the =CH bends is similar in the 100% biodiesel and 40% biodiesel/ASW. A noticeable leveling off of this degradation is apparent in the last few days; this is also visible by looking at these peaks in Figures 6.6 and 6.9. Towards the end of the experiment, the =CH scissor bend vibration almost is melded into the CH_2 bend at 1303 cm^{-1} and the =CH twist bend is significantly reduced indicating the isomerization may be almost complete. This isomerization was generally the only notable change to the spectra from the short biodiesel in actual sunlight experiment as is indicated in Figure 6.12 so it follows that isomerization is the first change that occurs to the FAMEs in biodiesel.

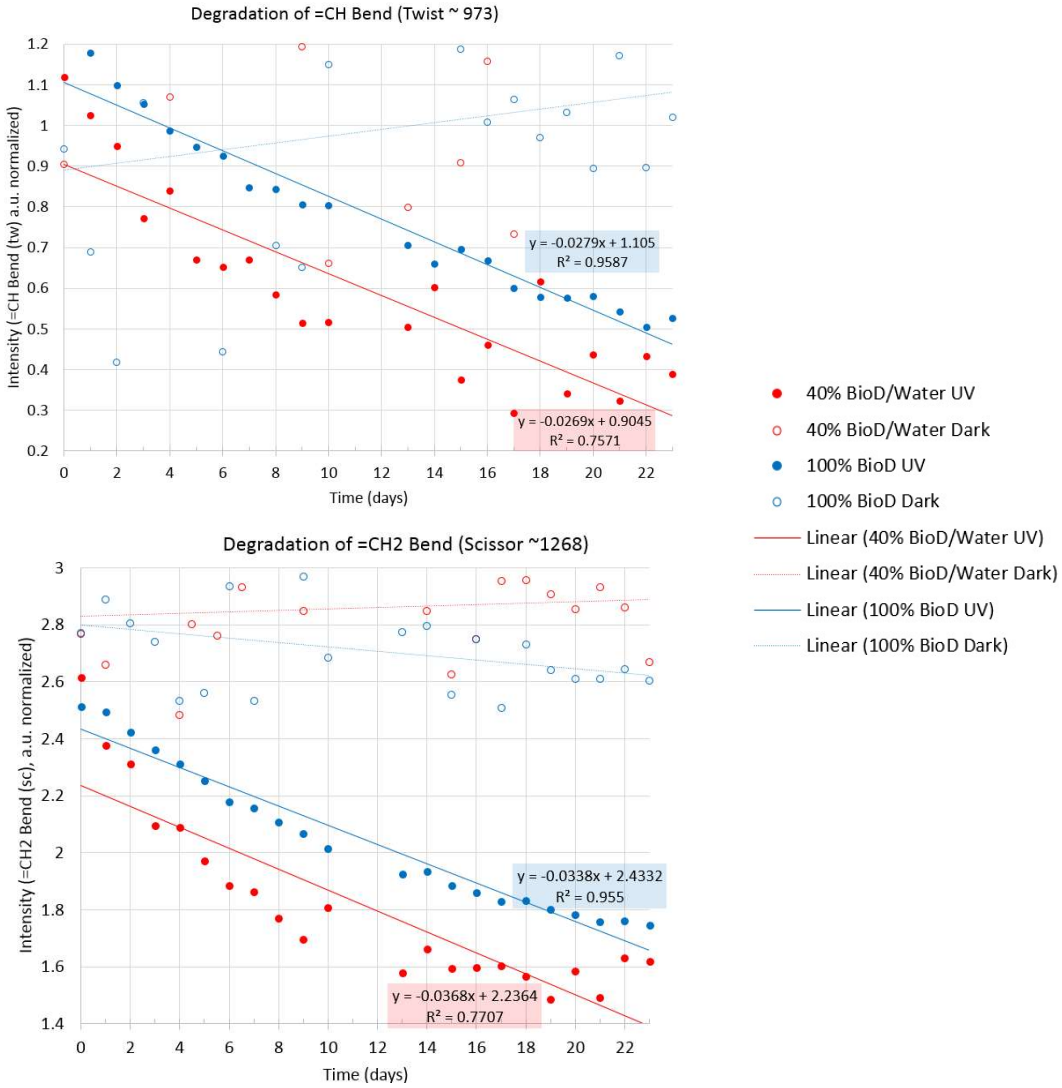

Figure 6.15 Degradation of =CH bends in biodiesel over 23 days under UV exposure. The isomerization begins to stabilize noticeably after approximately 14 days.

Photo-oxidation. The next most noticeable change to the spectra of the biodiesel and

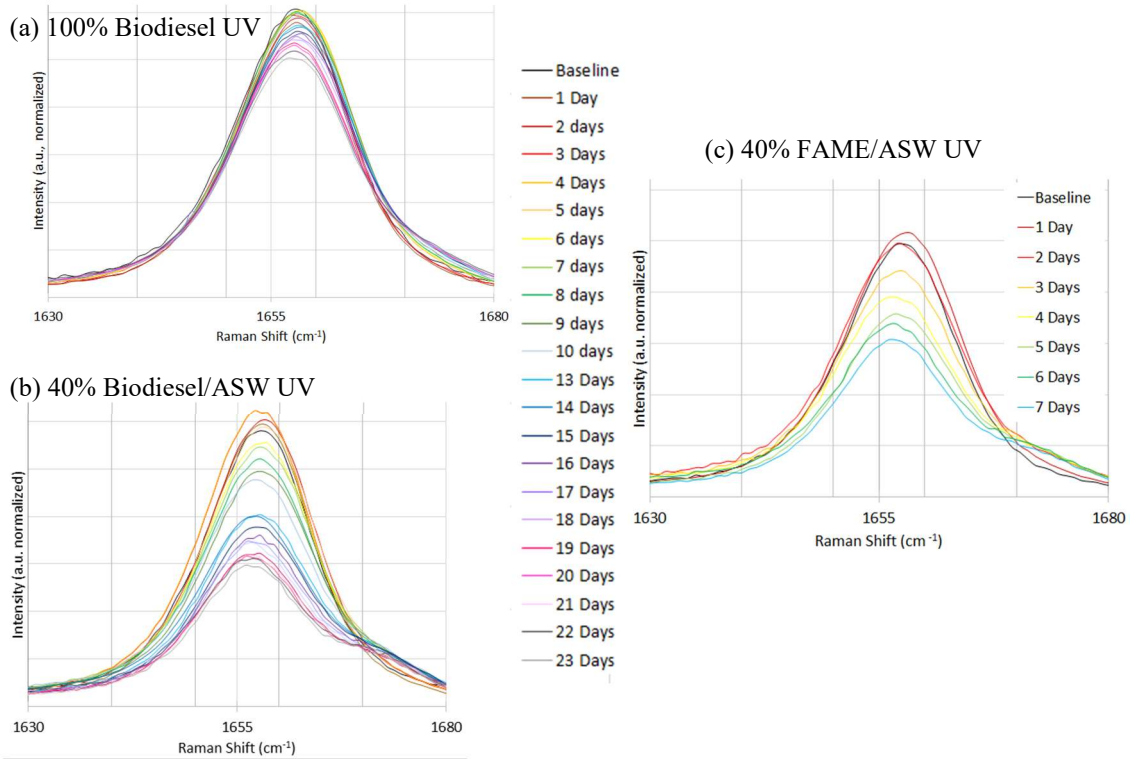

Figure 6.16 Detailed view of C=C stretch at ~1657 cm^{-1} from (a) 100% biodiesel (b) 40% biodiesel in ASW and (c) 40% FAMEs in ASW under UV exposure. The vibrational mode grows weaker over time indicating deterioration of the C=C bond.

FAMEs exposed to UV light was the weakening of the vibrational modes associated with the carbon double bonds. The =CH bends discussed in the previous paragraph weakened first due to isomerization, but they also declined due to the breakage of the double bond at the olefin group. Figure 6.16 is a more detailed view of the C=C degradation in the FAMEs in ASW and the biodiesel samples. All the samples under the UV exposure show signs of the unsaturated components in biodiesel and in the lab-made FAME mix degrading. However the biodiesel and FAMEs mixed with ASW show a much larger decline in this vibrational mode than the 100% biodiesel under UV conditions. This follows the results found by Khoury et al. and Yang et al. who found that the unsaturated components of biodiesel degraded first, and the higher the degree of unsaturation, the faster the degradation of those components [7, 19]. As the C=C vibrational

modes degrade, the remaining saturated FAME components in the mix and in biodiesel maintain the structure of the oil. Yang et al. suggested that photo-oxidation creates free radicals and other transient species [19].

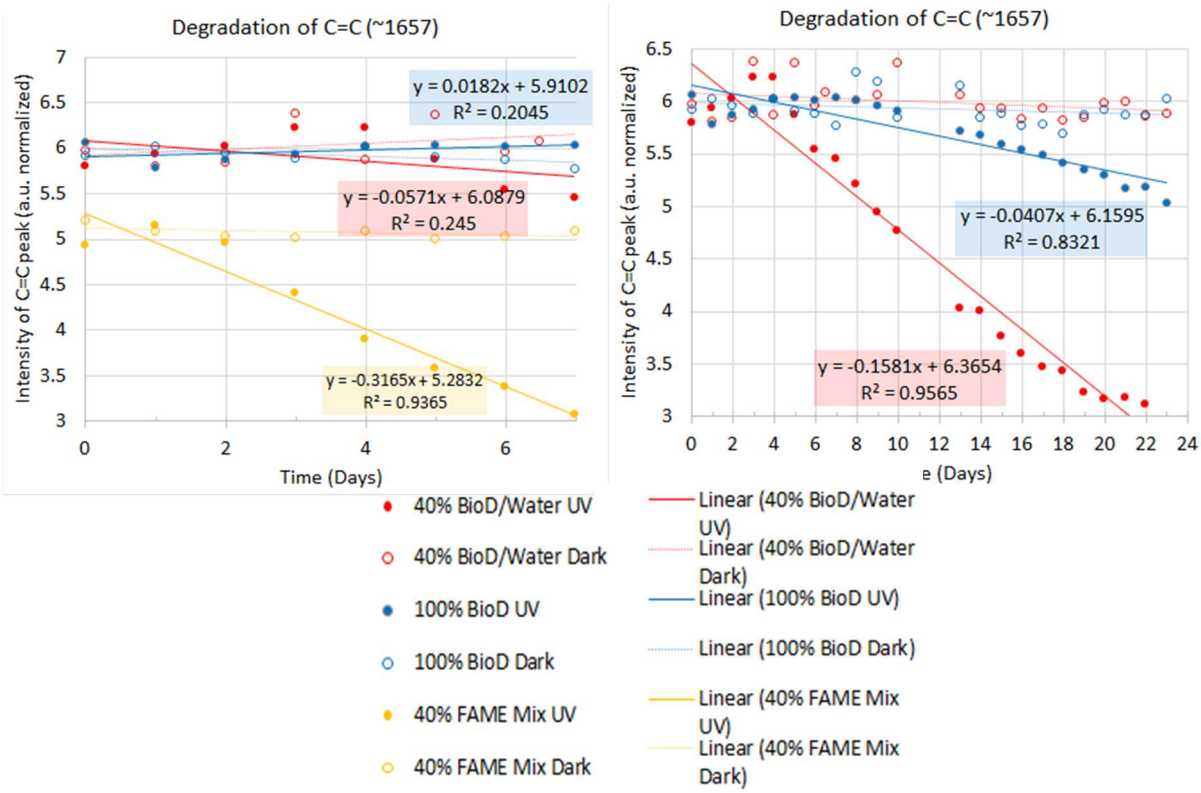

Figure 6.17 Degradation of C=C bond intensity caused by photo-oxidation. The top graph reveals the C=C in the lab made FAME mix degrades immediately. The biodiesel takes some days before it begins degrading due to the antioxidants in commercial biodiesel.

Table 6.2 Numeric analysis of the C=C degradation in biodiesel and a lab-made FAME mix over 7 days (top) and biodiesel over 7-23 days (bottom).

	Linear Correlation (R^2)	**Linear Slope**
100% Biodiesel	0.20	0.02
40% Biodiesel/ASW	0.25	-0.06
40% FAMEs/ASW	0.94	-0.32
From 0-7 Days		

	Linear Correlation (R^2)	**Linear Slope**
100% Biodiesel	0.99	-0.06
40% Biodiesel/ASW	0.95	-0.15
From 7-23 Days		

Hansen, Cyritsis and Lee indicated that high levels of unsaturated FAMEs in biodiesel

are susceptible to photo-oxidation and therefore unsaturated FAMEs in biodiesel should be controlled and/or additives like antioxidants should be added to the fuel to avoid this problem [6]. The commercial biodiesel used in this study clearly has anti-oxidants in it that slowed oxidation. This is illustrated in Figure 6.17. The top image shows the C=C intensity trend over 7 days. The lab-made FAME mix has a clear correlation (R^2>0.9) whereas the biodiesel samples have no correlation. After over 3 weeks however, the biodiesel samples show a clear correlation indicating photo-oxidation occurs, breaking the C=C bonds. Even once this photo-oxidation trend becomes strong from one week on, the speed at which this photo-oxidation occurs is still less than that observed in the FAME mix as documented in Table 6.2. The slope of the linear correlation for the 40% biodiesel in ASW from 7 days on is still only half of the slope of the linear correlation for the FAME mix in ASW.

Hydrolysis formation of methanol and FFAs. Khoury et al., Yang et al., and DeMello et al., suggested that biodiesel degrades into free fatty acids and methanol [7, 18, 19]. An indication of free fatty acid formation is observed in the carbonyl peak shift, especially notable in the 40% biodiesel/ASW sample under UV exposure. This carbonyl peak change is illustrated in more detail in Figure 6.18. Though subtle, it is apparent that the C=O peak begins to shift to a lower frequency as the peak broadens on the low frequency side and narrows on the higher frequency side. Another indication of the formation of FFAs discussed in section 6.1.2 is a change in the end group vibrations from 800-900 cm^{-1}. The ester end group of a fatty acid methyl ester is unique and its relative FFA instead had an OH end group. As hydrolysis occurs, the CH_3 end group of the FAME breaks off in the presence of water. It forms methanol (CH_3OH), and the free hydrogen from the water attaches to the oxygen left on the end group to form the FFA. For

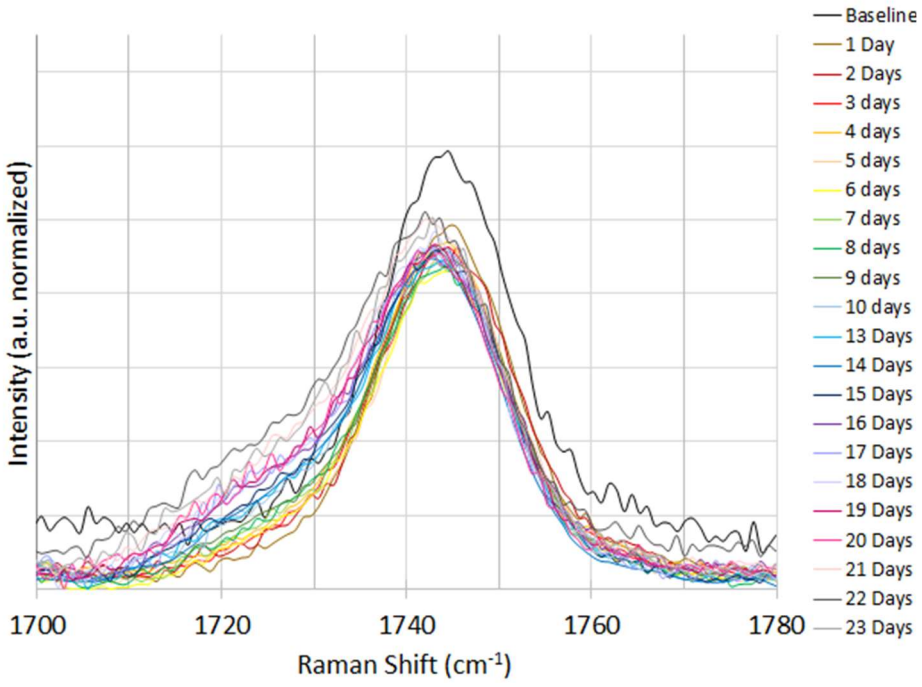

Figure 6.18 Raman spectra of 40% biodiesel in ASW under UV exposure focused on the carbonyl stretch. A shift in this peak towards the lower frequency indicates formation of the free fatty acids.

example in linear form, the hydrolysis reaction of oleic acid methyl ester is:

$CH_3(CH_2)_7CH=CH(CH_2)_7CO_2CH_3 + H_2O \rightarrow CH_3(CH_2)_7CH=CH(CH_2)_7COOH + CH_3OH$

As outlined in 6.3.1, the end group vibrations in the 40% biodiesel/ASW under UV exposure do change over the studied time period. There is an increase in intensity especially near 855 cm^{-1}. This region of the FAMEs was attributed to the CH_3 rock, C_1-C_2 acyl group (at 890 cm-1) and the C-O stretch. Unfortunately, it is unclear exactly why this region changed under UV and water exposure. The formation of the FFA could affect the location of the C-O stretch and the other stretches could also shift due to interactions of nearby atoms changing as hydrolysis takes place.

New peaks were expected to form indicating the presence of methanol from the hydrolysis reaction especially considering the long timeframe of this study. Unfortunately the presence of methanol in the 40% biodiesel/ASW under UV conditions was not identifiable in the Raman spectra. However, the obvious evaporation of this sample over the time studied shows that a volatile material was leaving the sample. Methanol has a vapor pressure that is almost 7 times greater than water at 20^oC and so methanol should evaporate quickly under the experimental circumstances [37]. This was discussed in section 6.3.1 and clearly illustrated in the photographs of Figure 6.7. The 40% biodiesel/ASW under UV exposure experienced significant evaporation as it was under the UV lamp with the top off. Its control was left in the dark with the top on so methanol could not have evaporated into an open space in that sample. From the findings of Leite et al., methanol was clearly formed in the water soluble fractions of biodiesel in seawater, and from the visual observation that a great amount of evaporation occurred in the 40% biodiesel/ASW sample, it is deduced that methanol was formed through hydrolysis but evaporated into the fume hood so that measurement of that substance was not possible [23].

6.4.2 Degradation Time of Biodiesel in ASW Compared to Literature Results

The degradation mechanisms are identifiable from these results, but the timing of the degradation is not as easy to evaluate with these Raman spectra. Khoury et al. found that after 10 days of sunlight exposure, none of the FAMEs with two or more double bonds remained and approximately 40% of the main component of biodiesel (oleic acid methyl ester) remained. In the current study, the C=C stretch of biodiesel in ASW was reduced in intensity by approximately 17% after 10 days (and 55% over 23 days). It is difficult to compare these two studies because Khoury et al. used actual sunlight and 100% biodiesel from a government source. In the current study, a monochromatic UV lamp was used in a commercial biodiesel sample mixed in saltwater.

Yang et al., found that after 5 hours of intense UV exposure over 80% of the total organic carbon was removed from a biodiesel sample in a water matrix. This study is also difficult to compare because of the strength of the UV lamp was ten times higher than the one in this study and it was at an unknown wavelength; also the measurement techniques were very different as to make the results incomparable in terms of degradation time.

The UV lamp used in this study was at 302 nm wavelength with a light intensity of 3.6 mW/cm^2 intensity. According to Diffey, the sunlight intensity at 302 nm measured in the summer (at noon on a clear day) in Albuquerque, New Mexico, USA is 0.00236 mW/cm^2 [20]. Therefore the UV lamp used in this study was significantly more powerful than the sun's irradiance at that specific wavelength. However, natural sunlight has a very large range of radiation from the UV-C low range of 100 nm through the visible range of 780 nm into the far infrared at 1 mm [20]. Though the UV lamp in this study was almost 1500 times greater in irradiance than the same wavelength contributed by actual sunlight, this study did not take into account the entire spectrum of sunlight. The three days that a concurrent experiment of biodiesel

samples was exposed to natural sunlight did not yield statistically valid results; this could be due to the antioxidants in biodiesel or also to the strength of the sun's radiation which varies with altitude, latitude, and weather factors [20]. Consequently, relating the timeframe of this study to actual environmental degradation under full sunlight conditions is not definitively possible.

6.5 Conclusions

Three concurrent experiments were performed over a 23 day time span. Pure biodiesel and 40% biodiesel mixed with ASW was evaluated under a monochromatic UV lamp through 23 days of exposure. Those same parameters were evaluated under actual sunlight through 3 days of exposure. Finally, a 40% lab-made FAME mix was blended with ASW and evaluated for 7 days. The results were similar for the FAME and biodiesel samples under UV exposure. The sunlight experiment was too short to yield viable results.

The mechanism of degradation identifiable through Raman spectroscopy included isomerization, photo-oxidation and hydrolysis. Isomerization appeared to be the first mechanism of degradation and was notable with the decline of the *cis* vibrations in the Raman spectra. This was also the first degradation method noted in a thermal study and the isomerization occurred in the pure biodiesel as well as the biodiesel/ASW samples [36]. Photo-oxidation was indicated through the break-down of the carbon double bonds. This was especially apparent in the samples placed in the artificial seawater. Photo-oxidation occurred quickly in the FAME mix, but took almost 7 days before it began in the biodiesel samples due to the antioxidants added to the commercial biodiesel to avoid this type of degradation during storage. The hydrolysis reaction occurred in the water samples and yielded free fatty acids and methanol. The FFA formation was notable in the carbonyl band shift and in the changes to the end groups. The methanol formation was not identifiable in the Raman analysis. However the obvious visual evaporation of the 40%

biodiesel/ASW sample and the relatively high vapor pressure of methanol showed that methanol was formed from this sample but evaporated in the fume hood.

The timeframe of the biodiesel degradation is challenging to relate to actual sunlight conditions. The study used a monochromatic UV lamp that was strong compared to the same UV wavelength produced by sunlight radiation, but it is problematic to correlate that to the entire sunlight spectrum and take into account the variables that affect sunlight radiation such as latitude, altitude and weather conditions. This study found similar results in terms of mechanistic degradation to analogous research in photolytic degradation; however other research was dissimilar in photolytic sources and in measurement techniques making the results incomparable in terms of degradation timeframe.

Chapter 7. Looking Ahead and Research Review

This study explored the degradation mechanics of commercial biodiesel exposed to saltwater and UV light to equate how this substance may break down in the marine environment. Several previous studies showed that biodiesel is considered readily biodegradable. The fatty acids that make up biodiesel were studied individually and as mixtures. Khoury et al. showed that unsaturated FAMEs break down faster than saturated FAMEs [7]. This was confirmed in another study by Yang et al [19]. Research into the thermal degradation of biodiesel found the same results [36].

Most research of biodiesel used gas chromatography for measurements due to its use in environmental forensics and its capability to separate components of a mixture. However little research on the Raman spectra of biodiesel was available. Beattie et al., produced a comprehensive study that identified major vibrational modes in individual FAMEs [13]. Miranda et al. specifically used Raman spectroscopy to characterize both common FAMEs of biodiesel and commercial biodiesel providing a good foundation for further characterization of biodiesel with this technique [15]. This current project identified the characteristic vibrational modes of the five major component FAMEs of biodiesel and further characterized a commercial biodiesel sample using Raman spectroscopy with results comparable to the findings of Miranda et al. and Beattie et al. FAMEs and biodiesel were mixed with ultra-pure water and artificial seawater to determine the concentration sensitivity of the spectrometer. At concentrations lower than 20% oil in water, the spectral resolution was not conducive to intense study. Comparatively, Khoury et al. and Yang et al. were able to use much lower concentrations of oil in water due their measurement techniques (GC and total organic carbon, respectively).

The degradation of biodiesel under a monochromatic UV lamp showed three mechanisms

for degradation: isomerization of the *cis* configuration, photo-oxidation of the carbon double bonds, and hydrolysis to form free fatty acids and methanol. The isomerization results were supported by Lin et al. and were the first mechanism of degradation. The photo-oxidation was indicated by Khoury et. al and Yang et. al who found that the more double bonds a component had, the faster and more complete the degradation [7, 19]. Photo-oxidation was illustrated to be slower in the commercial biodiesel sample than the lab-made FAME mix due to antioxidants added to the fuel to avoid oxidation. Hydrolysis contributed to the formation of free fatty acids and methanol. The formation of FFAs was demonstrated in the Raman spectra, but methanol was not detected by this form of measurement. However, the large amount of evaporation noted in the oil/water under UV sample indicated that a volatile substance was exiting the sample. Since methanol has a significantly higher vapor pressure than water, and Leite et al. showed that methanol was the main component formed in water soluble fractions of biodiesel, the evaporated substance was concluded to be methanol [23].

The experiment was conducted with a monochromatic UV lamp and though its irradiance was over 1,500 times higher than the sun's irradiance at that same wavelength, it is not comparable to the entire sunlight spectrum. Comparably, Khoury et al. used physical sunlight but not an oil/water mixture and Yang et al., used an extremely strong UV lamp but a different measurement technique. Therefore, correlating these results to a degradation time frame relative to actual physical oceanographic conditions was not feasible in this research.

7.1 Future Research

7.1.1 Procedural Improvements With Use of Alternate Research Instrumentation: SPME, SERS, GC

Raman spectroscopy provides a molecular level examination of a studied sample

allowing for intricate evaluation of the transformation of molecules. However, some vibrational modes are not active in Raman spectroscopy and the complexity of molecules can broaden peaks making some of the molecular vibrations difficult to evaluate. Further, these results showed that, especially in saltwater, mixtures of oil in water only yielded valid spectra at fairly high concentrations. Some enhanced Raman spectroscopy techniques are available and could resolve some of these issues including solid phase micro extraction (SPME) with Raman spectroscopy, and surface enhanced Raman spectroscopy (SERS).

In SPME, a fiber coated solid (usually coated with some kind of polymer) is placed into a liquid or gas sample. The coating is designed so that certain analytes (such as hydrocarbons or other organic molecules) attach to this fiber and then the entire solid can be evaluated under Raman spectroscopy [38]. Figure 7.1 shows an illustration of a SPME extraction directly into a liquid (a) and gas (b) sample. SPME can be used to analyze gas samples which could be applied for similar research to capture and measure the methanol evaporated from the oil/water under UV exposure sample [39]. Additionally, samples of low concentrations may attach to the fiber coating allowing for Raman resolution at low concentrations.

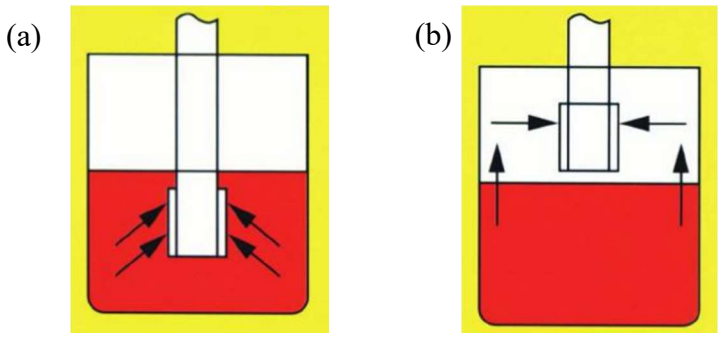

Figure 7.1 Illustration of solid-phase micro-extraction technique into an (a) liquid and (b) gas portion of a sample where the red substance is the analyte. [39]

In SERS, a solid substrate is engineered, often with metal or polymer nanoparticles that are specifically made to enhance the desired specimens' Raman signals [40]. In this method, low concentrations of an analyte will attach or be trapped near the substrate and this is analyzed by the Raman spectrometer; the properties of the substrate enhance the Raman active modes of the analyte making detection possible [40]. This method could be used to lower the concentration of the oil/water mix and potentially more specifically identify FFAs and methanol formed through hydrolysis. SPME and SERS are only two Raman spectroscopic enhancement techniques that may improve these results; many others also exist.

Alternatively, another form of measurement could be employed. As previously discussed, most fuel systems are analyzed using GC. This method is good at identifying each component which elutes from the main sample. Advancement techniques such as GC x GC (two dimensional gas chromatography) already is used extensively in environmental forensics because it can highly resolve very complex environmental samples [10]. GC can also detect gas samples which would be useful in detecting the evaporated methanol in this study. GC does require more complex sample preparation and it does not necessarily identify molecular-level changes.

7.1.2 Procedural Improvements and Enhanced Data Analysis

This research can be improved by taking multiple samples at each sampling time and specimen. From this, the Raman spectra could be averaged, and outliers discarded statistically. Further, studying the degradation of individual FAMEs exposed to water and UV will result in a more complete discussion of oxidation and the stability of the FAMEs that make up biodiesel in terms of saturation, carbon chain length and other features. Additionally, different UV lamp wavelengths or Xenon lamps (which better simulate full sunlight spectrum) can be used under comparative conditions to evaluate the time frame of biodiesel degradation. The specimens used

in this study were kept static under the UV lamp until they were shaken to use for the Raman analysis. Placing the specimens in a dynamic environment with stirring or rocking better emulates actual oceanographic conditions and could speed degradation.

Raman analysis yields simple "x, y" spectrographic data with the x-data corresponding to the wavelength of the Raman shift and the y-data corresponding to the intensity of the vibrational mode. There are very advanced statistical and numerical analyses that can be performed on spectroscopic data. Chemometrics is the term applied to the general discipline of advanced statistical and numerical evaluation to optimize chemical data results and is especially useful in chromatographic and spectral data sets [41]. Normalization and baseline subtraction, used in this research were the only two basic statistical techniques used to evaluate the data. Many other preprocessing methods exist from other normalization techniques to advanced multivariate and vector data processing [42]. A team of US Coast Guard researchers illustrate the capabilities of chemometrics, especially in environmental forensics by writing:

> Advanced numerical methods offer the advantages of multivariate analysis of correlated variables (i.e., diagnostic ratios) and a statistical basis for determining the similarities and/or differences between samples. In effect, these advanced data processing methods serve to elucidate significant differences between samples that have many similarities. [41]

Bringing together a group of researchers with statistical analysis skills working alongside chemical or environmental engineers could greatly enhance the amount, validity, and usefulness of the yielded results. If chemometrics were implemented alongside some of the more advanced Raman spectrographic techniques, this type of research could be extremely advantageous to multiple fields of study.

7.2 Implications for International Shipping

In returning to the original motivation for this research, it is critical to apply this new information to actuality. As discussed in section 1.1, vessels that ship biodiesel as cargo have an

option when travelling internationally to wash their empty tanks with seawater and discharge the residue in to the sea, given they follow some specific requirements. The US requirements are not aligned with this policy, requiring ships to clean their used cargo tanks dockside. As discussed in section 2.3, biodiesel is considered readily biodegradable, though it showed some toxicity to aquatic organisms such as microalgae, freshwater juvenile fish, and sea urchin larvae. The requirements for a ship discharging residual tank washings are made so that the concentration of residue cargo is not only low, but spread over a large area, far from land mases and sensitive ecosystems, avoiding conglomeration of residue and effectively diluting it with the almost infinite dilution capabilities of the oceans. Furthermore, natural physical oceanographic processes such as precipitation and weather, currents, waves, and other phenomenon are complex variables that will greatly affect how a discharged residue acts. Given this, it is unlikely that the discharged residue waste-washings occur in large enough concentrations to be of a major environmental concern to marine organisms, assuming that the vessel carefully follows the discharge requirements outlined by the International Maritime Organization. A critical piece of information that would elucidate this hypothesis is to understand the amount and concentration of biodiesel residue washings that could enter the marine environment from a ship. This data would require flow meters and concentration analysis at the output of the effluent which is possible, but would take international, corporate, and governmental cooperation.

This research showed that biodiesel will break down under UV exposure, which would occur on the top of the water where the residue would be discharged and these results were supported by other degradation research. Further, DeMello et al., and Khoury et al., showed that biological activity also degrades biodiesel as the free fatty acids formed from hydrolysis are a usable source of energy for biological activity [7,18]. An item of concern is the methanol that is

produced from the hydrolysis degradation. Previous studies from Brazilian researchers indicated that methanol is the main toxic outcome of biodiesel degradation and can cause harm to aquatic organisms [23]. However this current research showed that methanol evaporated readily from the biodiesel/water samples under UV exposure as methanol is very volatile. Further study into the production of methanol from biodiesel degradation and its fate would facilitate in determining the extent of the danger posed by methanol to the aquatic environment. With the actual exposure of biodiesel residue in the oceanic environment including sun/UV, wave, current, wind, weather, biological, and transport phenomena it is unlikely to remain in the environment in concentrations that could negatively impact aquatic organisms.

References

[1] M. Beck, Renewable Energy Directive and the challenges for the Biodiesel Industry, Hamburg: Anchor Academic Publishing, 2013.

[2] National Renewable Energy Laboratory, "Biodiesel Handling and Use Guide 4th Ed," U. S. Department of Energy, Oak Ridge, 2009.

[3] International Chamber of Shipping, "Shipping and World Trade," 2013. [Online]. Available: http://www.ics-shipping.org/shipping-facts/shipping-and-world-trade. [Accessed 05 05 2015].

[4] International Maritime Organization, "IMODOCS," 02 01 2013. [Online]. Available: https://docs.imo.org/. [Accessed 05 06 2015].

[5] International Maritime Organization, MARPOL Consolidated Edition 2011, London: International Maritime Organization, 2011.

[6] A. Hansen, D. Cyritsis and C. Lee, "Characteristics of Biofuels and Renewable Fuel Standards," in *Biomass to Biofuels - Strategies for Global Industries*, Chippenham, Wiley, 2010, pp. 3-26.

[7] R. Khoury, D. Ebrahimi, L. Hejazi, M. Bucknall, R. Pickcford and D. Hibbert, "Degradation of fatty acid methyl esters in biodiesels exposed to sunlight and seawater," *Fuel,* vol. 90, pp. 2677-2683, 2011.

[8] G. Keswani, Raman and His Effect, New Delhi: National Book Trust, 1980.

[9] HORIBA, "Raman Tututorial," HORIBA Scientific, 2016. [Online]. Available: http://www.horiba.com/us/en/scientific/products/raman-spectroscopy/raman-academy/raman-tutorial/. [Accessed 28 07 2015].

[10] G. Frysinger, R. B. Gaines and C. M. Reddy, "GC X GC - A new analytical tool for environmental forensics," *Environmental Forensics,* vol. 3, pp. 27-34, 2002.

[11] M. Ahmadjian and C. Brown, "Petroleum identification by laser Raman spectroscopy," *Analytical Chemistry,* vol. 48, no. 8, pp. 1257-1259, 1976.

[12] D. Cleveland, M. Carlson, E. Hudspeth, L. Quattrochi, K. Batchler, S. Balram, S. Hong and R. Michel, "Raman spectroscopy for the undergradtuate teaching laboratory: Quantification of ethanol concentration in consumer alcoholic beverages and qualitative identification of marine diesels usiing a miniature Raman spectrometer," *Spectroscopy Letters,* vol. 40, p. 903–924, 2007.

[13] J. R. Beattie, S. Bell and B. W. Moss, "A critical evaluation of raman spectroscopy for the analysis of lipids: Fatty acid methy esters," *Lipids,* vol. 39, no. 5, pp. 407-419, 2004.

[14] M. Silva, F. Teixeira, E. Torres, A. Rocha, F. Freires, T. Santos and a. P. Jong, "Biodiesel in Brazil: A market analysis and its economic effects," *Journal of Agricultural Sciences,* vol. 6, no. 8, pp. 160-178, 2014.

[15] A. Miranda, E. Castilho-Almeida, E. Ferreira, G. Moreira, C. Achete, R. Armond, H. D. Santos and A. Jorio, "Line shape analysis of the Raman spectra from pure and mixed biofuel esters componds," *Fuel,* vol. 115, pp. 118-125, 2014.

[16] K. G. Brown, E. Bicknell-Brown and M. Ladjadj, "Raman-active bands sensitive to motion and conformation at the chain termini and backboes of alkanes and lipids.," *Journal of Physical Chemistry,* vol. 91, pp. 3436-3442, 1987.

[17] C. Peterson and G. Moller, "Biodiesel fuels: Biodieegradability, biological and chemical oxygen demand, and toxicity.," in *The Biodiesel Handbook*, Urbana, AOCS Press, 2010, pp. 231-246.

[18] J. DeMello, C. Carmichael, E. Peacock, R. Nelson, J. Arey and C. Reddy, "Biodegradation and environmental behavior of biodiesel mixtures in the sea: An initial study," *Marine Pollution Bulletin,* vol. 54, pp. 894-904, 2007.

[19] Z. Yang, B. Hollebone, Z. Wang, C. Yang, C. Brown, M. L. G. Zhang and X. Ruan, "A preliminary study for the phtolysis behavior of biodiesel and its blends with petroleum oil in siimulated freshwater," *Fuel,* vol. 139, pp. 248-256, 2015.

[20] B. L. Diffey, "Sources and measurement of ultraviolet radiation," *Methods,* vol. 28, pp. 4-13, 2002.

[21] K. Bluhm, S. Heger, T. Seiler, A. Hallare, A. Schaffer and H. Hollert, "Toxicological and ecotoxicological potencies of biofuels used for the transport sector—a literature review," *Energy & Environmental Science,* vol. 5, pp. 7381-7392, 2012.

[22] N. Khan, M. Warith and G. Luk, "A comparison of acute toxicity of biodiesel, biodiesel blends, and diesel on aquatic organisms," *Journal of the Air & Waste Management Association ,* vol. 57, pp. 286-296, 2007.

[23] M. Leite, M. S. d. Araujo, I. Nascimento, A. S. D. Cruz, S. Pereira and N. C. D. Nascimento, "Toxcity of water soluble fractions of biodiesel fuels derived from castor oil, palm oil, and waste cooking oil," *Environmental Toxicology and Chemistry,* vol. 30, no. 4, pp. 893-897, 2011.

[24] S. Pereira, V. Araujo, M. Reboucas, F. Vieira, M. Almeida, F. Chinalia and I. Nascimento, "Toxicity of biodiesel, diesel and biodiesel/diesel blends: comparative sub-lethal effects of water-soluble fractions to microalgae species," *Bulletin of Environmental Contamination and Toxicology,* vol. 88, p. 234–238, 2012.

[25] I. Nascimento, S. Pereira, M. Leite, A. S. d. Cruz, J. Santos, D. Barros, T. Veras, H. Alvarez and M. Nascimento, "Is Biodiesel an eco-compatible fuel? Toxicity estimation to organisms of different trophic levels.," in *Industrial Pollution Including Oil Spills*, Portland, Ringgold Inc, 2009, pp. 61-90.

[26] N. Afseth, V. Segtnan and J. Wold, "Raman spectra of biological samples: A study of preprocessing methods.," *Applied Spectroscopy,* vol. 60, no. 12, pp. 1358-1367, 2006.

[27] F. Ya, L. Shuang and X. Da-Peng, "Raman spectra of oleic acid and linoleic acid," *Spectroscopy and Spectral Analysis,* vol. 33, no. 12, pp. 3240-3243, 2013.

[28] P. Larkin, Infrared and Raman Spectrometry; Principles and Spectral Interpretation, Amsterdam: Elsevier, 2011.

[29] E. Bicknell-Brown, K. Brown and W. Pearson, "Configuration-dependent Raman bands of phospholipid surfaces," *Journal of Raman Spectroscopy,* vol. 11, no. 5, pp. 356-362, 1981.

[30] S. Kint, P. Wermer and J. Scherer, "Raman spectra of hydrated phospholipid bilayers. 2. Water and head-group interactions," *Journal of Physical Chemistry,* vol. 96, no. 1, pp. 446-452, 1992.

[31] M. Hrovat, "Baseline Fit," 3 August 2009. [Online]. Available: http://www.mathworks.com/matlabcentral/fileexchange/24916-baseline-fit. [Accessed 1 May 2016].

[32] K. Sun, H. Su, Z. Yao and P. Huang, "Baseline correction for Raman spectra based on piecewise linear fitting," *Spectroscopy,* vol. 29, no. 2, pp. 54-61, 2014.

[33] S. Marinović, M. Krištović, B. Špehar, V. Rukavina and A. Jukić, "Prediction of diesel fuel properties by vibrational spectroscopy using multivariate analysis," *Journal of Analytical Chemistry,* vol. 67, no. 12, pp. 939-949, 2012.

[34] P. Brewer, G. Malby, J. Pasteris, S. White, E. Peltzer, B. Wopenka, J. Freeman and M. Brown, "Development of a laser Raman spectrometer for deep-ocean science," *Deep-Sea Research I,* vol. 51, p. 739–753, 2004.

[35] R. Grenlee and R. Lucas, "Electrical purification of gas turbine fuels," in *Manual on Requirements, Handling, and Quality Control of Gas Turbine Fuel*, ASTM, 1973, pp. 73-104.

[36] R. Lin, Y. Zhu and L. Tavlarides, "Mechanism and kinetics of thermal decomposition of biodiesel fuel," *Fuel,* vol. 106, pp. 593-604, 2013.

[37] National Center for Biotechnology Information, "PubChem: Open Chemistry Database," U.S. National Library of Medicine, 2016. [Online]. Available: https://pubchem.ncbi.nlm.nih.gov. [Accessed 1 May 2016].

[38] I. Nwaneshiudu, Q. Yu and D. Schwartz, "Quantitative solid-phase microextraction - Raman spectroscopy for the detection of trace organics in water," *Applied Spectroscopy,* vol. 66, no. 12, pp. 1487-1491, 2012.

[39] J. Pawliszyn, K. Jinno and R. Smith, Application of Solid Phase Microextraction, Cambridge: Royal Society of Chemistry, 2007.

[40] J. Popp and T. Mayerhofer, "Surface-enhanced raman spectroscopy," *Analytical and Bioanalytical Chemistry,* vol. 394, pp. 1717-1718, 2009.

[41] R. Gaines, G. Hall, G. Frysinger, W. Gronlund and K. Juaire, "Chemometric determination of target componds used to fingerprint unweathered diesel fuels," *Environmental Forensics,* vol. 7, pp. 77-87, 2006.

[42] S. Li, J. Nyagilo, D. Dave and J. Gao, "Models and methods for quantitative analysis of surfance-enhanced Raman spectra," *IEEE Journal of Biomedical and Health Informatics,* vol. 18, no. 2, pp. 525-536, 2014.

[43] Royal Society of Chemistry, "ChemSpider," Royal Society of Chemistry, 2015. [Online]. Available: http://www.chemspider.com/. [Accessed 15 06 2015].

[44] N. Colthup, L. Daly and W. Stephen, Introduction to Infrared and Raman Spectroscopy, 2nd Ed., New York: Academic Press, 2012.